

International Journal of Modern Physics D  
 © World Scientific Publishing Company

## COSMIC RAYS IN GALAXY CLUSTERS AND THEIR NON-THERMAL EMISSION

GIANFRANCO BRUNETTI

*IRA-INAf, via P. Gobetti 101, 40129 Bologna, Italy  
 brunetti@ira.inaf.it*

THOMAS W. JONES

*School of Physics and Astronomy, University of Minnesota, 116 Church St SE, Minneapolis, MN 55455, USA  
 twj@msi.umn.edu*

Received Day Month Year

Revised Day Month Year

Radio observations prove the existence of relativistic particles and magnetic field associated with the intra-cluster-medium (ICM) through the presence of extended synchrotron emission in the form of radio halos and peripheral relics. This observational evidence has fundamental implications on the physics of the ICM. Non-thermal components in galaxy clusters are indeed unique probes of very energetic processes operating within clusters that drain gravitational and electromagnetic energy into cosmic rays and magnetic fields. These components strongly affect the (micro-)physical properties of the ICM, including viscosity and electrical conductivities, and have also potential consequences on the evolution of clusters themselves. The nature and properties of cosmic rays in galaxy clusters, including the origin of the observed radio emission on cluster-scales, have triggered an active theoretical debate in the last decade. Only recently we can start addressing some of the most important questions in this field, thanks to recent observational advances, both in the radio and at high energies. The properties of cosmic rays and of cluster non-thermal emissions depend on the dynamical state of the ICM, the efficiency of particle acceleration mechanisms in the ICM and on the dynamics of these cosmic rays. In this review we discuss in some detail the acceleration and transport of cosmic rays in galaxy clusters and the most relevant observational milestones that have provided important steps on our understanding of this physics. Finally, looking forward to the possibilities from new generations of observational tools, we focus on what appear to be the most important prospects for the near future from radio and high-energy observations.

*Keywords:* Galaxies: clusters: general; Radiation mechanisms: non-thermal; Acceleration of particles.

*PACS numbers:* 95.30.Cq; 95.30.Gv; 95.30.Qd; 98.65.Cw; 98.65.Fz; 98.65.Hb

### 1. Introduction

Clusters of galaxies and the filaments that connect them are the largest structures in the present universe in which the gravitational force due to the matter overdensity overcomes the expansion of the universe. Massive clusters have typical total masses of the order of  $10^{15} M_{\odot}$ , mostly in the form of dark matter ( $\sim 70 - 80\%$  of the total mass), while baryonic matter is in the form of galaxies ( $\sim \text{few}\%$ ) and especially in the form of a hot

2 *G. Brunetti & T. W. Jones*

( $T \sim 10^8 K$ ) and tenuous ( $n_{gas} \sim 10^{-1} - 10^{-4} cm^{-3}$ ) gas ( $\sim 15 - 20\%$ ), the intra-cluster-medium (ICM)<sup>1,2</sup> (Figure 1). That ICM emits thermal X-rays, mostly via bremsstrahlung radiation, and also Compton-scatters the photons of the cosmic microwave background, leaving an imprint in the mm-wavelengths band that provides information complementary to the X-rays<sup>6</sup> (Figure 1). In the current paradigm of structure formation, clusters are thought to form via a hierarchical sequence of mergers and accretion of smaller systems driven by dark matter that dominates the gravitational field. Mergers, the most energetic phenomena since the Big Bang, dissipate up to  $10^{63} - 10^{64}$  ergs during one cluster crossing time ( $\sim$  Gyr). This energy is dissipated primarily at shocks into heating of the gas to high temperature, but also through large-scale ICM motions.<sup>2,7,8</sup> Galaxy clusters are therefore veritable crossroads of cosmology and astrophysics; on one hand they probe the physics that governs the dynamics of the large-scale structure in the Universe, while on the other hand they are laboratories to study the processes of dissipation of the gravitational energy at smaller scales. In particular, a fraction of the energy that is dissipated during the hierarchical sequence of matter accretion can be channeled into non-thermal plasma components, i.e., relativistic particles (cosmic rays, or “CRs”) and magnetic fields in the ICM. Relativistic particles in the ICM are the main subject of our review.

The evidence for non-thermal particles in the ICM is routinely obtained from a variety of radio observations that detect diffuse synchrotron radiation from the ICM (Figure 1). They also open fundamental questions of their origins as well as their impact on both the physics of the ICM and the evolution of galaxy clusters more broadly.<sup>9</sup> Cosmological shock waves and turbulence driven in the ICM during the process of hierarchical cluster formation are obvious potential accelerators of cosmic ray electrons (CRe) and protons (hadrons or CRp).<sup>10-15</sup> In addition, clusters host other accelerators of CRs, ranging from ordinary galaxies (especially as a byproduct of star formation) to active galaxies (AGN)<sup>16-19</sup> and, potentially, regions of magnetic reconnection.<sup>20</sup> The long lifetimes of CRp (and/or nuclei) against energy losses in the ICM and their likely slow diffusive propagation through the disordered ICM magnetic field, together with the large size of galaxy clusters, make clusters efficient storehouses for the hadronic component of CRs produced within their volume or within the individual subunits that later merged to make each cluster.<sup>16-18</sup> The consequent accumulation of CRs inside clusters occurs over cosmological times, with the potential implication that a non-negligible amount of the ICM energy could be in the form of relativistic, non-thermal particles. An important result of trapped CRp above a few hundred MeV kinetic energy is that they will necessarily produce secondary pions (and their decay products, including  $e^\pm$  and  $\gamma$ -rays) through inelastic collisions with thermal target-protons. Consequently, they can be traced and/or constrained by secondary-particle-generated radio and  $\gamma$ -ray emission.<sup>16, 17, 19, 21-25</sup>

The most direct way to pin-point CRp in galaxy clusters is through the detection of  $\gamma$ -ray emission generated by the decay of secondary  $\pi^0$  particles. However to date, despite the advent of the orbiting Fermi-LAT and deep observations from ground-based Cherenkov arrays, no ICM has been firmly detected in the  $\gamma$ -rays.<sup>26-33</sup> Cluster  $\gamma$ -ray upper limits, together with several constraints from complementary approaches based on radio observa-

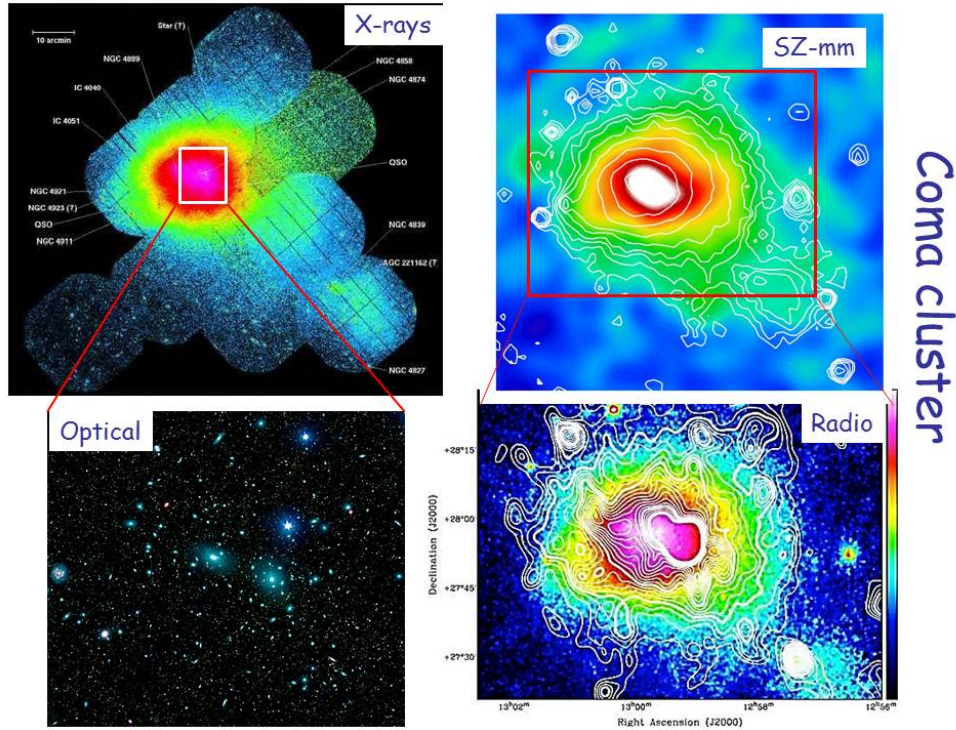


Fig. 1. Multi-frequency view of the Coma cluster: the thermal ICM emitting in the X-rays (top left, adapted from<sup>3</sup>), the overlay between thermal SZ signal (colors) and X-rays (contours) (top right, adapted from<sup>4</sup>), the optical emission from the galaxies in the central region of the cluster (bottom left, from Sloan Digital Sky Survey, credits NASA/JPL-Caltech/ L.Jenkins (GSFC)), and the synchrotron (radio halo) radio emission (contours) overlaid on the thermal X-rays (colors) (bottom right, adapted from<sup>5</sup>).

tions<sup>34–36</sup> suggest that the energy in the form of CRp is less than roughly a percent of the thermal energy of the ICM, at least if we consider the central Mpc–size region. This result contradicts several optimistic expectations derived in the last decades, based mostly on estimates for CRp production in structure formation shocks, and poses important constraints on the efficiency of CRp acceleration and transport in galaxy clusters.

On the other hand, the existence of CRe and magnetic fields in the ICM of many clusters is in fact demonstrated by radio observations. CRe are indeed very well traced to the ICM of clusters through their radio emission. Cluster-scale ( $\sim$  Mpc-scale) diffuse synchrotron emission is frequently found in merging galaxy clusters. It appears in the form of so-called *giant radio halos*, apparently unpolarized synchrotron emission associated with the cluster X-ray emitting regions, and *giant radio relics*, elongated and often highly polarized synchrotron sources typically seen in the clusters’ peripheral regions with linear extents sometimes exceeding  $\sim$  Mpc.<sup>37,38</sup> The locations, polarisation and morphological properties of radio relics suggest a connection with large scale shocks that cross the ICM during mergers and that may accelerate locally injected electrons or re-accelerate pre-existing energetic

electrons to energies where they emit observable synchrotron emission.<sup>39,40</sup> Electrons responsible for giant radio halo emissions, on the other hand, require virtually cluster-wide generation, as we outline below. There are good reasons to believe that radio halos trace gigantic turbulent regions in the ICM, where relativistic electrons can be re-accelerated through scattering with MHD turbulence and/or injected by way of inelastic collisions between trapped CRp and thermal protons.<sup>25,40,41</sup> As we will discuss in this review, one of the most interesting consequences of the present theoretical scenario for CRe production in clusters is that cluster-scale radio emission should be more common than presently seen, especially at lower radio frequencies. Specifically, we may expect to find many more clusters through radio emission in the frequency range that will be explored in the next few years by the new generation of low frequency radio telescopes, such as LOFAR<sup>a</sup>, MWA<sup>b</sup> and LWA<sup>c</sup>. Another important consequence of current ICM CR models is that, despite a current dearth of detections, clusters should be sources of high energy photons at a level that could be detectable by the next generation of X-ray and  $\gamma$ -ray telescopes. Successful, firm detection of galaxy clusters in the hard X-rays and in  $\gamma$ -rays would lead to a fundamental leap forward in our understanding, as it will provide a unique way to measure the energy content of magnetic fields, as well as CRe and CRp in cosmic large scale structure. Since it seems likely that radio halos and relics are signposts of the dissipation of gravitational energy into non-thermal components and emission, they can also be used as valuable (indirect) probes of the merging rate of clusters at different cosmic epochs.<sup>14,42</sup> In this respect the upcoming radio surveys both at lower and higher radio frequencies, with LOFAR, MWA, and ASKAP<sup>d</sup>, and on longer time-scales with the SKA<sup>e</sup>, have the potential to provide important complementary data for cosmological studies.

Diffuse synchrotron radio emission on smaller scales,  $\sim 100 - 300$  kpc, known as *radio mini-halos*, is also found at the centers of relatively relaxed clusters with cool cores.<sup>37,38</sup> The existence of mini halos indicates that mechanisms other than major cluster-cluster mergers can power non-thermal emission in the ICM. As we will discuss in this review, also in this case, gravity is likely to provide the ultimate energy reservoir to power the non-thermal emission, potentially extracted, for example, from the sloshing of the gas in response to motions of dark matter cores in and near the cluster. However, AGNs that are usually found at the center of these sources and also frequently distributed over larger cluster volumes may be players. In addition, at the present time any relationships between mini and giant halos are still poorly defined.

Starting from this background, the goals of this review are to discuss the most relevant aspects of the origin and physics of CRs and non-thermal emission in galaxy clusters and to elaborate on the present theoretical framework. We will place emphasis on the most important current observational constraints, along with the observational prospects for the near future. In Sect.2 we will discuss the physics of CRs acceleration by different

---

<sup>a</sup><http://www.lofar.org/>

<sup>b</sup><http://www.mwatelescope.org/>

<sup>c</sup><http://www.phys.unm.edu/lwa/>

<sup>d</sup><http://www.atnf.csiro.au/projects/askap/>

<sup>e</sup>[www.skatelescope.org](http://www.skatelescope.org)

sources/mechanisms, whereas in Sect.3 we will discuss the relevant energy losses and the dynamics of CRs in the ICM. In Sect.4 we will discuss the most important observational properties of diffuse radio sources in galaxy clusters, their origin and the main prospects for the near future. Specifically giant radio halos, mini halos and relics are discussed in Sects. 4.2, 4.3, and 4.4, respectively, whereas in Sect. 4.1 we will briefly discuss current observational constraints on the magnetic field in the ICM. In Sect. 5 we will discuss current observational constraints on the high-energy emission from galaxy clusters, the most relevant theoretical aspects and prospects for the near future. Sect. 6 provides our Summary.

## 2. Cosmic ray sources and acceleration

Consensus has been reached in the past decade that shocks produced during the hierarchical formation of the large scale structure in the universe are likely sources of CRs in galaxy clusters,<sup>10,13,43</sup> thus implying a direct connection between the generation of CRs and the formation and evolution of the hosting clusters. Similarly, there is consensus on the fact that turbulence can be induced in the ICM as a result of the same processes of clusters formation and that such turbulence affects the propagation of CRs, while also providing a potentially important mechanism for re-acceleration of CRp and CRe.<sup>14,44-46</sup>

Several additional sources can supply (inject) relativistic particle populations (electrons, hadrons or both) into the ICM. For instance, particles can be accelerated in ordinary galaxies as an outcome of supernovae (SN) and then expelled into the ICM with a CRp luminosity as high as  $\sim 3 \times 10^{42} \text{erg s}^{-1}$ .<sup>16</sup> Alternatively, high velocity outflows from AGNs may plausibly contribute up to  $\sim 10^{45} \text{erg s}^{-1}$  in CRs over periods of  $\sim 10^8$  years.<sup>18</sup>

### 2.1. Galaxies, Starbursts and Active Nuclei

Individual normal galaxies are certainly sources of CRs as a consequent of current and past star formation. Massive clusters of galaxies contain more than a hundred galaxies where SN and pulsars accelerate CRs. The efficiency of CR acceleration at these sites is constrained from complementary observations of Galactic sources. However, the amount of CR energy available to the ICM depends also on the way these CRs are transported from their galactic sources into the ICM.

Voelk et al. 1996<sup>16</sup> pioneered the studies of the role of SN explosions, including starbursts, in cluster galaxies. The number of SNe experienced by a typical cluster since its formation epoch,  $N_{SN}$ , can be estimated from the metal enrichment of the ICM, assuming those metals are released by SNe. This gives a total energy budget in the form of CRp :

$$E_{CR}^{SN} = N_{SN} \eta_{CR}^{SN} E_{SN} \leq \frac{[Fe]_{\odot} X_{cl} M_{cl, gas}}{\delta M_{Fe}} E_{SN} \eta_{CR}^{SN} \quad (1)$$

where  $[Fe]_{\odot} X_{cl} M_{cl, gas}$  is the mass of iron in the ICM ( $[Fe]_{\odot} \sim 4/10^5$  is the iron abundance,  $X_{cl} \sim 0.35$  the typical metallicity measured in galaxy clusters, and  $M_{cl, gas}$  the baryon mass of the cluster),  $\delta M_{Fe}$  is the iron mass available to the ICM from a single SN explosion,  $E_{SN} \sim 10^{51} \text{erg}$  is the SN kinetic energy and  $\eta_{CR}^{SN}$  is the fraction of SN kinetic energy in

the form of CRp;  $\eta_{CR}^{SN} \sim 0.2 - 0.3$  is constrained from observations of SN in the Galaxy. Note that the efficiency for acceleration of CRe in SNRs is apparently several orders of magnitude smaller than for CRp.<sup>47,48</sup> Eq.1 implies a ratio between the CRp and thermal energy budget in galaxy clusters  $E_{CR}^{SN}/E_{gas} \sim 10^{-3}$ , assuming  $\delta M_{Fe} \sim 0.1 M_{\odot}$  (appropriate for type II SN) and  $T_{gas} \sim 10^8$  K. This is an optimistic estimate of the expected energy content of CRp in galaxy clusters from this source, because it does not account for adiabatic losses in the likely event that CRp from SN are transported into the ICM by SN-driven galactic winds.

On the other hand, clusters of galaxies contain AGNs, which, by way of their synchrotron-emitting jets and radio lobes, are known to carry CRe.<sup>49</sup> The majority of cool-core clusters contain central, dominant galaxies that are radio loud.<sup>50-52</sup> The radio lobes of these AGNs are seen frequently to coincide with X-ray dark volumes (“cavities”) that have turned out to be the best calorimeters of the total energy deposited by AGN outflows. The cavities, being filled with relativistic and some amount of very hot thermal plasma at substantially lower density than their surroundings, are poor thermal X-ray emitters. Such cavities have been seen in something like 1/4 of the clusters observed by Chandra,<sup>53</sup> despite the fact that they often exhibit low contrast. From an assumption of pressure balance between the cavity and the surrounding ICM the cavity energy contents have been estimated generally in the range  $\sim 10^{55} - 10^{61}$  erg.<sup>53,54</sup> These approach  $\sim 1\% E_{gas}$  for an entire ICM in some cases. Dynamical estimates of cavity lifetimes are typically  $\sim 10^7 - 10^8$  yr, roughly representing buoyancy timescales. These lead to AGN power deposition estimates within an order of magnitude of the X-ray cooling rate of the host cluster,<sup>55</sup> at least while the AGN jets are active. The bubble forming duty cycles, estimated from the fraction of cool-core clusters that harbor clear bubbles, range as high as 70%.<sup>56</sup> Simulations suggest that roughly 1/2 of the power of the AGN outflow is immediately deposited irreversibly as ICM heat through shocks and entrainment.<sup>57</sup> These may also drive ICM turbulence that would contribute to CR acceleration and to the dynamics of CRs (Sects. 2.2.2, 3.2). Given their large energy inputs, AGN outflows are widely invoked to account for heating needed to limit the effects of strong radiative cooling in cluster cores, e.g.<sup>53,54,58</sup> So, the total energy deposition into the ICM by AGNs is likely to be substantial.

However, the energy in CRe and CRp is harder to establish in radio lobes of cluster radio galaxies. In a few cases the absence of observed inverse Compton X-rays has been used to establish that most of the energy filling the radio lobes must be in some form other than radiating electrons,<sup>59</sup> although CRe energy fractions as high as 10% are not ruled out. Meaningful CRp energy content estimates in the lobes do not exist at present, although recent detailed comparisons of internal-lobe and external pressure suggest that models in which CRp transported by the jet dominate lobe energetics are unlikely.<sup>60</sup> Remarkably, various theoretical arguments have been made suggesting that much of the direct energy flux in AGN jets is carried by cold, non-radiating particles or electromagnetic fields.<sup>61</sup> Even if much of the energy filling the cavities is carried by CRs, it is not yet clear how efficiently those CRs can be dispersed through diffusion and convective/turbulent mixing over the full cluster volume, and how much of the energy would remain in CRs, after

accounting for adiabatic and other energy losses. Large scale magnetic fields, for instance, can help confine lobe contents.<sup>62–64</sup> A connected problem that will be discussed in Sect.4.3 is the possible role of relativistic outflows from the central AGNs in the origin of radio mini halos in cool core clusters.

While most discussions of AGN energy deposition in clusters have focused on central, dominant galaxies, there are other populations of AGNs in clusters that could contribute to the CR population, either directly or indirectly. Low luminosity AGNs are quite commonly distributed throughout clusters. Stocke et al.<sup>65</sup> have argued, in fact, that virtually all bright red sequence galaxies in rich clusters are likely to be low-luminosity blazars with relativistic jets that could collectively dominate AGN energy inputs to the ICM. In that case their CR outputs would be more easily distributed across the cluster by way of ICM turbulence and large scale “weather” (e.g., sloshing). In addition, tailed radio galaxies, quite common and widely distributed in both relaxed and merging clusters, show clear evidence of strong interactions with the ICM that includes entrainment and the generation of turbulence.<sup>66,67</sup>

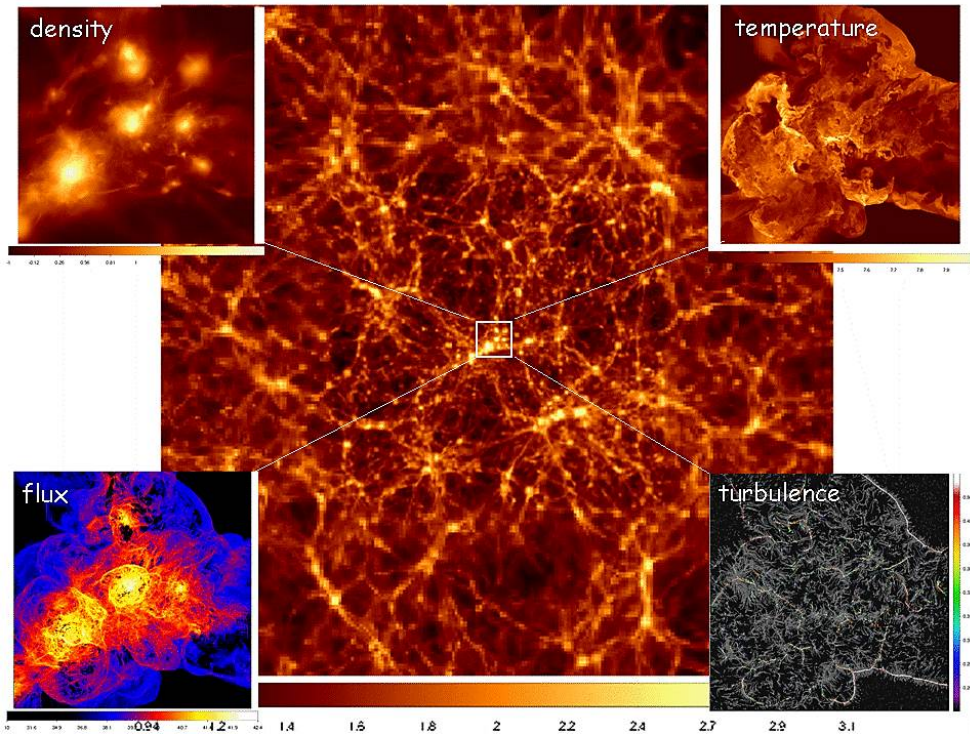


Fig. 2. Projection of matter density for a volume of size 187 Mpc/h simulated with ENZO AMR (velocity and density refinement technique) with peak spatial resolution 25 kpc/h. The two panels on the left are  $8 \times 8 \times 2$  Mpc/h zooms of the central region showing the projected density (top-left) and the kinetic energy-flux (bottom-left). The two panels on the right are  $8 \times 8 \times 0.025$  Mpc/h zooms of the same region showing the temperature distribution (top-right) and the overlay of shock map and turbulent velocity-vectors (obtained with a filtering of laminar motions on 300 kpc scale). Images are obtained at  $z = 0.6$  from simulations presented in.<sup>79</sup>



## 2.2. Particle acceleration in the ICM

The current prevailing view is that the process of structure formation may contribute directly and indirectly most of the energetics of non-thermal components (CRs, magnetic fields and turbulence) in galaxy clusters.<sup>8, 11, 13, 14, 23, 25, 39, 44, 45, 68–76</sup> Mergers between two or more clusters are observed to heat clusters through shocks.<sup>77, 78</sup> Although more difficult to constrain observationally, the additional process of semi-continuous accretion of material onto clusters, especially from colder filaments, is expected to drive quasi-stationary, strong shocks and turbulent flows at Mpc distances from cluster centers that should impact on the ICM physics and acceleration of CRs over wide volumes.

Particle acceleration during mergers should occur at shock waves that are driven to cross the ICM. Particle acceleration is also expected to result from several mechanisms that may operate within turbulent regions also driven in the ICM during these mergers (e.g., turbulent acceleration and magnetic reconnection, etc).<sup>20</sup> The intricate pattern of shocks and large-scale turbulent motions and their interplay is still difficult to establish observationally, but can be traced in some detail by cosmological simulations of galaxy cluster formation. Fig.2 provides a view of the complex dynamics of the ICM as seen in simulations. In particular, a complex pattern of strong and weak shocks is naturally driven in the ICM, largely by gravity variations reflecting dark matter dynamics (Sect. 2.2.1). This shock distribution, where most of the kinetic energy flux is dissipated within clusters, is morphologically correlated to some extent with the distribution of the turbulent motions in the ICM, that are, indeed, partly driven by those shocks (Sect. 2.2.2). In the following we will focus on the physics of shocks and particle acceleration at shocks (Sect. 2.2.1), and on the physics of turbulence and turbulent acceleration in galaxy clusters (Sect. 2.2.2).

### 2.2.1. Shocks in galaxy clusters as CRs accelerators

The total gravitational energy dissipated by baryonic matter in a merger of two clusters with roughly equal mass,  $M = 10^{15} M_{\odot}$ , is  $E \approx 10^{64}$  erg. With the assumption that the gaseous components of the initial clusters are at the associated virial temperatures, it is easy to show that the merging components approach each other at slightly supersonic relative speed, therefore implying the formation of weak,  $M \sim 2$ , shock waves.<sup>11, 70, 80</sup> Those shocks will typically strengthen moderately as they emerge into lower density and low temperature regions outside the cluster cores. Additional, remote, accretion shocks that result from the continuous accretion of matter at several Mpc-distances from clusters center (also called “external shocks” when they form due to the accretion of never-shocked gas), are typically much stronger; that is, they have higher Mach numbers, since they develop in cold, un-virialised external cluster regions. On the other hand, since gas densities are also quite low in those environments, the energy available for dissipation through such shocks is relatively smaller than through lower Mach number shocks that dissipate energy in higher density regions closer to cluster centers during mergers. Simple (analytical or semi-analytical) but accurate estimates of the amount of kinetic energy associated with accretion/external shocks are very challenging. A leap forward in understanding in this area, however, has been achieved in the last decade through extensive cosmological simulations



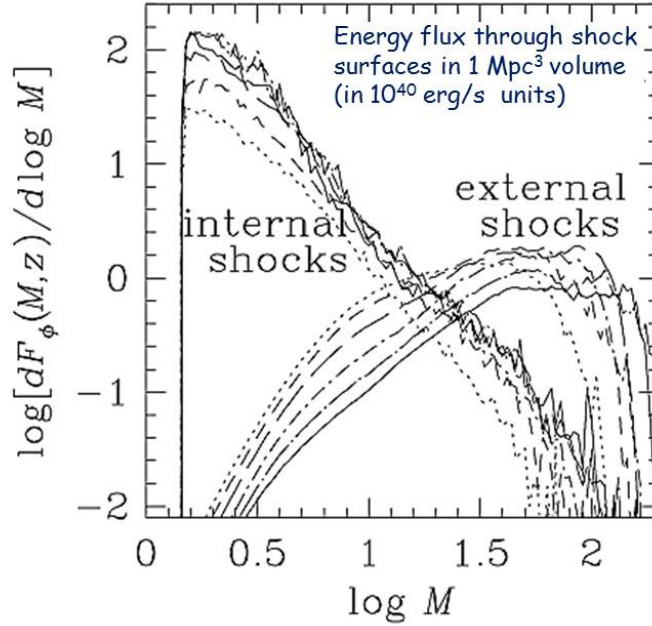


Fig. 3. Distribution of the energy flux at shocks surfaces as a function of the shock-Mach number from numerical (cosmological) simulations (adapted from<sup>13</sup>). Units are in  $10^{40}$  erg/s  $(1+z)^3 h^3 \text{Mpc}^{-3}$ . Shocks are divided into internal and external categories. External shocks are defined as shocks forming when never-shocked, low-density, gas accreted onto nonlinear structures, such as filaments etc. Internal shocks form within the regions bounded by external shocks.

that allow one to study the formation of shocks in clusters, from their outskirts to more internal regions with increasing detail.<sup>13,71–73,79,81,82</sup>

Figure 3 illustrates these points. It shows the kinetic energy flux through shock surfaces, that is,  $1/2\rho V_{sh}^3 S$ , measured in clusters formed during cosmological simulations. Here,  $\rho$  is the upstream gas density, while  $V_{sh}$  and  $S$  are shock velocity and surface area, respectively. The distribution of energy fluxes shows that most of the gravitational energy is dissipated at relatively weak, “internal” (merger) shocks, with Mach number  $M \sim 2 - 3$ . A modest fraction of the kinetic energy-flux passes through related stronger internal-shocks developed during merger activity as they propagate outwards after merging cores have their closest approach. Figure 3 shows that only a few % of the energy flux is dissipated at strong, “external” shocks.

If even a small percentage of the merger and accretion shock-dissipated energy can be converted into non-thermal particles through a first order Fermi process, then the ICM could be populated with an energetically significant population of non-thermal, CR particles.<sup>13,25,74,81,83,84</sup> This prospect has drawn considerable focus to potential consequences

of shock generated CRs and the refinement of early estimates of CR production in ICMs.

### 2.2.1.1. Shock acceleration of CRs

The acceleration of CRs at shocks is customarily described according to the diffusive shock acceleration (DSA) theory.<sup>85–88</sup> In effect diffusing particles are temporarily trapped in a converging flow across the shock if their scattering lengths across the shock are finite but much greater than the shock thickness. Particles escape eventually by convection downstream. Until they do, they gain energy each time they are reflected upstream across the shock, with a rate determined by the velocity change they encounter across the shock discontinuity and a competition between convection and diffusion on both sides of the shock. The hardness (flatness) of the resulting spectrum reflects the balance between energy gain and escape rates. In other words, it depends on the energy gain in each shock crossing combined with the probability that particles remain trapped long enough to reach high energies. Mathematically this balance can be conveniently described through the diffusion-convection equation for a pitch angle averaged CRs distribution function  $f(p, t)$  in a compressible flow<sup>f</sup> that is:<sup>87</sup>

$$\frac{\partial f}{\partial t} + (\mathbf{V} \cdot \nabla)f - \nabla \cdot \{ \mathbf{n} D (\mathbf{n} \cdot \nabla) f \} = \frac{1}{3} (\nabla \cdot \mathbf{V}) p \frac{\partial f}{\partial p} \quad (2)$$

where  $p$  is the modulus of the particle's momentum,  $\mathbf{V}$  is the velocity of the background medium (assuming  $c \gg V \gg V_A$ , with  $V_A$  the Alfvén velocity), while  $\mathbf{n}$  is the unit vector parallel to the local magnetic field, and  $D$  is the particle spatial diffusion coefficient (see Sect. 2.2.2). The 2nd and 3rd terms account for convection and diffusion, respectively, while the right hand side takes account of the adiabatic energy gains (losses) suffered by particles in a converging (expanding) flow. As written, Eq.2 omits non adiabatic losses, such as from radiation, that can be important especially for CRE (CRs energy losses are discussed in Sect. 3.1), momentum diffusion and effects such as CR energy transfer to wave amplification/dissipation (turbulent-CRs coupling is discussed in Sect. 2.2.2).

Under these conditions, if all particles are injected at low energies and “see” the same velocity change across the shock, the steady state spectrum of test-particle CRs at a plane shock is a power law in momentum,  $f(p) = K p^{-(\delta_{inj}+2)}$ , where the slope is

$$\delta_{inj} = 2 \frac{M^2 + 1}{M^2 - 1}. \quad (3)$$

$M = V_{sh}/c_s$  is the Mach number of the shock. For strong shocks,  $M \rightarrow \infty$ , this slope tends to  $\delta_{inj} \rightarrow 2$ . Thus, in the strong shock limit, the energy and pressure in the resulting CRs are broadly distributed towards the highest energies that are achieved. On the other hand, for weak shocks,  $M^2 \approx 1 + \varepsilon$  with  $\varepsilon \ll 1$ , this tends to  $\delta_{inj} \approx 2 + 4/\varepsilon \gg 2$ . In this case the fractional velocity jump across the shock is small, so the energy in CRs accelerated

<sup>f</sup>  $f$  is the number of CRs per unit phase-space volume,  $d^3 p dV$

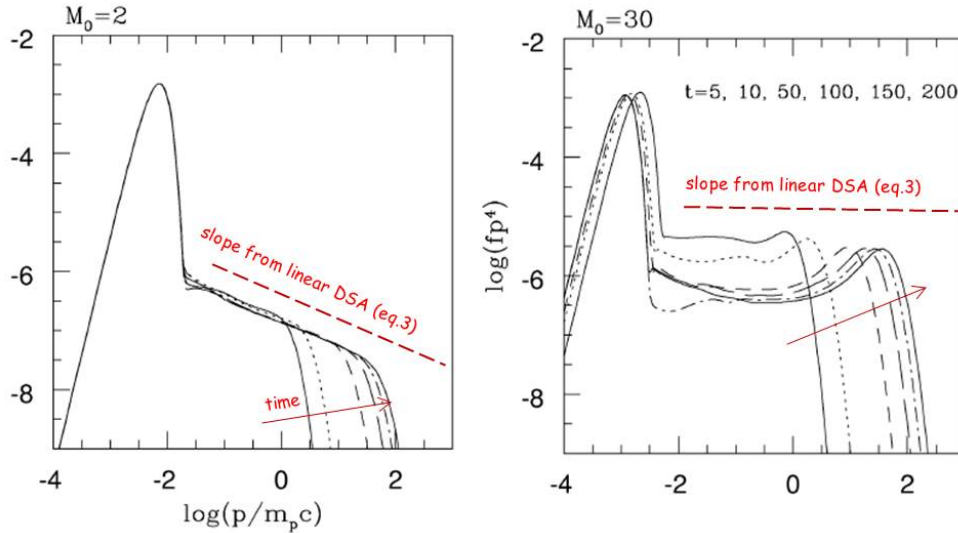


Fig. 4. Time evolution of the spectrum of protons accelerated from a Maxwellian upstream distribution at shocks with Mach number 2 (left) and 30 (right) (adapted from<sup>95</sup>). The spectral slope predicted by (test-particle) DSA is represented as a red-dashed line.

from suprathermal values is concentrated in the lowest energy CRs. That is, the CRs gain relatively little energy before they escape downstream. Consequently, for the same number of CRs and the same kinetic energy flux through the shock,  $\sim \rho V_{sh}^3$ , the energy input to locally injected CRs through DSA is much greater in strong shocks than in weak shocks.

As a consequence of this theory, it is apparent that even a modest injection of particles at a strong shock can lead to a substantial fraction of the kinetic energy flux into strong, initially purely hydrodynamical shocks going into CRs. Those, in turn backreact on and modify the structure of the shocks themselves. Under these conditions the process of particle acceleration is described using nonlinear theory.<sup>86,88–92</sup> The main outcome of that development is the formation of a compressive precursor to the shock, leading to an increase in the total shock compression, upstream turbulence and magnetic field amplification, followed by an actual weakening of the fluid shock transition (the so-called ‘sub-shock’). In a highly CR-modified shock a large part of the DSA process at high CR energies actually takes place in the precursor when the spatial diffusion coefficient,  $D$  is an increasing function of particles momentum. Then, the subshock is responsible mostly for the acceleration process at low energies<sup>93</sup> and injection of seed DSA particles.

The importance and detailed outcomes of nonlinear evolution in *strong* shocks depend on

the size of the CR population at the shock, the hardness of the CR spectrum being accelerated at the shock, the efficiency and distribution of turbulent magnetic field amplification upstream of the shock and the geometry of the shock.<sup>94</sup> These physical details are important, since they regulate how much energy is extracted from the flow into the shock and, accordingly how much pressure will develop from these CRs and amplified magnetic field within the shock transition. On the other hand, unless they include much larger total CR populations or interact with a pre-existing CR population with a hard spectrum, *weak shocks* are minimally affected by nonlinear effects, because of the steeper CR spectra generated in these shocks. Fig.4 shows the time evolution of CRp spectra accelerated at simulated weak and stronger shocks. In the case of weak shocks the spectrum agrees with the prediction of test particle DSA theory, while the spectrum becomes concave and flatter than test particle DSA for stronger shocks, due to the non-linear back-reaction of CRp. The quality of comparisons between real and theoretical strong, DSA-modified shocks is still an open question (see the discussion at the end of this section).

The acceleration time-scale at the shock (i.e. the time necessary for CRs of energy  $E$  to double that energy) depends on the time interval between shock crossings for the CR,  $\sim 4D/(V_p V_{sh})$ ,  $V_p$  is the particle velocity, and on the ratio of the CR velocity to the fluid velocity change across the shock, so  $\sim V_p/\Delta V_{sh}$ . Thus, it primarily depends on the spatial diffusion coefficient of particles, and inversely on the shock velocity,  $V_{sh}$ , and the compression through the shock. In the simplified case that the spatial diffusion coefficient does not change across the shock, the mean acceleration time to a given momentum in an unmodified shock can be written as :

$$\tau_{acc}(p) \simeq \frac{4D(p)}{(c_s M)^2} \frac{M^2(5M^2 + 3)}{(M^2 + 3)(M^2 - 1)} \quad (4)$$

that approaches  $\tau_{acc} \approx 20D/(c_s M)^2$  for strong shocks.

In order to derive a maximum energy of the accelerated CRs in a given time interval we assume a Bohm diffusion coefficient,  $D(p) = (1/3)r_L(p)c$ , (see also Sect 2.2.2) where,  $r_L(p)$ , is the particle Larmor radius. This is optimistically small, thus giving us an optimistic upper energy bound, since it assumes a mean free path equal to the CR gyroradius. The spatial diffusion coefficient for relativistic particles then becomes in practical terms,

$$D(p) \sim 3 \times 10^{22} \frac{(cp/\text{GeV})}{(B/\mu\text{G})} \text{ cm}^2 \text{ s}^{-1}, \quad (5)$$

resulting in an acceleration time scale to GeV energies of the order of 1 yr, if we assume a typical shock velocity in galaxy clusters,  $V_{sh} = c_s M \sim \text{few } 10^3 \text{ km/s}$ , and  $B \sim 1 \mu\text{G}$ . Then, from eqs.4-5,  $p_{max} \sim (\tau/\text{yrs}) \text{ GeV}$ , implying for realistic available acceleration times ( $\gg$  years) that the power law distribution of the accelerated particles should extend up to very high energies, where energy losses or diffusion from the acceleration region quenches the acceleration process (spatial diffusion in the ICM is discussed in Sect. 3.2).

The energy losses for CRe, due especially to synchrotron and inverse Compton processes (see Sect. 3), are much more significant than those for CRp. For CRe the maximum energy

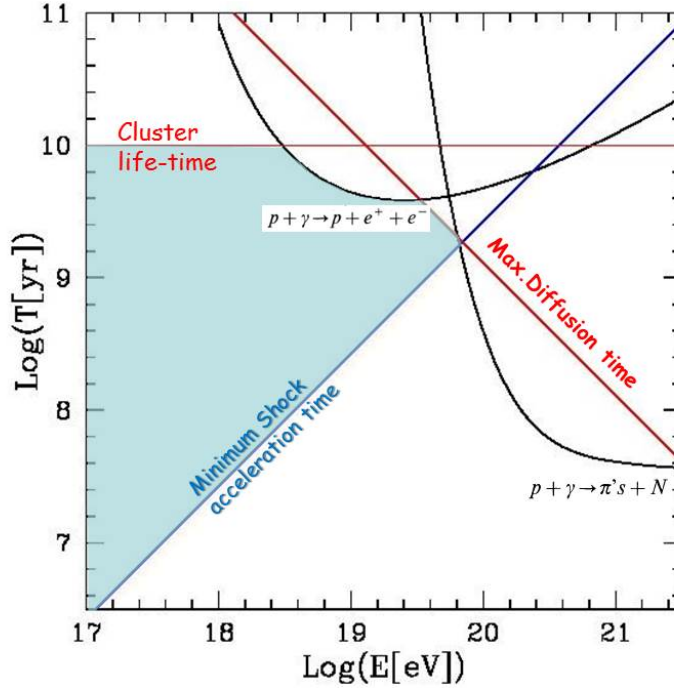


Fig. 5. The life-time of CRp in the ICM as a function of energy due to photo-pion and photo-pair production (solid curves) are compared to a reference life-time of clusters  $\sim 10$  Gyrs, to the maximum diffusion time-scale of CRp (assuming Bohm-diffusion on 3 Mpc scales and using an optimistic value  $B = 5\mu\text{G}$ ) and to the minimum acceleration time-scale of CRp by shocks (assuming an optimistic configuration with Bohm-diffusion with  $B = 5\mu\text{G}$ , and a shock velocity = 4000 km/s). The allowed region, marking the energies of CRp that can be obtained via shock acceleration, is highlighted in blue.

accelerated at shocks in galaxy clusters can be of the order of several tens of TeV.<sup>96,97</sup> Once these CRe are advected downstream of the shock, radiative cooling due to inverse Compton scattering (ICS) with the CMB (and if the magnetic fields are strong enough, synchrotron, Sect. 3) will steadily reduce the maximum electron energy, so that it scales asymptotically as  $\gamma_{e,max} \propto 1/x$ , where  $x = V_d t$  is the propagation distance downstream from the shock reached over a time,  $t$ . This causes the “volume integrated” electron spectrum to steepen by one in the power law index,  $\delta = \delta_{inj} + 1$  above energies reflecting this loss over the lifetime of the accelerating shock.<sup>98,99</sup> Consequently, the “spatially unresolved” synchrotron spectrum “from the downstream region” will show a steepened spectral slope,  $\alpha = (\delta - 1)/2 = \alpha_{inj} + 1/2$ .

By contrast, CRp in these shocks are not subjected to significant energy losses until they reach extremely high energies where they suffer inelastic collisions with CMB photons. CRp with energies above a few hundred PeV will produce  $e^\pm$  when they collide with CMB photons, limiting their life-times to a period below a few Gyr<sup>100</sup> (Figure 5). Most impor-

tant, at energies above about  $5 \times 10^{19}$  eV, such collisions produce pions, and each such collision extracts a significant fraction of the CRp energy (this is the same physics that determines the so-called Greisen-Zatsepin-Kuzmin (GZK) cutoff in the ultra-high energy CR spectrum). For example, for energies above  $\sim 10^{20}$  eV the CRp life-time drops rapidly below  $\sim 10^8$  yr (Fig. 5). In Figure 5 we compare these relevant time-scales with the shock-acceleration time-scale (eqs. 4-5) and with the life-time of shocks and clusters themselves. It follows that CRp acceleration at cluster shocks can reach at most maximum energies of a few  $10^{19}$  eV.<sup>43,96</sup> We note that this is an *optimistic* estimate, as we are implicitly assuming that such high-energy CRp are still effectively confined in galaxy clusters<sup>§</sup> (CRs diffusion/confinement is discussed in Sect. 3.2).

#### 2.2.1.2. Shock acceleration in the ICM & open questions

Particle acceleration efficiency at strong shocks is becoming constrained by studies of SN-driven shocks in our Galaxy.<sup>47,48</sup> Those shocks transfer  $\sim 10\%$  or more of the energy flux through them into CRp. It is important to keep in mind that the shocks mostly responsible for acceleration of observable Galactic CRs are very strong, with Mach numbers upwards of  $10^3$ , and that they are found in low beta-plasma,  $\beta_{pl} = P_{gas}/P_B$ , environments. By contrast, and as discussed above, the ICM is a high- $\beta_{pl}$  environment and most of the kinetic energy flux penetrating galaxy cluster shocks is associated with much weaker shocks where, the acceleration efficiency is probably much less, although still poorly understood.<sup>92,101,102</sup> In this respect galaxy clusters are special environments, as they are unique laboratories for constraining the physics of particle acceleration at (Mpc-scale) weak shocks. It remains an open issue whether these weak shocks can accelerate CRs in the ICM at meaningful levels.

A critical, unresolved ingredient in shock acceleration theory is the minimum momentum of the seed particles that can be accelerated by DSA; i.e., the minimum momentum that leads to diffusive particle transport across the shock. This, along with the detailed processes that control this minimum momentum are crucial in determining the efficiency with which thermal particles are injected into the population of CRe and CRp. Particles must have momenta at least several times the characteristic postshock thermal ion momenta in order to be able to successfully recross into the preshock space. Quasi-thermalized particles are inherently less likely to recross in the upstream direction in weak shocks than strong shocks, because of the weaker dissipation in weak shocks; i.e., the ratio of the postshock thermal speed to the postshock convection speed is relatively smaller. Injection is expected to depend sensitively on the charge/mass ratio of the injected species, since that determines the rigidity ( $\propto p/q$ ) of particles at a given energy. For this reason, nonrelativistic electrons appear to be very difficult to inject from the thermal population (because  $p = \sqrt{2mE}$ ), so are likely to be far fewer than injected protons. Typically some kind of upstream, pre-injection process, often involving protons reflected by the shock that gener-

<sup>§</sup>e.g., confinement of CRp with energies  $10^{19} - 10^{20}$  eV for a Hubble time would require conditions comparable to Bohm diffusion at distances of several 100 kpc from the shock

ate upstream waves that can resonate with nonrelativistic electrons, is invoked to enable electron injection at shocks.<sup>103–106</sup> The processes “selecting” the particles that can recross define so-called *thermal-leakage injection*. It is important to realize that they are poorly understood, especially in the relatively weak shocks with large  $\beta_{pl}$  expected in cluster media. Existing collisionless shock simulations, hybrid and PIC simulations, have focused on strong shocks or low beta-plasma.<sup>106–108</sup> The orientation of the magnetic field with respect to the shock normal is also important, since it strongly influences the physics of the shock structure.<sup>106, 109</sup>

A connected, unresolved ingredient in nonlinear CR shock theory is the level of amplification of the magnetic field and its distribution within the shock due to CR-driven instabilities. The evolution of the magnetic field through the full shock structure is important, since the magnetic field self-regulates the diffusion process of supra-thermal particles on both sides of the shock and also affects the injection process.<sup>91, 110</sup> There are several proposed models to amplify magnetic fields significantly within the CR-induced shock precursor;<sup>111–113</sup> none of them applies until some degree of shock modification already takes place. This means they only apply in strong shocks, so probably not in cluster merger shocks. Some magnetic field generation and/or amplification downstream of curved or intersecting shocks may result when the electron density and pressure gradients are not parallel (the so-called Biermann Battery effect<sup>114</sup>), due to the Weibel filamentation instability<sup>115, 116</sup> or when the downstream total plasma and pressure gradients are not parallel (so-called baroclinic effects that amplify vorticity<sup>8, 117</sup>). Amplification of turbulence and magnetic fields only downstream, however, have minimal impact on DSA, which depends essentially on those properties on both sides of the shock.

As a final remark we mention that there is still discussion on the spectrum of CRs resulting from shock acceleration. Although calculations in the last decade agreed on the conclusion that the spectra of CRs accelerated at strong shocks are concave (flat) as a result of the dynamical back-reaction of CRs (Figure 4), current data for SNRs seem to favour steeper spectra and suggest a partial revision of the theory.<sup>118</sup> Specifically, the absence of CR spectral concavity in modified shocks requires a relative reduction in acceleration efficiency or increased escape probability for the highest energy CRs.<sup>94</sup>

### 2.2.2. Turbulence in the ICM and CR reacceleration

Galaxy clusters contain many potential sources of turbulence. These include cluster galaxy motions,<sup>119, 120</sup> the interplay between ICM and the outflowing relativistic plasma in jets and lobes of AGNs,<sup>121, 122</sup> and buoyancy instabilities such as the magnetothermal instability (MTI) in the cluster outskirts.<sup>123</sup> However, the most important potential source of turbulent motions on large scales is the process that leads directly to the formation of galaxy clusters.<sup>14, 75, 124, 125</sup> Mergers between clusters deeply stir and rearrange the cluster structure. In this case turbulence is expected from core sloshings, shearing instabilities, and especially from the complex patterns of interacting shocks that form during mergers and structure formation more generally<sup>79, 126–137</sup> (Figure 2). Such a complex ensemble of mechanisms should drive in the ICM both compressive and incompressive turbulence, as also supported



by the analysis of numerical simulations;<sup>137,138</sup> in Figure 6 we report a sketch of the turbulent properties of the ICM.

Large scale turbulent motions that are driven during cluster-cluster mergers and dark matter sub-halo motions are expected on scales comparable to cluster cores scales,  $L_o \sim 100 - 400$  kpc, and might have typical velocities around  $V_o \sim 300 - 700$  km/s, e.g.<sup>125</sup> These motions are sub-sonic, typically with  $M_s = V_o/c_s \approx 0.2 - 0.5$ , but they are strongly super-Alfvénic, with  $M_A = V_o/V_A \approx 5 - 10$ , e.g.<sup>45</sup> This implies a situation in which magnetic field lines in the ICM are continuously advected/stretched/tangled on scales larger than the Alfvén scale; that is, the scale where the velocity of turbulent eddies equals the Alfvén speed,  $l_A \sim L_o(V_o/V_A)^{\frac{2}{a-1}}$  ( $a$  is the slope of the turbulent velocity power-spectrum,  $W(k) \propto k^{-a}$ ). Below this scale, turbulent, “Reynolds stresses” are insufficient to bend field lines and turbulence becomes MHD (Fig. 6). Under these conditions the effective particle mean-free-path in the ICM should be  $l_{mfp} \sim l_A$  rather than the value of the classical Coulomb ion-ion mean free path,  $l_C \sim 10 - 100$  kpc<sup>45,139</sup> (Fig. 6)<sup>h</sup>.

However the ICM is a “weakly collisional” plasma and can be very different from collisional counterparts, because it is subject to various plasma instabilities, e.g.<sup>140,141</sup> In many cases, as a result of plasma instabilities the (relatively weak) magnetic field is perturbed on very small scales. That provides the potential to strongly reduce the effective thermal particle (and CRs) mean free path<sup>142-145</sup> and also the effective viscosity of the fluid, below the classical Braginskii viscosity determined by thermal ion-ion Coulomb collisions.

All these considerations about the velocities of large-scale motions and the effective particle mean-free-path in the ICM allow us to conclude that the effective Reynolds number in the inner ICM is  $Re \gg 10^3$ ; that is, much larger than it would be if it were determined by the classical ion-ion mean free path ( $Re \sim 100$ ). Theoretically this suggests that a cascade of turbulence and a turbulent inertial range could be established from large to smaller scales (Fig. 6). In addition plasma/kinetic instabilities in the ICM generate waves at small, resonant, scales (Fig. 6). Among the many types of waves that can be excited in the ICM we mention the slab/Alfvén modes that may be excited for example via streaming instability<sup>146</sup> and gyro-kinetic instability,<sup>145</sup> and the whistlers that may be excited for example via heat-flux driven instabilities.<sup>143,147</sup> Also coherent wave phenomena in MHD turbulence can generate non-linear electrostatic waves; for example lower hybrid electrostatic waves in the ICM might be excited through the non-linear modulation of density in large amplitude Alfvén wave-packets.<sup>148</sup> Both large-scale motions (and their cascading at smaller scales) and the component of self-excited turbulent waves at small scales have a strong role in governing the micro-physics of the ICM through the scattering of particles and the perturbation of the magnetic field.

Current X-ray observations do not allow one to derive stringent constraints on the turbulent motions in dynamically active (i.e. merging or non cool core) clusters<sup>149,150</sup> (see however the pioneering attempt by<sup>151</sup>) (constraints on cool core clusters are discussed in Sect. 4.3).

<sup>h</sup>the effective mfp should be the smaller of the two scales, however under typical ICM conditions  $l_A < l_C$ , see<sup>45</sup>

This will hopefully change in the next years thanks to the ASTRO-H satellite<sup>i</sup> that will allow measurement of ICM turbulence through the Doppler broadening and shifting of metal lines induced by turbulent motions and the effect of turbulence on resonant lines properties.<sup>127,136,152–156</sup>

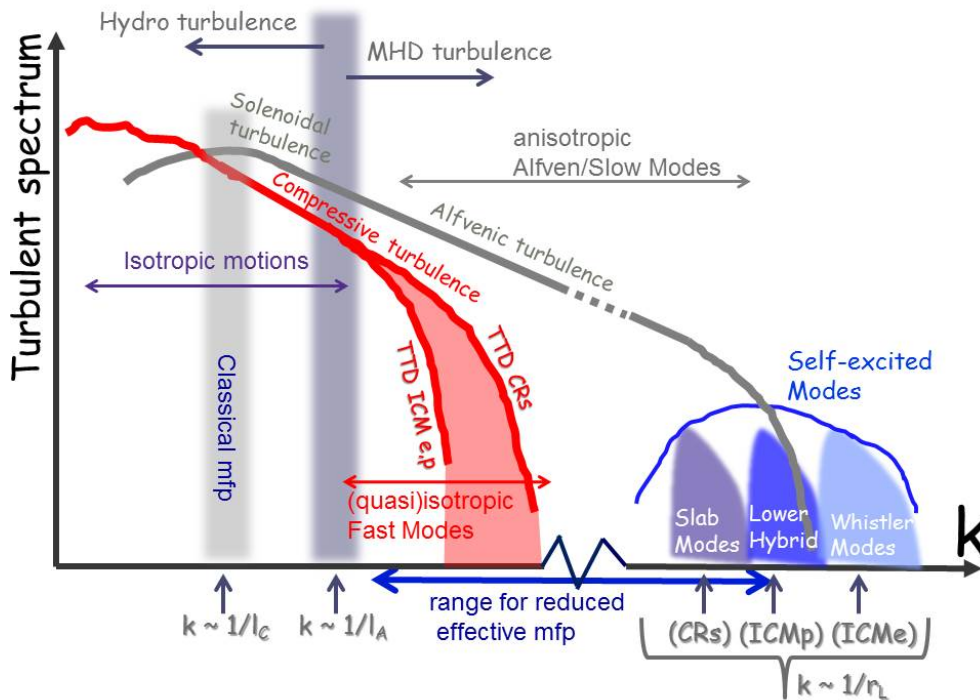


Fig. 6. A schematic view of turbulence in the ICM. The transition from hydro- to MHD turbulence is marked (see text). The expected spectral features of both solenoidal and compressive turbulence generated at large scales are illustrated: solenoidal turbulence develops an Alfvénic cascade at small (micro-) scales whereas the compressible part (fast modes in the MHD regime) is presumably dissipated via TTD resonance with electrons and protons in the ICM (or eventually via TTD resonance with CRs in case of reduced effective mean free path, see text). A schematic illustration of relevant examples of “self-excited” modes, excited via CRs- or turbulent-induced instabilities, is also shown together with the relevant scales: slab modes, lower hybrid electrostatic waves, and whistler waves (see text). A schematic illustration of the scales of the Alfvén scale,  $l_A$ , classical mean-free-path due to Coulomb ion-ion collisions,  $l_C$ , and reduced particles mean-free-path is also given.

### 2.2.2.1 Turbulent Acceleration

Turbulence in the ICM can potentially trigger several mechanisms of particle acceleration. The non-linear interplay between particles and turbulent waves/modes is a stochastic

<sup>i</sup><http://astro-h.isas.jaxa.jp/en/>

process that drains energy from plasma turbulence to particles.<sup>157, 158</sup> In addition, reconnection of magnetic fields may be faster in turbulent regions than in stationary media or laminar flows,<sup>159</sup> potentially providing an additional source of particle acceleration in the ICM.<sup>20</sup> In this Section we will focus on stochastic re-acceleration of CRs due to resonant interaction with turbulence, in particular with low-frequency waves, because this turbulent-acceleration mechanism has the best developed theory and is the most commonly adopted in the current literature. Acceleration of CRs directly from the thermal pool to relativistic energies by MHD turbulence in the ICM is very inefficient and faces serious problems due to associated energy arguments.<sup>160, 161</sup> Consequently, turbulent acceleration in the ICM is rather a matter of re-acceleration of pre-existing (seed) CRs rather than *ab initio* acceleration of CRs, e.g.<sup>162, 163</sup>

The (re)acceleration of CRs by turbulence is customarily described according to the quasi-linear-theory (QLT), where the effect of linear waves on particles is studied by calculating first-order corrections to the particle orbit in the uniform/background magnetic field  $\mathbf{B}_0$ , and then ensemble-averaging over the statistical properties of the turbulent modes.<sup>164–166</sup> In QLT one works in the coordinate system in which the space coordinates are measured in the Lab system and the particle momentum coordinates are measured in the rest frame of the background plasma that supports the turbulence and in which turbulence is homogeneous. Then the gyrophase-averaged particle density distribution,  $f(x, p, \mu, t)$ ,  $\mu$  is the cosine of the particle pitch angle, evolves in response to electromagnetic turbulence according to the Fokker-Planck equation:<sup>158</sup>

$$\frac{df}{dt} = \frac{\partial}{\partial \mu} \left[ \left( D_{\mu\mu} \frac{\partial}{\partial \mu} + D_{\mu p} \frac{\partial}{\partial p} \right) f(p, \mu, t) \right] + \frac{1}{p^2} \frac{\partial}{\partial p} \left[ p^2 \times \left( D_{\mu p} \frac{\partial}{\partial \mu} + D_{pp} \frac{\partial}{\partial p} \right) f(p, \mu, t) \right] \quad (6)$$

where  $D_{pp}$ ,  $D_{\mu\mu}$  and  $D_{p\mu}$  are the fundamental transport coefficients describing the stochastic turbulence–particle interactions. These are determined by the electromagnetic fluctuations in the turbulent field.

Much attention has been devoted to the interaction with the low-frequency Alfvén and magnetosonic MHD waves<sup>j</sup>. For these waves the relevant Fokker-Planck coefficients are given by:<sup>165, 168</sup>

<sup>j</sup>Following<sup>167</sup> here we define low frequency waves as those having frequency  $\omega \ll \Omega_i/\beta_{pi}$ , where  $\Omega_i$  is the Larmor frequency of nonrelativistic ions

$$\begin{aligned}
 \begin{pmatrix} D_{\mu\mu} \\ D_{pp} \end{pmatrix} &= \frac{\Omega^2(1-\mu^2)}{2B_0^2} \mathcal{R}e \sum_{n=-\infty}^{n=\infty} \int_{\mathbf{k}_{\min}}^{\mathbf{k}_{\max}} d^3k \begin{pmatrix} \left(1 - \frac{\mu\omega}{vk_{\parallel}}\right)^2 \\ \left(\frac{pc}{v}\right)^2 \end{pmatrix} \int_0^{\infty} dt e^{-i(k_{\parallel}v_{\parallel} - \omega + n\Omega)t} \\
 &\left\{ J_{n+1}^2(x) \begin{pmatrix} P_{RR}^{\mathbf{k}} \\ R_{RR}^{\mathbf{k}} \end{pmatrix} + J_{n-1}^2(x) \begin{pmatrix} P_{LL}^{\mathbf{k}} \\ R_{LL}^{\mathbf{k}} \end{pmatrix} + J_{n+1}(x)J_{n-1}(x) \left[ e^{2i\Psi} \begin{pmatrix} -P_{RL}^{\mathbf{k}} \\ R_{RL}^{\mathbf{k}} \end{pmatrix} \right. \right. \\
 &\left. \left. + e^{-2i\Psi} \begin{pmatrix} -P_{LR}^{\mathbf{k}} \\ R_{LR}^{\mathbf{k}} \end{pmatrix} \right] \right\} \quad (7)
 \end{aligned}$$

where  $\omega$  is the wave frequency,  $k$  the wave-number,  $k_{\perp}$  and  $k_{\parallel}$  the wave-number components perpendicular and parallel to the background field,  $\Psi = \arctan(k_x/k_y)$ ,  $\Omega = (q/|q|)\Omega_0/\gamma$  ( $\Omega_0 = qB/(mc)$  is the non-relativistic gyrofrequency) and where we define  $x = k_{\perp}v_{\perp}/\Omega$  as the argument for the Bessel functions,  $J_n$ . The relevant electromagnetic fluctuations are :

$$\langle B_{\alpha}(\mathbf{k})B_{\beta}^*(\mathbf{k}') \rangle = \delta(\mathbf{k} - \mathbf{k}')P_{\alpha\beta}^{\mathbf{k}} \quad (8)$$

and

$$\langle E_{\alpha}(\mathbf{k})E_{\beta}^*(\mathbf{k}') \rangle = \delta(\mathbf{k} - \mathbf{k}')R_{\alpha\beta}^{\mathbf{k}} \quad (9)$$

where  $\alpha$  and  $\beta = R, L$  indicate right-hand and left-hand wave polarizations.

Under conditions of negligible damping  $\omega = \omega_r + i\Gamma \rightarrow \omega_r$  and the integral in eq.(7) is

$$\int d^3k \int_0^{\infty} dt e^{-i(k_{\parallel}v_{\parallel} - \omega + n\Omega)t} (\dots) \rightarrow \pi \int d^3k \delta(k_{\parallel}v_{\parallel} - \omega + n\Omega) (\dots), \quad (10)$$

where  $\delta(k_{\parallel}v_{\parallel} - \omega + n\Omega)$  selects the resonant conditions between particles and waves; namely,  $n = \pm 1, \dots$  (gyroresonance that is important for Alfvén waves) and  $n = 0$  (*Transit Time Damping*, *TTD*, or wave surfing that is the most important for magnetosonic waves).<sup>157, 165</sup> In the MHD approximation the polarisation and dispersion properties of the waves are relatively simple. For Alfvén waves,  $P_{RR}^{\mathbf{k}} = P_{LL}^{\mathbf{k}} = -P_{RL}^{\mathbf{k}} = -P_{LR}^{\mathbf{k}}$ ,  $R_{RR}^{\mathbf{k}} = R_{LL}^{\mathbf{k}} = R_{RL}^{\mathbf{k}} = R_{LR}^{\mathbf{k}}$  and  $\omega = v_A k_{\parallel}$ , while for (fast) magnetosonic waves,  $P_{RR}^{\mathbf{k}} = P_{LL}^{\mathbf{k}} = P_{RL}^{\mathbf{k}} = P_{LR}^{\mathbf{k}}$ ,  $R_{RR}^{\mathbf{k}} = R_{LL}^{\mathbf{k}} = -R_{RL}^{\mathbf{k}} = -R_{LR}^{\mathbf{k}}$  and  $\omega = V_f k$  (see<sup>157, 158</sup> for details);  $V_f = c_s$  in high beta-plasma such as the ICM.

In the case of low-frequency MHD waves with phase velocities,  $V_{ph}$ , much less than the speed of light the magnetic-field component is much larger than the electric-field component,  $\delta B \sim c/V_{ph} \delta E$ . Then the particle distribution function,  $f$ , adjusts very rapidly to quasi-equilibrium via pitch-angle scattering, approaching a quasi-isotropic distribution. In this case the Fokker-Planck equation (eq. 6) simplifies to a diffusion-convection equation:<sup>169, 170</sup>

20 *G. Brunetti & T. W. Jones*

$$\frac{\partial f(p,t)}{\partial t} = \frac{1}{p^2} \frac{\partial}{\partial p} \left( p^2 \mathcal{D}_{pp} \frac{\partial f}{\partial p} - p^2 \left| \frac{dp}{dt} \right|_{\text{loss}} f \right) + \frac{\partial}{\partial z} \left( D \frac{\partial f}{\partial z} \right) + Q(p,t) \quad (11)$$

where the momentum diffusion coefficient parallel to the magnetic field,  $\mathcal{D}_{pp}$ , is:

$$\mathcal{D}_{pp} = \frac{1}{2} \int_{-1}^1 d\mu D_{pp} \quad (12)$$

and the spatial diffusion coefficient,  $D$ , is :

$$D = \frac{v^2}{8} \int_{-1}^1 d\mu \frac{(1-\mu^2)^2}{D_{\mu\mu}}. \quad (13)$$

and where we added two terms in eq. (11),  $f p^2 |dp/dt|$  and  $Q$ , that account for energy losses (see Sect. 3.1) and injection of CRs, respectively. To avoid confusion, we mention that the basic physics behind the two diffusion convection equations (2) and (11) is similar. The principal differences are that eq. (11), which targets CR interactions with local turbulence, ignores large-scale spatial variations in the background velocity,  $V$ , while eq.(2) ignores the momentum diffusion coefficient,  $D_{pp}$ , because in strongly compressed flows at shocks it is sub-dominant (note that eq.2 also omits energy losses and injection of CRs).

From eqs. (7)-(9) and (12) and (13) it is clear that the momentum and spatial diffusion coefficients depend on the electric field and magnetic field fluctuations, respectively. Simple, approximate forms for these coefficients can be written in some circumstances that are useful in several astrophysical situations, including galaxy clusters.

For instance, if one assumes isotropic pitch angle scattering by resonant (linearly polarized and undamped) Alfvén waves with  $k \sim r_L^{-1}$ , the spatial diffusion coefficient from eq. (13) can be written for relativistic CRs as:<sup>171</sup>

$$D \approx A c r_L \frac{B_0^2}{(\delta B)^2}, \quad (14)$$

where  $\delta B$  represents the net amplitude of (resonant) magnetic field fluctuations defined in eq. (8) and where  $A \sim 1$  (in Sect.3.2 we will give a equivalent formula in terms of the Alfvén wave spectrum, eq. 25). We note that for  $\delta B \sim B_0$  the result is equivalent to the classical Bohm diffusion formula,  $D \sim (1/3) c r_L$ , that has been used in Sect. 2.2.1.

Similarly, if we assume momentum diffusion due to Transit-Time-Damping, TTD, ( $n = 0$ ) interactions with isotropic magnetosonic waves, we can write approximately for relativistic CRs:<sup>45</sup>

$$\mathcal{D}_{pp} \approx A_1 p^2 \frac{c_s^2}{c l} \frac{(\delta B)_f^2}{B_0^2}, \quad (15)$$

where  $A_1$  ( $A_1 \sim 5$ ) depends on details of the turbulence,  $l$  is the scale on which magneto-sonic waves are dissipated, and now  $(\delta B)_f$  represents magnetic field fluctuations associated with those waves through eq.(8) ( $\delta B_f/B_0 \sim V_t/c_s$ , e.g.,<sup>45</sup> where  $V_t$  is the velocity of large-scale turbulent eddies).

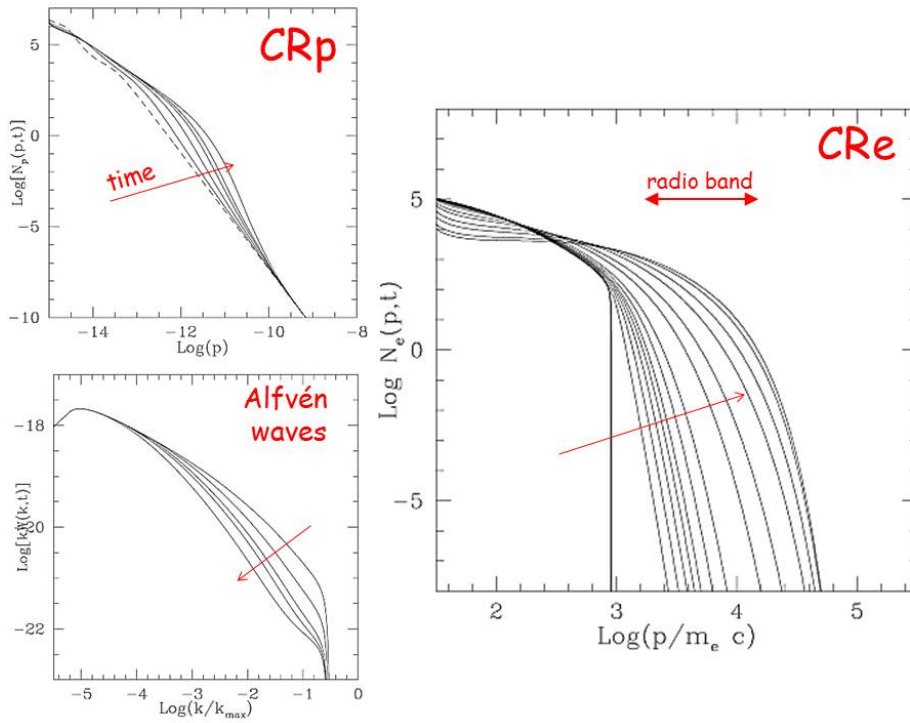


Fig. 7. The coupled evolution with time of the spectra of CRp (upper-left;  $p$  is in cgs units), CRe (right) and Alfvén waves (bottom-left); Alfvén waves are continuously injected assuming an external source (adapted from<sup>174</sup>). Panels highlight the non-linear interplay between the acceleration of CRs and the evolution of waves that, indeed, are increasingly damped with time as they transfer an increasing amount of energy to CRs. Saturation of CRe acceleration at later times is due to the combination of radiative losses and the damping of the waves that limits acceleration efficiency.

#### 2.2.2.2. Application to the ICM & open questions

To account for the turbulence–particle interaction properly, one must know both the scaling of turbulence down to resonant interaction lengths (Eqs. 8–9), the changes with time of the turbulence spectrum on resonance scales due to the most relevant damping processes, and the interactions of turbulence with various waves produced by CRs. This is extremely challenging. However, in the last decade several modeling efforts attempted to study turbulent acceleration in astrophysical environments, including galaxy clusters, by using physically motivated turbulent scalings and the relevant collisionless damping of the

turbulence.

Several calculations suggest that there is room for turbulence in galaxy clusters to play an important role in the acceleration of CRs. This outcome depends on the fraction of the turbulent energy that goes into (re)acceleration of CRs in the ICM.

Presumably the many types of waves generated/excited in the ICM, both at large and very small scales (Fig. 6), should jointly contribute to the scattering process and (re)acceleration of CRs. Much attention has been devoted to CR acceleration due to compressible (fast mode) turbulence that is driven at large scales in the ICM from cluster mergers and that cascades to smaller scales. Under this hypothesis, and as expected for typical conditions in galaxy clusters (i.e., high temperature, high beta plasma and with likely forcing and dissipation scales), it is the compressible fast modes that are the most important in the acceleration of CRs in ICMs. Most of the energy of these modes is converted into the heating of the thermal plasma via the TTD resonance. However current calculations show that TTD can drain as much as a few to  $\sim 10$  percent of the total turbulent-energy flux into the CR component of the ICM plasma.<sup>14,45,172</sup> In this case CRe in the ICM can be re-accelerated up to energies of several GeV, provided that the energy budget of fast modes on scales of tens of kpc is larger than about 3-5 percent of the local thermal energy budget<sup>k</sup>. We expect that this conclusion is important for understanding the origin of radio halos (Sect. 4).

Moreover there are several circumstances under which the fraction of the turbulent energy that is transferred into CRs may be much larger than a few %, thus making the acceleration process also more efficient than in the previous case. For example, if we consider the scenario discussed above, where compressive (fast mode) turbulence is generated at large scales, a large fraction of the energy of the fast modes can be converted into the acceleration of CRs if the CR particle collision frequencies in the ICM are much larger than those due to the classical process of ion-ion Coulomb collisions.<sup>144</sup> Potentially this may occur if the interactions between particles are mediated by magnetic perturbations generated by plasma instabilities. Instabilities may be driven by compressive turbulence and CRs in the ICM.<sup>144,145</sup> Another case where a large fraction of the turbulent energy is potentially dissipated into the (re)acceleration of CRs in galaxy clusters is that of incompressible turbulence, where acceleration is driven by Alfvén modes via gyro-resonance ( $n = \pm 1$ ).<sup>44,173,174</sup> In this case the important caveat is that Alfvén modes develop an anisotropic cascade toward smaller scales, below the Alfvén scale, that quenches the efficiency of the gyro-resonance,  $n = \pm 1$ , scattering (acceleration) process.<sup>168,175,176</sup> Consequently models of Alfvénic acceleration assume that waves are generated in the ICM at small (quasi-resonant) scales (Fig. 6), although it remains still rather unclear whether such small-scale waves can be efficiently generated in the ICM.

In all these cases, where a fairly large fraction of the turbulent energy is drained into CRs,

---

<sup>k</sup>We note that if compressive turbulence is generated at larger (e.g. a few 100 kpc) scales, this condition in terms of energy budget, essentially implies that a large fraction of the energy of such turbulence is transported to smaller scales. It implies, for example, that weak shocks generated by compressive turbulence and viscosity do not dissipate most of the turbulent energy budget into heat.

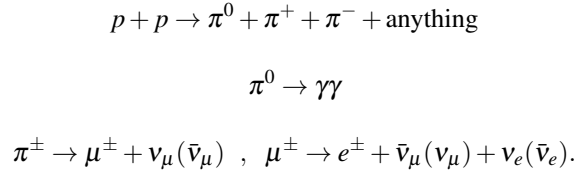


the efficiency of acceleration is essentially fixed by the damping of turbulence by the CRs themselves.<sup>144,174,177</sup> Figure 7 shows an example of CRp and CRe acceleration under these conditions. As time proceeds during the acceleration, the CRs gain energy and extract an increasing energy budget from the turbulent cascade. Consequent modifications are induced in the spectrum of the turbulence, causing a decrement in the acceleration efficiency. This differs from the cases where a smaller fraction of turbulent energy is dissipated into CRs acceleration. In these cases indeed the turbulent properties and the efficiency of turbulent acceleration depend only weakly on the CRs properties and energy budget.<sup>45,172</sup>

### 2.3. Generation of secondary particles

If we assume that CRp remain in galaxy clusters for a time-period,  $\tau$ , the grammage they encounter during their propagation is  $X_g \sim n_{ICM} m_p c \tau \sim 1.6 \times \frac{n_{ICM}}{10^{-3}} \times \frac{\tau}{\text{Gyr}} \text{g cm}^{-2}$ . On cosmic time scales that would often be comparable in the ICM with the nuclear grammage required for an inelastic collision,  $X_{nuc} \approx 50 \text{g cm}^{-2}$ . This implies that the generation of secondary particles due to inelastic collisions between CRp and thermal protons in the ICM is an important source of CRe.

The decay chain for the injection of secondary particles is:<sup>19</sup>



A threshold reaction requires CR protons with kinetic energy just larger than  $T_p \approx 300$  MeV to produce  $\pi^0$ . The injection rate of pions is given more generally by:<sup>19,178</sup>

$$Q_{\pi^{\pm,o}}(E, t) = n_{th}^p c \int_{p_*} dp N_{CRp}(p, t) \frac{F_\pi(E_\pi, E_p) \sigma^{\pm,o}(p)}{\sqrt{1 + (m_p c/p)^2}}, \quad (16)$$

where  $N_{CRp}$  is the CRp spectrum,  $F_\pi$  is the spectrum of pions from the individual collisions of CRp (of energy  $E_p$ ) and thermal protons<sup>177–185</sup> and  $\sigma^{\pm,o}(p)$  is the pp cross section for  $\pi^o$ ,  $\pi^+$  and  $\pi^-$ .<sup>182,183,185</sup>

Neutral pions decay into  $\gamma$ -rays with spectrum<sup>19,182,183,185</sup> :

$$Q_\gamma(E_\gamma) = 2 \int_{E_{min}}^{E_p^{max}} \frac{Q_{\pi^o}(E_{\pi^o})}{\sqrt{E_\pi^2 - m_\pi^2 c^4}} dE_\pi, \quad (17)$$

where  $E_{min} = E_\gamma + 1/4 m_\pi^2 c^4 / E_\gamma$ . Neutral pions produced near threshold will decay into a pair of  $\gamma$ s with average energy  $E_\gamma \simeq 67$  MeV. This provides a rough measure of the low energy end of the expected  $\gamma$ -ray spectrum. Charged pion decays produce muons, which then produce secondary electrons and positrons (as well as neutrinos) as they decay. The injection rate of relativistic electrons/positrons then becomes:

$$Q_{e^\pm}(p, t) = \int_{E_\pi} Q_\pi(E_{\pi^\pm}, t) dE_\pi \int dE_\mu F_{e^\pm}(E_\pi, E_\mu, E_e) F_\mu(E_\mu, E_\pi), \quad (18)$$

where  $F_{e^\pm}(E_e, E_\mu, E_\pi)$  is the spectrum of electrons and positrons from the decay of a muon of energy  $E_\mu$  produced in the decay of a pion with energy  $E_\pi$ ,<sup>19,185</sup> and  $F_\mu(E_\mu, E_\pi)$  is the muon spectrum generated by the decay of a pion of energy  $E_\pi$ .<sup>19,177,178</sup>

Secondary electrons continuously generated in the ICM are subject to energy losses (Sect. 3.1). If these secondaries are not accelerated by other mechanisms, their spectrum approaches a stationary distribution because of the competition between injection and energy losses:<sup>186</sup>

$$N_{e^\pm}(p) = \frac{1}{\left[ \frac{dp}{dt} \right]_L} \int_p^{p_{\max}} Q_{e^\pm}(p) dp, \quad (19)$$

where  $\frac{dp}{dt}_L$  accounts for CRE energy losses (see Sect. 3.1). Assuming a power law distribution of CRp,  $N_p(p) = K_p p^{-s}$ , the spectrum of secondary electrons at high energies,  $\gamma > 10^3$ , is  $N_e(p) \propto p^{-\delta}$ , with  $\delta = s + 1 - \Delta$ , where  $\Delta \sim 0.05$  approximately accounts for the log-scaling of the p-p cross-section at high energies.<sup>177,185,187</sup> The radio synchrotron emission from these electrons ( $e^\pm$  actually) would have a spectral slope,  $\alpha = (\delta - 1)/2$ .

### 3. The life-cycle of CRs in galaxy clusters

In this Section we discuss the energy-evolution and dynamics of relativistic CRp and CRE that are released in the cluster volume from the accelerators described in the previous Section. In this Section we also discuss the constraints on CR acceleration efficiency and propagation that come from the current  $\gamma$ -ray and radio observations.

#### 3.1. Energy Losses

Cosmic rays, especially electrons for energies above  $\sim$  GeV, are subject to energy losses that limit their life-time in the ICM and the maximum energy at which they can be accelerated by acceleration mechanisms.

##### 3.1.1. Electrons

The energy losses of ultra-relativistic electrons in the ICM are essentially dominated by ionization and Coulomb losses at low energies<sup>11</sup>

$$\left[ \frac{dp}{dt} \right]_i = -3.3 \times 10^{-29} n_{\text{th}} \left[ 1 + \frac{\ln(\gamma/n_{\text{th}})}{75} \right], \quad (20)$$

where  $n_{\text{th}}$  is the number density of the thermal plasma protons, and by synchrotron and inverse Compton losses at higher energies,<sup>11</sup>

$$\left[ \frac{dp}{dt} \right]_{\text{rad}} = -4.8 \times 10^{-4} p^2 \left[ \left( \frac{B_{\mu G}}{3.2} \right)^2 + (1+z)^4 \right], \quad (21)$$

where  $B_{\mu G}$  is the magnetic field strength in units of  $\mu G$ , and we assumed isotropic magnetic fields and distributions of CRe momenta. The factor in the square brackets can alternatively be expressed as  $B_{IC}^2 + B^2$ , where  $B_{IC} = 3.2(1+z)^2 \mu G$  is the equivalent magnetic field strength for energy losses due to ICS with CMB photons.

The life-time of CRe,  $\tau_l \sim p/(dp/dt)$ , from Eqs. 20–21, is :

$$\begin{aligned} \tau_e(\text{Gyr}) \sim 4 \times \left\{ \frac{1}{3} \left( \frac{\gamma}{300} \right) \left[ \left( \frac{B_{\mu G}}{3.2} \right)^2 + (1+z)^4 \right] \right. \\ \left. + \left( \frac{n_{\text{th}}}{10^{-3}} \right) \left( \frac{\gamma}{300} \right)^{-1} \left[ 1.2 + \frac{1}{75} \ln \left( \frac{\gamma/300}{n_{\text{th}}/10^{-3}} \right) \right] \right\}^{-1}. \end{aligned} \quad (22)$$

This depends on the number density of the thermal medium, which can be estimated from X-ray observations, on the IC-equivalent magnetic field (i.e., redshift of the cluster), and on the magnetic field strength, which is important only in the case  $B^2 \gg B_{IC}^2$  and eventually can be constrained from Faraday rotation measures (Sect. 4.1).

### 3.1.2. Protons

For relativistic CRp, the main channel of energy losses in the ICM is provided by inelastic p-p collisions (Sect. 2.3). This sets a CRp life-time

$$\tau_{pp}(p) \simeq \frac{1}{c n_{\text{th}} \sigma_{pp}} \quad (23)$$

$\sigma_{pp}$  is the inclusive p-p cross-section.<sup>182, 183</sup>

For trans-relativistic and mildly relativistic CRp, energy losses are dominated by ionization and Coulomb scattering. CRp more energetic than the thermal electrons have<sup>158</sup>

$$\left( \frac{dp}{dt} \right)_i \simeq -1.7 \times 10^{-29} \left( \frac{n_{\text{th}}}{10^{-3}} \right) \frac{\beta_p}{\frac{3}{4} \sqrt{\pi} \beta_e^3 + \beta_p^3} \quad (\text{cgs}) \quad (24)$$

where  $\beta_e = v_e/c \simeq 43\beta_p \simeq 0.18(T/10^8 K)^{1/2}$  is the RMS velocity of the thermal electrons, while  $\beta_p$  is the corresponding thermal proton velocity.

### 3.1.3. General energy loss considerations

Figure 8 shows the (total) time scales for losses of CRe and CRp. CRp with energy 1 GeV – 1 TeV are long-living particles with life-times in the cores of galaxy clusters  $\sim$  several Gyrs. At higher energy the CRp time-scale gradually drops below 1 Gyr, while at very high

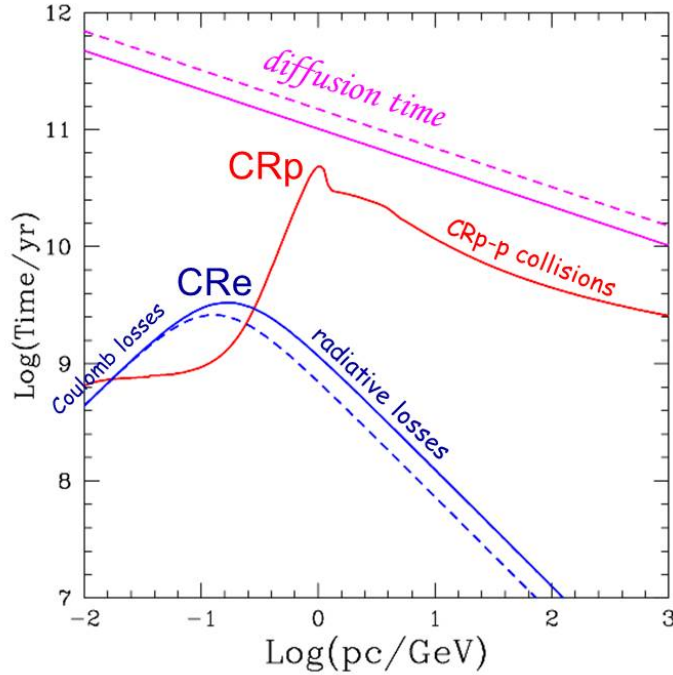


Fig. 8. Life-time of CRp (red) and CRE (blue, lower curves) in the ICM at redshift  $z = 0$ , compared with the CR diffusion time on Mpc scales (magenta, upper curves) (adapted from<sup>25</sup>). The most relevant channels of CR energy losses at different energies are highlighted in the panel. Adopted physical parameters are :  $n_{th} = 10^{-3} \text{cm}^{-3}$ ,  $B = 1$  (solid) and  $3 \mu\text{G}$  (dashed). Diffusion is calculated assuming a Kolmogorov spectrum of magnetic fluctuations with  $L_{max} = 100 \text{kpc}$  and  $f = 1$ .

energy, in the regime of ultra high energy CRp, the life-time is limited by inelastic  $p - \gamma$  collisions with CMB photons, as discussed in Section 2.2.1 (Fig. 5).

On the other hand, CRE are short-lived particles at the energies where they radiate observable emissions, due to the unavoidable radiation energy-losses (mainly ICS and synchrotron). The maximum life-time of CRE, about 1 Gyr, is at energies  $\sim 100 \text{MeV}$ , where radiative losses are roughly equivalent to Coulomb losses. On the other hand, CRE with energy  $\sim$ several GeV that emit synchrotron radiation in the radio band (GHz), have shorter life-times,  $\sim 0.1 \text{Gyrs}$ . The life-times of CRE at high energies do not vary much from cluster cores to periphery, because for weak magnetic fields they are determined by the unavoidable losses from ICS off CMB photons. On the other hand, CRE ICS lifetimes will scale strongly and inversely with cluster redshift according to  $(1+z)^{-4}$  (eqs. 21-22).

### 3.2. Dynamics of CRs in the ICM

The propagation of CRs injected in the ICM is mainly determined by diffusion and convection.

The time necessary for CRs to diffuse over distances  $L$  is  $\tau_{diff} \sim (1/4)L^2/D$ . This implies that the spatial diffusion coefficient necessary for diffusion of CRs over Mpc-scales within a few Gyrs is extremely large,  $D > 2 \times 10^{31} \text{cm}^2 \text{s}^{-1}$ . For CRs with GeV energy this is several orders of magnitude larger than that in our Galaxy. This simple consideration suggests that galaxy clusters are efficient containers of CRs.

More specifically, according to QLT the diffusion coefficient for gyro-resonant scattering of particles with Alfvénic perturbations of the magnetic field is<sup>146, 188</sup> (see also Sect. 2.2.2):

$$D(p) = \frac{1}{3} r_{Lc} \frac{B^2}{\int_{2\pi/r_L}^{\infty} dk P(k)}, \quad (25)$$

where  $P(k)$  is the power spectrum of turbulent field-perturbations on a scale  $k$  (that interacts resonantly with particles with momentum  $p \propto 1/k$ ), such that  $\int_{k_{min}}^{\infty} dk P(k) = fB^2$  and  $f \leq 1$ ;  $k_{min}$  is the minimum wavenumber (maximum scale) of turbulence<sup>1</sup>. In Figure 8 we show a comparison between the life-time of CRs and their diffusion-time on Mpc scales assuming a Kolmogorov spectrum of the Alfvénic fluctuations,  $fB^2 \propto k^{-5/3}$ , with a maximum scale  $L_{max} = 2\pi k_{min}^{-1} = 100$  kpc and  $f = 1$ . The diffusion time of CRs in this case is substantially larger than a Hubble time, implying that CRp can be accumulated in the volume of galaxy clusters and that their energy budget increases with time, as first realized by.<sup>16–18</sup> Figure 8 suggests that even a fairly small level of magnetic field fluctuations in the ICM,  $f \ll 1$ , should be sufficient to confine most of the CRs in the gigantic volume of galaxy clusters for a time-period comparable to the age of clusters themselves.

Formally eq.25, which has been originally adopted to support CRs confinement in clusters, assumes an isotropic distribution of Alfvénic fluctuations at resonant scales. This is not true in the case of the strong<sup>m</sup> incompressible turbulence, because its cascading process is anisotropic with respect to the mean field.<sup>189, 190</sup> Consequently, particle scattering is strongly reduced.<sup>168, 175, 176</sup> However, in general this does not imply that CRs scattering is inefficient because, even limiting to the particular case of strong incompressible turbulence<sup>n</sup>, we can think that the non-resonant mirror interactions with the slow-mode perturbations provide a lower limit to the rate of scattering that is still orders of magnitude more efficient than that due to the gyroresonant scatter calculated according to QLT<sup>191</sup> We also note that Alfvén waves can be excited directly at resonant scales, for example, due to the streaming instability that is driven by CRs streaming along the field lines, eg.<sup>146, 158</sup> (Fig. 6). In this case the streaming speed (the effective “drift speed”) of CRs gets limited to the Alfvén speed. If this process is efficient in the ICM, CRs drift at the Alfvén speed and the time-scale necessary for CRs to cover Mpc distances is  $\sim$  Hubble time using a reference value,  $v_A \sim 10^7$  cm/s. In the presence of background turbulence, the streaming instability

<sup>1</sup>We note that if turbulent field-perturbations are on scales  $\leq r_L$ , i.e.  $k_{min} \geq 2\pi/r_L$ , and  $f \approx 1$  eq. (25) is the coefficient of parallel Bohm diffusion,  $D \sim 1/3 r_{Lc}$

<sup>m</sup>We note, from the MHD turbulence literature, that the notion “strong,” refers to the strength of the non-linear interaction between turbulent waves, not to the amplitude of the turbulent fluctuations.

<sup>n</sup>If a fraction of the turbulence is compressible, scattering is efficient and dominated by fast modes.

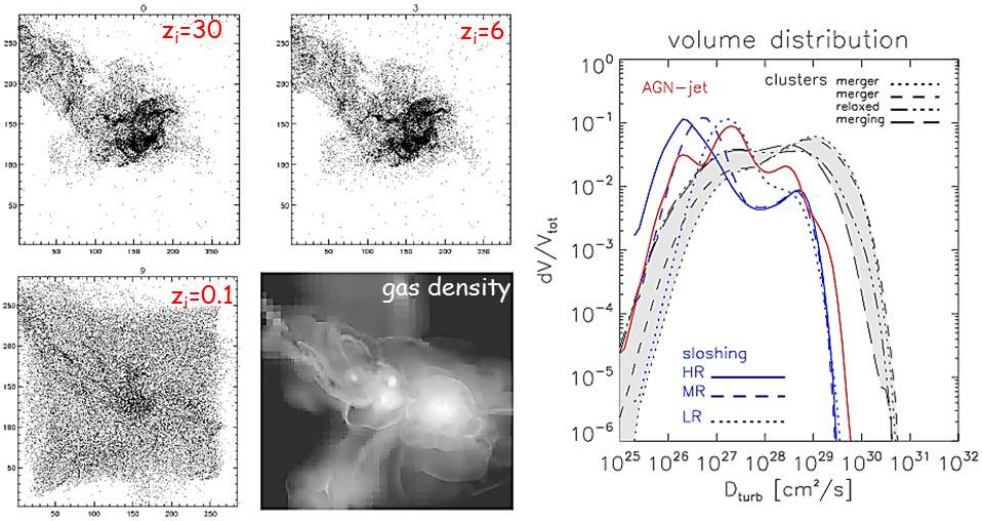


Fig. 9. Left panel: spatial distribution of tracers particles in a galaxy clusters at  $z = 0$  that have been uniformly generated in the cluster region in the simulated box at  $z = 30, 6$  and  $0.1$ . The bottom-right panel shows the gas density at  $z = 0$  (adapted from<sup>153</sup>). Right panel: volume-filling distribution of the turbulent spatial-transport coefficient,  $D \sim V_l l_o$ , that is estimated from the analysis of numerical simulations of galaxy clusters. Curves refer to cases where turbulent motions are driven by cluster mergers, AGN-jets and sloshing (from<sup>135</sup>).

can be partially suppressed.<sup>168,192</sup> This is because turbulence suppresses the waves responsible for self-confinement of CRs, since they cascade to smaller scales before they have the opportunity to scatter CRs. Such a background turbulence, however, also limits the “free flight” of CRs, through the scattering with the fluctuations of the magnetic field induced by turbulence itself. In the most “favourable” case, where we neglect small scale fluctuations, CRs can “fly” along the magnetic field lines over maximum distances that are of the order of the smallest scale on which the magnetic field is effectively advected by turbulent motions. That is the MHD, Alfvén scale,  $l_A \simeq l_o/M_A^3$ , where  $l_o$  is the turbulent-injection scale and  $M_A$  is the Alfvénic Mach number of the turbulence on that scale, eg.<sup>45,139</sup> (Sect. 2.2.2, Fig. 6). The resulting *maximum* diffusion coefficient is  $D \sim 1/3cl_A \approx 10^{31} (\frac{l_A}{0.3kpc}) cm^2 s^{-1}$ , still implying a diffusion time over Mpc-scales of several Gyrs. In conclusion, we believe that the wealth of waves that can be naturally generated in the ICM, on both small and large scales, supports the paradigm of confinement of CRp in galaxy clusters; namely, that most of the energy budget of CRp is accumulated in the cluster volume over the cluster life-time.

Assuming, in the light of this discussion, that parallel diffusion of CRs of some energy  $E$  is strongly suppressed by fluctuations on relatively small scales, the cluster-scale dynamics of these CRs is controlled by advection via gas flows accompanied by a process of turbulent-transport (Figure 9, left). This process is analogous to the transport of passive scalars by a turbulent flow, and it induces the CR particles to exhibit a random walk behaviour, eg.,<sup>193</sup> within the bulk flow. This regime is known as *Richardson* diffusion in hydro-turbulence.<sup>194</sup> In this regime the transport is super-diffusive,  $L^2 \propto \tau_{diff}^{3/2}$ , on scales smaller than the injection scale of turbulent eddies and diffusive,  $L^2 \sim 4D\tau_{diff}$ , on larger scales. Because it is controlled by the fluid motions, the CR transport-coefficient is energy-independent and can be estimated as  $D \sim V_{l_o} l_o$ , where  $V_{l_o}$  and  $l_o$  are the velocity and scales of the largest turbulent eddies. According to numerical simulations of galaxy clusters the largest values,  $D \sim 10^{30-31} \text{cm}^2 \text{s}^{-1}$ , are derived in the case of merging systems<sup>135</sup> (Figure 9, right) as a result of large scale motions and mixing generated during these events in the ICM. This has the potential implication that turbulence might transport CRs on a scale that could be of the order of cluster-cores, thus, potentially inducing a spatial distribution of CRs that is broader than that of the thermal plasma. Similarly, we note that the same mechanism could also spread metals through the ICM leading to the formation of the flat spatial distributions of metals that are observed in non-cool core clusters.<sup>153,195</sup>

To avoid confusion from the complexity of the above discussion, we clarify that the relative importance of particle scattering-based diffusion parallel to the local mean magnetic field and bulk fluid turbulence-based transport of CRs in the ICM depend on particle energies and the fluid turbulence properties, with the dynamics of very high energy CRs being dominated by scattering-based diffusion.

### 3.3. Limits on CRp

The expected confinement and accumulation of CRp generated during cluster formation (Sect. 3.2) motivate the quest for CRp in galaxy clusters. Most of the thermal energy in the ICM is generated at shocks, as previously noted. Estimates of CRp acceleration efficiency suggest as much as  $\sim 10\%$  of the kinetic energy flux at cosmological shocks may be converted into CRs.<sup>196</sup> Then, one might claim that the resulting energy budget of CRs should be a substantial fraction of the ICM thermal energy. If true, the presence of the CRp could influence many aspects of ICM dynamics, including, for examples, contribution to ICM pressure support and a partial quenching of radiative cooling in core regions.

The most direct approach to constraining the energy content of CRp in ICMs consists in the searches for  $\gamma$ -ray emission from the decay of the neutral pions due to CRp-p collisions in the ICM. Early space-based  $\gamma$ -ray upper limits from EGRET observations provided limits  $E_{CR}/E_{ICM} < 0.3$  in several nearby galaxy clusters.<sup>26</sup> Subsequently, more stringent limits have been derived from deep, pointed observations at energies  $E_\gamma > 100$  GeV with ground-based Cherenkov telescopes.<sup>27,29,31,197-199</sup> These limits, unfortunately, depend on the unknown spectral shape of the CRp-energy distribution and the spatial distribution of CRp in the clusters. The most stringent limits are obtained assuming  $\delta = 2.1$  ( $N_{CR}(p) \propto p^{-\delta}$ ) and a linear scaling between CRp and thermal energy densities (Fig. 10); under these assump-



tions a particularly deep limit  $E_{CR}/E_{ICM} < 0.016$  is derived for the Perseus cluster.<sup>31</sup> Constraints are significantly less stringent for steeper spectra and for flatter spatial distributions of the CRp component in the cluster. The recent advent of the orbiting Fermi-LAT observatory has greatly improved the detection prospects thanks to its unprecedented sensitivity at MeV/GeV energies. However, after almost 5 years of operations, no firm detection of any ICM has been obtained. Only upper limits to the  $\gamma$ -ray emission have been obtained for both individual nearby clusters and from the stacking of samples of clusters.<sup>30,32,33,199–201</sup> Under the assumption that the spatial distribution of CRp roughly follows that of the thermal ICM, in the most stringent cases (including stacking procedures) these limits constrain  $E_{CR}/E_{ICM} < \text{about } 1\%$  (Fig. 10), with only a weak dependence on  $\delta$ . Similar limits are derived by assuming a spatial distribution of CRp that is slightly broader than that of the ICM,<sup>32</sup> such as that expected from simulations by.<sup>202</sup> Limits on the CRp total energy become gradually less stringent if one assumes a flatter spatial distribution compared to the ICM, since then more CRp reside in regions where the number density of thermal-targets protons is lower and where they consequently produce fewer  $\pi^0$  and  $\gamma$ -rays.

Radio observations of galaxy clusters also provide limits on  $E_{CR}/E_{ICM}$ , since these observations allow one to constrain the generation rate of secondary CRe in the ICM.<sup>34–36</sup> Only a fraction of clusters show diffuse, cluster scale synchrotron emission at the sensitivity level of present observations (Sect. 4). Most do not. Radio upper limits to the cluster-scale emission limit the combination of the energy densities of the magnetic field and secondary CRe, and consequently the energy budget in the form of primary CRp as a function of the magnetic field strength. Faraday rotation measurements provide an indication that the central,  $\text{Mpc}^3$ -volume, regions of galaxy clusters are magnetized at  $\approx \mu\text{G}$  level.<sup>203–205</sup> This information allows one to break the degeneracy between CRp and magnetic field energy densities, resulting in limits  $E_{CR}/E_{ICM} \leq \text{few} \times 0.01$  (Fig. 10).

Current upper limits violate optimistic expectations for the CRp energy content and  $\gamma$ -ray emission from galaxy clusters derived in the last decade.<sup>16,25,83,202,206–209</sup> Consequently the available limits now suggest that the efficiency of CRp acceleration that has been previously assumed for the most important mechanisms operating in galaxy clusters was too optimistic, or that eventually CRp diffusion and turbulent-transport (Sect. 3.2) play an important role. In this respect we notice that current observational constraints refer mainly to the innermost ( $\sim \text{Mpc}$ ) regions of clusters where both the number density of thermal protons (targets for  $\pi^0$  production) and the magnetic field are largest. In fact no tight constraints are available for the clusters outskirts where the CRp contribution might be relatively larger.

As a final remark on this point we note that future radio telescopes, including the phase 1 of the SKA, will have a chance to obtain constraints one order of magnitude deeper. These constraints will be better than current constraints from  $\gamma$ -ray observations even if we assume that the magnetic fields in the ICM are significantly weaker than those estimated from Faraday rotation measurements (Fig. 10). We note however that current limits on the hard X-ray and  $\gamma$ -ray emission<sup>30</sup> from galaxy clusters exclude the possibility that the magnetic fields in the ICM are smaller than 0.1–0.2  $\mu\text{G}$ . Weaker fields than these in clusters hosting

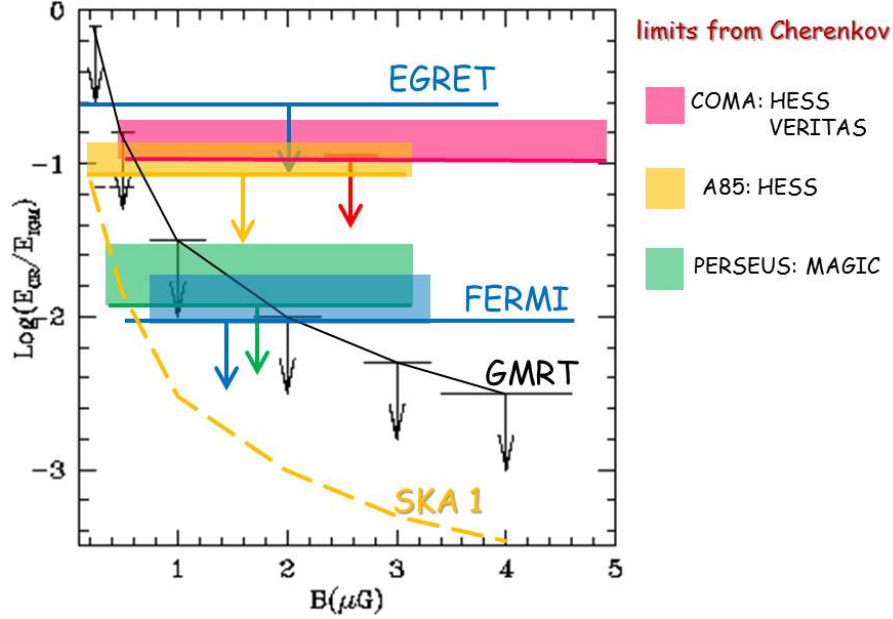


Fig. 10. A collection of representative upper limits to the ratio of the energy in CRp and thermal ICM as derived from  $\gamma$ -ray and radio observations. Radio-based upper limits depend on the magnetic field strength in a  $\text{Mpc}^3$  volume. Limits from observations with Cherenkov telescopes include the case of Coma,<sup>197,199</sup> A85<sup>29</sup> and Perseus.<sup>31</sup> In<sup>29,197</sup>  $\delta = 2.1$  and a spatially constant ratio of CRp and ICM energy densities are assumed. In the case of Coma<sup>199</sup> we report the limits obtained by these authors by adopting a spatial distribution and spectrum of CRp from numerical simulations. In the case of Perseus<sup>31</sup> the reported region (green) encompasses limits obtained using  $\delta = 2.1$  and a spatially constant ratio of CRp and ICM energy densities and limits obtained by adopting a spatial distribution and spectrum of CRp from numerical simulations. Limits from EGRET and Fermi-LAT are taken from<sup>26</sup> and<sup>32,33</sup> respectively. In<sup>26,33</sup> limits are obtained assuming a spatially constant ratio of CRp and ICM energy densities, whereas we report the limits obtained by<sup>32</sup> by assuming the spatial distribution of CRp from simulations. Upper limits derived from radio observations are taken from<sup>35</sup>. The sensitivity level to CRp from future SKA 1 observations is also reported for clusters at  $z = 0.25$ .

giant radio halos would, as we explain in Sect. 5, necessarily require inverse Compton hard X-rays above current upper limits from the same CRp population responsible for the radio synchrotron emission.

#### 4. Diffuse synchrotron radio sources in galaxy clusters: radio halos and relics

Steep spectrum ( $\alpha \geq 1$ , with  $F(\nu) \propto \nu^{-\alpha}$ ), diffuse radio emission extended on cluster scales is observed in a number of galaxy clusters. The emission is clearly associated with the ICM and not individual sources, implying the existence of relativistic electrons and magnetic fields mixed with the ICM. Without entering in the details of the morphological zoology that is observed, see e.g.,<sup>37,38</sup> in this Section we focus on the two main classes of

diffuse radio sources in galaxy clusters: radio halos and giant radio relics.

Halos and relics have different properties and presumably also a different origin. Radio halos are classified in *giant* (Figure 11) and *mini radio halos* (Figure 15), peaking in intensity near the centre of galaxy clusters and having good spatial coincidence with the distribution of the hot X-ray emitting gas. Radio relics (Figure 16) are typically elongated and located at the cluster periphery. Some clusters include both. The two classes of radio sources differ also in their polarization properties. Halos are generally unpolarised, while relics are strongly polarised. Synchrotron polarisation in the relics is a signature of significant anisotropy in the magnetic field on large scales, probably due either to compression (e.g., shocks) or possibly to shear (e.g., tangential discontinuities). The absence of observed polarization in radio halos and their morphological connection with the thermal X-ray emission suggest that the relativistic plasma that generates that synchrotron radiation occupies a large fraction of the volume filled by the hot X-ray emitting ICM.

Faraday rotation measurements and limits to ICS X-rays (and  $\gamma$ -rays) indicate that the ICM is magnetised at  $\mu\text{G}$  levels<sup>204</sup> (Sects. 4.1, 5), in which case the relativistic CRe emitting in the radio band have energies of a few GeV (Lorentz factor  $\gamma \sim 10^4$ ) that have lifetimes  $\approx 0.1$  Gyr in the ICM (Sect. 3, Figure 8). This short life-time, combined with the excessively long time that is needed by these CRe to diffuse across a sizable fraction of the Mpc-scale of the observed emissions, requires that the emitting particles in halos and relics are continuously accelerated or generated *in situ* in the emitting regions;<sup>119</sup> this is known as the *diffusion problem*.

The hierarchical sequence of mergers and accretion of matter that leads to the formation of clusters and filaments dissipates enormous quantities of gravitational energy in the ICM through processes on microphysical scales. Even if a small fraction of this energy is converted into CRs acceleration we may expect non-thermal emission from galaxy clusters and from the Cosmic Web more generally. Cluster-scale radio sources may probe exactly this process and consequently they are extremely important crossroads of cosmology, astrophysics and plasma physics. However, the very low radio surface brightness of the Mpc-scale radio sources in galaxy clusters<sup>o</sup>, combined with their steep radio spectra (average values reported for  $\alpha$  are in the range 1.2–1.4), make their detection difficult.<sup>38,218,219</sup> Presumably this implies that we are currently detecting only the *tip of the iceberg* of the non-thermal radio emission from the Cosmic Web,<sup>220</sup> which also implies that current observational classification is possibly subject to a revision in the next years (for observational hints of diffuse emission on possibly very large scales, such as radio bridges and complex emissions, see also<sup>38</sup> and ref. therein).

Theoretically several mechanisms that are directly or indirectly connected with the formation of galaxy clusters may contribute to the origin of the observed radio emission. In this respect it is commonly accepted that radio halos and relics are due to different mechanisms and consequently probe different pieces of the complex physics in these environments. Specifically giant radio halos probably trace turbulent regions in the ICM where particles are trapped and accelerated by some mechanism, while, on the other hand, radio relics

---

<sup>o</sup> $\sim 1\mu\text{ Jy arcsec}^{-2}$  at 1 GHz

are associated with cosmological shock waves where particles can be accelerated. As discussed in Sect 2.2 shocks and turbulent motions in the ICM are tightly connected, and this ultimately may provide a possible physical link between relics and halos.<sup>78</sup>

#### 4.1. A brief note on $B$ estimates in the ICM

In the following Sections we shall use cluster-scale radio sources as probes of the physics of CRs in the ICM. The origin and distributions of magnetic fields in galaxy clusters are not the main focus of our review. However, for clarity we briefly comment on the current ideas for the origin of magnetic fields in these systems. In particular, they rely on the possibility that seed magnetic fields, of cosmological origin or injected in the volume of galaxy clusters by galaxies and AGNs, are mixed and amplified by compression and stretching through accretion and turbulent-motions induced by shocks and clusters dynamics.<sup>8, 75, 76, 125, 221–226</sup> However, given the importance of ICM magnetic field strength estimates from Faraday rotation in constraining CR populations, it is appropriate here to outline briefly how they are currently obtained. They depend, of course, on the circular birefringence at radio frequencies of a magnetized plasma. Propagating through such a medium, the plane of linear polarization (generally in synchrotron emission) rotates through an angle  $\chi = RM \times \lambda^2$ , where  $RM = 812 \int_0^L n_e B_{\parallel} dl$  rad/m<sup>2</sup>, with  $B_{\parallel}$  the magnetic field component along the line of sight in  $\mu\text{G}$ ,  $n_e$  is the electron number density in units of cm<sup>-3</sup>, and  $dl$  the differential path in kpc. Examination of the wavelength variation in polarization seen through the ICM is used to measure distributions of RM across the observed sources. The RM distribution carries essential information about the ICM magnetic field strength and structure when combined with X-ray data to establish the electron density distribution. As already noted (Sects. 2-3), the ICM magnetic field is expected to be turbulent. In that case  $B_{\parallel}$  will fluctuate (around zero if the turbulence is isotropic), reducing the mean rotation measure,  $\langle RM \rangle$ , towards zero if the mean aligned field vanishes, but adding a nonzero dispersion,  $\sigma_{RM} = 812 \bar{n}_e \sigma_{B_{\parallel}} \Lambda \sqrt{L/\Lambda}$ , where  $\bar{n}$  the mean number density,  $\sigma_{B_{\parallel}}$  the rms strength of the line-of-sight magnetic field,  $L$  the path length, and  $\Lambda = (3/2)L_B$ , with  $L_B$  the 3D correlation length of the magnetic field.<sup>227, 228</sup> The units are the same as before. In practice the magnetic field estimates depend on estimations for  $\sigma_{RM}$  (or sometimes  $RM_{RMS}$ ) and  $\Lambda$ . Accuracies in these are controlled by limited statistics in the RM distribution (since available coverage of the ICM is generally rather sparse), by the indirect connection between the 2D RM coherence scale and the 3D magnetic field correlation scale,  $L_B$  (but see<sup>229</sup>), and often by uncertainties in the total ICM path to a polarized source, if it is embedded. Typically, RM samples are taken from several moderately extended background and embedded synchrotron sources distributed across an area comparable to or larger than the cluster core. By adopting simple models for the systematic radial scaling between the magnetic field and the ICM density, along with simple parameterization of the magnetic field turbulence spectrum several such analyses have been conducted, with typical resulting central ICM magnetic field values  $B_0 \sim 1 - \text{few } \mu\text{G}$ .<sup>204, 205, 229–235</sup> While uncertainties in individual cluster results are probably at least a factor  $\sim 2$ , the general pattern of results seems fairly robust.

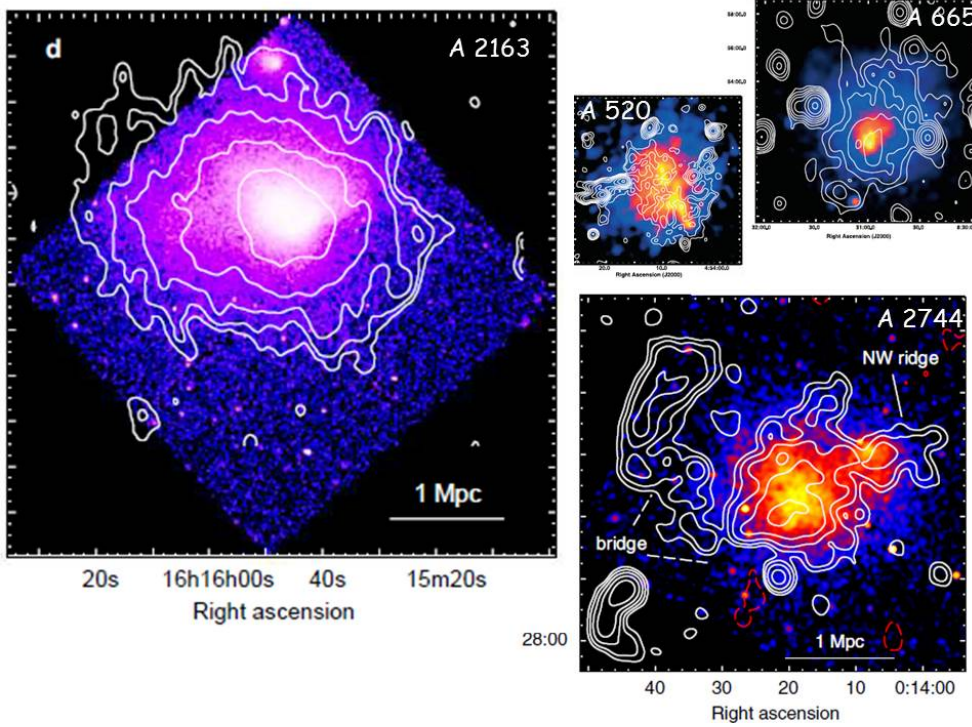


Fig. 11. Radio images of giant radio halos (contours) overlaid on the thermal X-ray emission of the hosting clusters. Images are reported with the same physical scale (credits : Giacintucci in prep. for A2163,<sup>210</sup> for A520 and A665,<sup>211</sup> for A2744).

#### 4.2. Giant Radio Halos

Returning to CRs, we note that two principal mechanism proposals are presently advocated to explain the origin of CRe emitting in giant radio halos: i) (re)-acceleration of relativistic particles by MHD turbulence in the ICM<sup>14, 15, 44, 45, 138, 162, 163, 173, 174, 236, 237</sup> and, ii) continuous production of secondary electron-positron pairs by inelastic hadronic collisions between accumulated CRp and thermal protons in the ICM,<sup>19, 23, 24, 46, 238, 239</sup> and their combination.<sup>172, 177</sup>

The hadronic scenario is based on the physics described in Sect. 2.3 and allows one to resolve the *slow diffusion problem*<sup>P</sup>, because CRe are continuously injected *in situ* throughout the ICM. Also the morphological connection between radio and X-ray emission in galaxy clusters can be explained by this scenario because the X-rays trace the thermal matter that provides the targets for the hadronic collisions. An unavoidable consequence of this scenario is the emission of  $\gamma$ -rays due to the decay of  $\pi^0$  that are produced by the same decay chain that is responsible for the injection of secondary CRe (Sect. 2.3).

<sup>P</sup>As mentioned before, slow CR diffusion in the ICM is incompatible with unavoidably rapid electron energy loss rates unless observed electrons are injected or accelerated throughout radio halo volumes.

The turbulent acceleration model is based on the physics described in Sect. 2.2.2 and assumes that turbulence is generated strongly during cluster mergers and that a fraction of its energy is dissipated into (re)acceleration of CRe via Fermi II –type mechanisms. In this case the slow diffusion problem is also solved, because the emitting CRe are (re)accelerated *in situ*, for a fairly long period (of about 1 Gyr) by merger–induced turbulence that is assumed to fill a substantial fraction of the volume of clusters. The most obvious expectation of this model is a tight connection between giant radio halos and cluster mergers, because of the finite decay time for merger-generated turbulence. According to this model radio halos could have complex, spatially varying (and potentially very steep) spectra due to the breaks and cut-offs that are produced in the spectrum of the emitting CRe as a result of the balance between (spatially varying) acceleration and cooling (Sect. 2.2.2, see also Fig. 7).

#### 4.2.1. *Observational milestones and origin of giant radio halos*

Pioneering studies using Arecibo and the NVSS and WENSS radio surveys suggested that radio halos are not common in galaxy clusters.<sup>240–242</sup> Current observations show that not all clusters have diffuse radio emission, with only  $\sim 1/3$  of X-ray luminous systems hosting giant radio halos. This provides one of the most relevant constraints for understanding the origin of CRe in radio halos. In this respect an important step has been achieved in the last few years, thanks to meter wavelength radio observational campaigns at the GMRT<sup>9</sup> combined with observations at higher radio frequencies and in the X-ray band.<sup>68,243–247</sup> The high sensitivity surveys with the GMRT found that clusters with similar thermal X-ray luminosity, and presumably similar mass, branch into two populations, one hosting radio halos and a second one with no evidence for halo-type cluster-scale radio emission at the sensitivity level of current observations<sup>35,248</sup> (Figure 12, left). Related to this finding, another observational milestone that has been achieved in the last decade is the connection between giant radio halos and the dynamics of the hosting clusters, with halos always found only in merging systems.<sup>38,249</sup> Firm statistical evidence of that has been recently obtained from combined radio – X-ray studies of galaxy clusters in the GMRT surveys<sup>68,246</sup> (Figure 12, right). These studies have shown that the generation of giant radio halos occurs during mergers between galaxy clusters. This leads to a number of possible physical interpretations. The most obvious are that turbulence generated during cluster mergers may rapidly accelerate CRs (Sect. 2.2.2)<sup>35,236,248</sup> or that the cluster magnetic field can be amplified by the turbulence during these mergers.<sup>239,250</sup> Less obvious hypotheses to connect halos and mergers have been proposed, including the possibility that spatial diffusion or streaming of CRs plays a role in modifying the level of synchrotron emission in galaxy clusters, provided that the diffusion or streaming depends strongly on the dynamical state of the cluster.<sup>46,192</sup> More recent studies attempt to better constrain the occurrence of radio halos in galaxy clusters by selecting clusters using the SZ-effect,<sup>251</sup> that is a better indicator of cluster mass with respect to the clusters X-ray emission.<sup>6</sup> The combination of the GMRT surveys, mentioned above, with the Planck SZ catalog<sup>252</sup> shows that clusters branch into

<sup>9</sup><http://gmrt.ncra.tifr.res.in/>

two populations (radio halos and limits) also in a radio–SZ diagram (although this bimodal behaviour appears weaker than that in X-ray diagrams), and that the two populations correlate with the cluster dynamics<sup>246</sup> as in previous X-ray based studies. However the fraction of clusters hosting radio halos using SZ selected samples appears larger than that measured using X-ray clusters samples.<sup>253</sup> That may be due to the combination of a distinct time evolution of the SZ and X-ray signals from the ICM during cluster mergers and a bias toward cool-core systems in X-ray selected samples,<sup>253</sup> and opens to complementary ways to study the connection of thermal and non-thermal components in galaxy clusters.

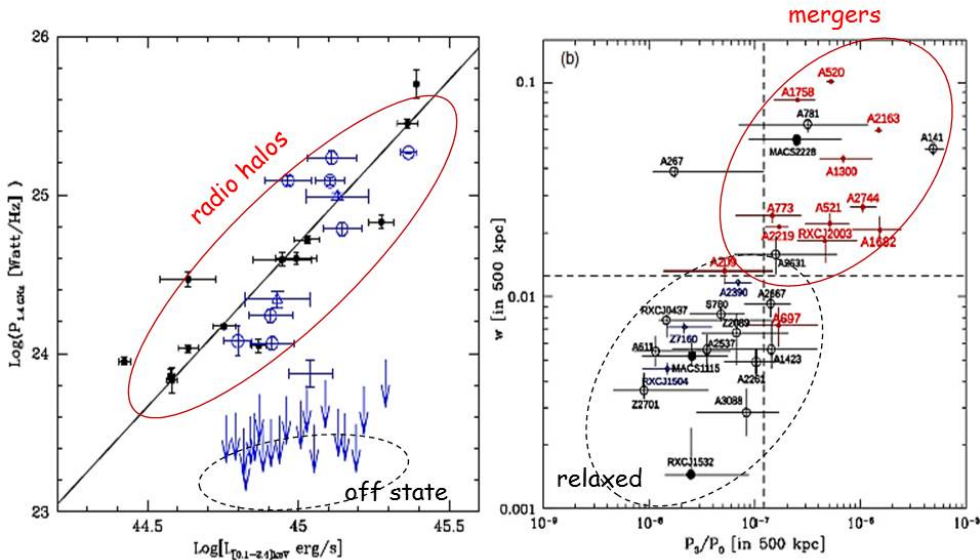


Fig. 12. Left panel: distribution of galaxy clusters of the GMRT sample<sup>244</sup> in the radio power – X-ray luminosity diagram, showing that clusters branch into two : giant radio halos (the merging systems in the left panel of the figure) and off state”, undetected, systems (the relaxed systems in the left panel of the figure) (adapted from<sup>248</sup>). Right panel: distribution of galaxy clusters in the centroid-shift variance  $w$  vs power ratio  $P_3/P_0$  diagram. Mergers are reported in the top-right panel, relaxed systems in the bottom-left panel. Clusters hosting giant radio halos are reported in red (adapted from<sup>68</sup>).

The existence of a connection between thermal and non-thermal ICM components is also highlighted by point-to-point correlations discovered between the synchrotron brightness of giant radio halos and the X-ray brightness of the hosting clusters<sup>38,254</sup> and, in the case of the Coma cluster, between the Compton  $y$ -parameter and the radio brightness.<sup>255</sup> These correlations have been used to claim that the spatial distribution of CRs in galaxy clusters is generally broader than that of the thermal ICM, with implications on the physics discussed



in Sect. 3.2. In addition a number of authors have identified the very broad (flat) spatial profiles of giant radio halos as a potential challenge for a purely hadronic origin of these sources, because in some cases a large, or radially increasing, energy density of CRp and/or magnetic field is required to generate the observed radio emission from radially distant, low target- ICM density, regions.<sup>255–259,274</sup> Potential constraints on the thermal – non-thermal connection and on the physics of radio halos also come from possible trends between the local synchrotron spectral indices and ICM temperatures.<sup>38</sup> Still, these relationships are only hints at the full picture. Only future radio observations that combine extreme brightness sensitivity and high angular resolution, for example using the SKA and its precursors, will provide the opportunity to exploit adequately the physical information encoded in the above correlations, including the interplay between particle acceleration and transport in the ICM and their connections with the magnetic field properties.

Important constraints on the origin of giant radio halos already come from the combination of radio and  $\gamma$ -ray observations. Current upper limits to the  $\gamma$ -ray emission from galaxy clusters, including clusters hosting radio halos, (Sect. 3.3, Figure 10) put especially stringent constraints on the role of hadron-hadron collisions and their secondary products for the origin of these sources. Specifically, this information can strongly constrain cluster magnetic field requirements. From eq.(17), (19) and (21) the ratio of synchrotron luminosity from secondary CRe and  $\gamma$ -ray luminosity due to  $\pi^0$  decay depends on the magnetic field strength in the ICM as,

$$\frac{P_{syn}}{P_{\gamma}} \propto \left\langle \frac{B^{1+\alpha}}{B^2 + B_{IC}^2} \right\rangle, \quad (26)$$

where  $\langle .. \rangle$  indicates an emission-weighted quantity and  $\alpha$  is the synchrotron spectral index. Consequently,  $\gamma$ -ray upper limits derived for clusters hosting giant radio halos provide corresponding lower limits to the strength of the magnetic field in the volume occupied by radio halos. For a few giant (and nearby) radio halos, including their prototype in the Coma cluster, current limits challenge a pure hadronic origin, because the values allowed for the magnetic fields are inconsistent (or in tension) with those estimated from studies based on Faraday rotation measures.<sup>260–262</sup> Figure 13 (left) shows the case of the Coma cluster radio halo, where the allowed region for the magnetic field is derived within a pure hadronic model by combining the Fermi-LAT limits with both the spectrum of the halo and its brightness distribution at 330 MHz.<sup>262</sup> In other words, assuming that rotation measures give a relatively fair view of the magnetic fields in clusters (Sect. 4.1, Fig. 13) and more explicitly do not seriously underestimate their strengths, the energy budget required for the CRp component to explain radio halos in the context of hadronic models is larger than that allowed by the existing limits to the cluster  $\gamma$ -ray emission.

The spectra of radio halos provide crucial information for the origin of the emitting CRe in the central Mpc-region of the hosting clusters. The accurate measurement of the integrated spectra of radio halos is a difficult task. Radio halos usually embed a number of individual sources and, sometimes, projected foreground and background sources, whose flux density needs to be carefully subtracted from the total diffuse emission. This requires

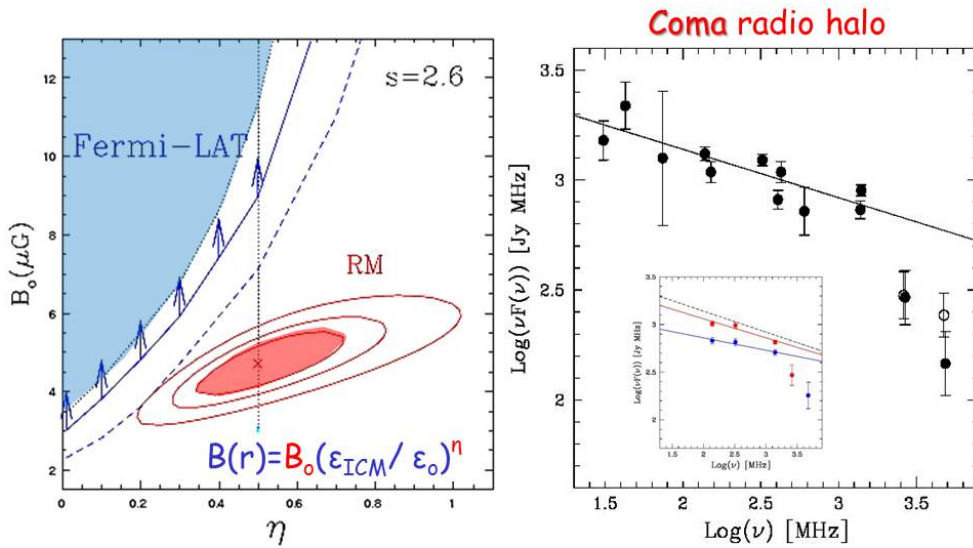


Fig. 13. Left panel: the allowed region for the central magnetic field  $B_0 - \eta$  parameter (defined in the bottom of the panel) derived from the combination of Fermi-LAT limits and the properties of the radio halo at 330 MHz (blue region), is compared with that derived from the analysis of RM (red region) (adapted from<sup>262</sup>). Right panel: the spectrum of the Coma halo (empty points at 2.7 and 4.8 GHz are corrected for the SZ-decrement). The inset is the spectrum of the Coma halo (corrected for the SZ decrement) extracted using an aperture of 13 (lower-blue) and 17.5 arcmin radius (upper-red). The spectra show the steepening at higher frequencies (adapted from<sup>266</sup>).

high quality imaging over a range of resolutions. Moreover, because of their steep spectra, diffuse cluster sources are best imaged at low frequencies. High quality, high resolution imaging at frequencies below 1.4 GHz has become available only very recently. For this reason, a meaningful spectrum with data points at three or more frequencies spread over  $\sim 1$  order of magnitude is currently available only for a few objects, e.g.<sup>218</sup>

The radio halo in the Coma cluster is the prototype of this class of radio sources.<sup>5,263,264</sup> It is a unique case, with spectral measurements spanning almost 2 orders of magnitude in frequency<sup>265</sup> (Figure 13, right). The measured spectrum significantly steepens at frequencies above about 1 GHz. A power-law that fits the data at lower frequencies overestimates the (SZ-corrected) flux measured at 2.7 and 5 GHz by factors of 2 and 3, respectively.<sup>266</sup> This suggests a break (or cut-off) in the spectrum of the emitting CRe at a maximum energy,  $E_{max}$ , around a few GeV. Establishment of the steepening of the spectrum of the Coma halo is an observational milestone, because it allows one to estimate the acceleration time-scale (or equivalently the efficiency) of the mechanism responsible for the origin of the CRe responsible for the radio halo. The maximum energy of accelerated CRe is given by

the competition between the acceleration rate and (for observable, GeV electrons) radiative losses. From eq. (22) the lifetime of radio-emitting CRe using viable magnetic fields in the Coma cluster is  $\tau_e \sim \text{few} \times 10^8$  yrs, which is then also the time-scale of the acceleration mechanism<sup>f</sup>. The existence of this spectral break implies that the mechanisms responsible for CRe acceleration must be of relatively low efficiency (long acceleration time-scale), or alternatively that they must intrinsically produce a break in the distribution of CRe at  $E_{max} \sim \text{few GeV}$ .

In the case of turbulent acceleration (Sect. 2.2.2) we can roughly estimate an acceleration time-scale (see eq. (15) with  $\delta B^2/B_0^2 \sim V_t^2/c_s^2$ )

$$\tau_{acc} \sim \frac{p^2}{\mathcal{D}_{pp}} \sim \frac{cl}{v_t^2}, \quad (27)$$

where  $V_t$  is the ICM turbulent velocity. With  $l \sim \text{kpc}$  and  $V_t \sim 100 \text{ km s}^{-1}$  the acceleration times,  $\tau_{acc} \sim 10^8$  yrs, providing a relative match at energies  $E_{max} \sim \text{few GeV}$  between acceleration and cooling. The spectrum of higher energy electrons will be steepened by the increasing relevance of cooling (see Figure 7 for a representative re-accelerated spectrum), thus leading to the observed break in the radio synchrotron spectrum at a frequency

$$\nu_{max} \approx C_{SYN} E_{max}^2 B \propto \frac{\mathcal{D}_{pp}^2 B}{(B^2 + B_{IC}^2)^2}. \quad (28)$$

where  $C_{SYN} \sim 2 \times 10^7$  if frequency, energy and magnetic field are measured in Hz, GeV and  $\mu\text{G}$ , respectively.

Schlickeiser et al (1987)<sup>267</sup> first realized the importance of the measurements of the spectrum of the Coma radio halo and indeed suggested an origin of the CRe based on stochastic acceleration due to turbulence, disfavouring other mechanisms that included the generation of secondary electrons by hadronic collisions. In this latter case the CRe spectrum extends in principle, to very high energies, if CRp extends to very high energies (say  $E_{CRp} > 100$  GeV), as indeed expected from the discussion in Sect. 2. Therefore, no intrinsic cut-off would be expected in the radio spectrum.<sup>25,96</sup>

Spectral behaviours qualitatively similar to that of the Coma halo are expected in other radio halos if they are powered by turbulent acceleration. However, the generality of this behaviour is still unclear from the observational side, because of the observational difficulties in obtaining reliable measurements of radio halos spanning an adequately large frequency range. As a matter of fact, the spectra of most giant radio halos are constrained by only a few data-points (typically 2-3) spanning less than one order of magnitude in frequency range, and are consistent with a simple power law<sup>s</sup>. Most importantly, however, in the last decade it has been found that the observed values of the slopes of the integrated spectrum

<sup>f</sup>This match applies, provided the acceleration process operates for a time-period that is not short compared to the required acceleration time-scale (energy doubling time). Otherwise, a balance between acceleration and losses obviously cannot be achieved.

<sup>s</sup>see however e.g.<sup>268,269</sup> for A2256

of radio halos span a broad range of values,  $\alpha \sim 1 - 2$  ( $F(\nu) \propto \nu^{-\alpha}$ , e.g.<sup>38,211,218</sup>). This implies (at least) that the synchrotron spectrum of radio halos is not a *universal* power law, and puts constraints on the mechanisms responsible for the acceleration of the CRe. Particularly stringent constraints derive from halos with extreme spectral properties,  $\alpha \sim 1.5 - 2$ . In these cases the energy budget of CRs that would follow from the assumption that the energy distribution of CRe is a power law extending to lower energies, is unacceptably large.<sup>15,24,257,270,271</sup> One possibility is that the spectrum of the emitting CRe breaks towards high energies, producing a very steep radio spectral shape within the observed frequency range. This requires, of course, that such a break in the CRe spectrum is formed at suitable energies (i.e., in the GeV range responsible for the radio emissions).<sup>15,272</sup> Under this hypothesis the constraints on the acceleration mechanisms are similar to those derived above for the Coma radio halo.

#### 4.2.2. *Open problems and Future Efforts*

Despite the discussion above (and in Sect. 2.2.2) that provides arguments that are consistent with the hypothesis that giant radio halos trace turbulent regions in merging clusters and possibly originate due to (some type of) turbulent-related mechanism of CRs acceleration, many important points are still open. First of all, the role of secondary CRe is still unclear. It is true in the case of several radio halos that  $\gamma$ -ray limits and arguments connected with the observed radio spectra (and brightness distributions) seriously challenge a purely hadronic, simply injected  $e^{\pm}$  population for the observed emission. However, it is also fair to say that in general the existing data are still insufficient to discriminate clearly among different more complex scenarios. Most important, secondaries will exist at some level, since CRp are virtually certain to exist in clusters and will undergo inelastic collisions with the thermal ICM (Sects. 2.3 and 3). Consequently Mpc-scale radio emission should be generated at some level in “all” clusters with luminosities that should vary depending on the cluster dynamical histories (e.g., accretion shock histories) and/or magnetic properties (e.g., histories of magnetic flux injection and amplification).<sup>23,36,239,273,274</sup> In this respect future radio surveys with sensitivities to diffuse cluster-scale emission much better than current surveys, will provide unique and critical constraints to the role played by secondaries. For reference, *Hybrid models*, that assume radio halos to be generated by the (re)acceleration of secondary particles by turbulence in cluster mergers,<sup>172,177</sup> predict that secondaries generated in more relaxed systems produce radio emission with luminosity marginally smaller than current upper limits in Figure 12.<sup>36,172</sup>

Future radio surveys are likely to produce a big step forward in our understanding of the formation and evolution of radio halos. The measure of the formation rate of radio halos in galaxy clusters and its dependence on the cluster thermal properties (dynamics, mass, temperature etc) provides unique information on the physics of these sources. One of the main limitations of current studies is that only X-ray luminous clusters have been scrutinized with adequate radio observations, whereas only very poor information is available for less luminous systems<sup>38,219</sup> that are expected to host fainter halos according to the correlation in Fig. 12. A similar limitation applies also to the most recent studies that focus

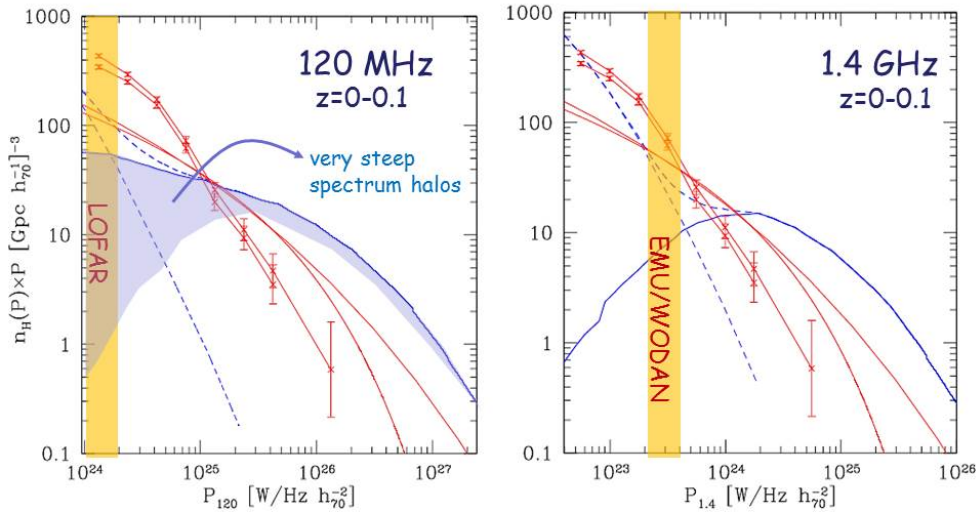


Fig. 14. Radio luminosity functions of giant radio halos at  $z = 0 - 0.1$  predicted by different models at 1.4 GHz (right) and 120 MHz (left). Blue lines are based on turbulent re-acceleration models (solid line) and secondary emission (thin dashed lines) from ‘off state’ systems (i.e. undetected halos in Fig. 12); the thick dashed-lines represent the sum of the two contributions (adapted from<sup>273</sup>). Red-solid lines are from<sup>276</sup> while the red-points are from numerical simulations by<sup>274</sup> that are based on secondary models and assume that 10% of systems host radio halos (note that those simulations include both giant and mini halos). The blue region in the left panel shows the contribution to the luminosity function at 120 MHz due to very steep spectrum halos that are predicted in the turbulent re-acceleration model and do not contribute at higher frequency. The nominal sensitivity level of LOFAR and EMU/WODAN surveys is also reported.

on mass-selected cluster samples, that are based on SZ-catalogs, that are indeed limited to cluster masses  $M_{500} \geq 6 \times 10^{14} M_{\odot}$ .<sup>246</sup> These limitations are due to the limited sensitivity of present radio observations, but soon will be eliminated thanks to a new generation of radio telescopes, such as LOFAR, ASKAP, and in the longer period, the SKA, that will survey the sky with unprecedented sensitivities to the cluster scale diffuse emission.

LOFAR and, to a somewhat lesser extent, MWA and LWA, will be particularly important because they will observe at lower frequencies, between 10 MHz and 200 MHz, stepping into a basically unexplored frequency range. LOFAR observations and their combination with JVLA<sup>4</sup> observations and, for nearby radio halos, observations with single dish radio telescopes (such as GBT and Effelsberg), will allow derivation of spectral mea-

<sup>4</sup><https://science.nrao.edu/facilities/vla>

measurements of radio halos over unprecedented, wide frequency coverage, thus providing crucial constraints on theoretical models. In particular, one of the most intriguing theoretical hypotheses is the existence of radio halos with very steep spectra that are undetected by radio surveys at higher frequencies and that should be discovered by observations at lower frequencies.<sup>15,272,273,275</sup> Such a hypothesis is based on turbulent acceleration models that predict that less energetic merger events (less turbulent) generate radio halos with very steep spectra. Since these less energetic mergers are more common, one can speculate that steep spectrum halos constitute a large population of halos that is presently invisible. According to present calculations that use the crude assumption that a *fixed* fraction of the cluster-merger energy goes into MHD turbulence available for particle acceleration on Mpc-scale, the LOFAR surveys should detect about 500 new radio halos. About half of these halos should have very steep spectra.<sup>273,275</sup> Despite their still-early development and need for greater sophistication, current models have been able to make some notable predictions<sup>u</sup>. For instance, re-acceleration models predict that the shape of the Luminosity Functions of radio halos change with observing frequency due to the contributions of the expected population of steeper-spectrum halos at lower frequencies (Figure 14). This differs from predictions based on other scenarios, including the hadronic model, where all halos should have to a first approximation similar spectra (independent of the mass of the hosting clusters and of the energy released during mergers), and provides a valuable way to put constraints on the origin of these sources with future radio surveys. In particular, as shown in Figure 14, the most powerful way will be probably the combination of LOFAR surveys, at low frequencies, with future surveys with ASKAP or Apertif<sup>v</sup>, at higher frequencies.

### 4.3. Mini Halos

In addition to the disturbed, merging clusters that have been found to host giant radio halos, a number of relaxed, cool-core clusters host faint, diffuse radio emission with a steep spectrum and a size comparable to that of the cool-core region<sup>38</sup> (Figure 15), so substantially smaller than the giant halos. As a first approximation one might have thought these sources as a version of giant radio halos scaled on smaller scales of the order of few 100 kpc in size rather than Mpc size. However, the two classes of radio sources show prominent differences. First of all, in clear contrast to giant radio halos, mini halos are always found in dynamically relaxed systems suggesting that cluster mergers do not play a major role for their origin. Also the synchrotron volume emissivity of mini halos differs from that of giant halos, being typically larger.<sup>277,278</sup> Whether the underlying physical mechanisms that accelerates the CRE in mini halos differ substantially from the analogous mechanisms in giant radio halos is still unclear. Clusters hosting mini halos always have central radio-loud AGNs exhibiting outflows in the form of radio lobes and bubbles inject CRE into the central

<sup>u</sup>We note that, independent of the theoretical scenario that is adopted for the origin of radio halos, predictions of the formation rate of radio halos and their number counts are severely limited by uncertainties in the properties of cluster magnetic fields - including their evolution with cluster mass and cosmic epoch - and CR dynamics.

<sup>v</sup><http://www.astron.nl/general/apertif/apertif>

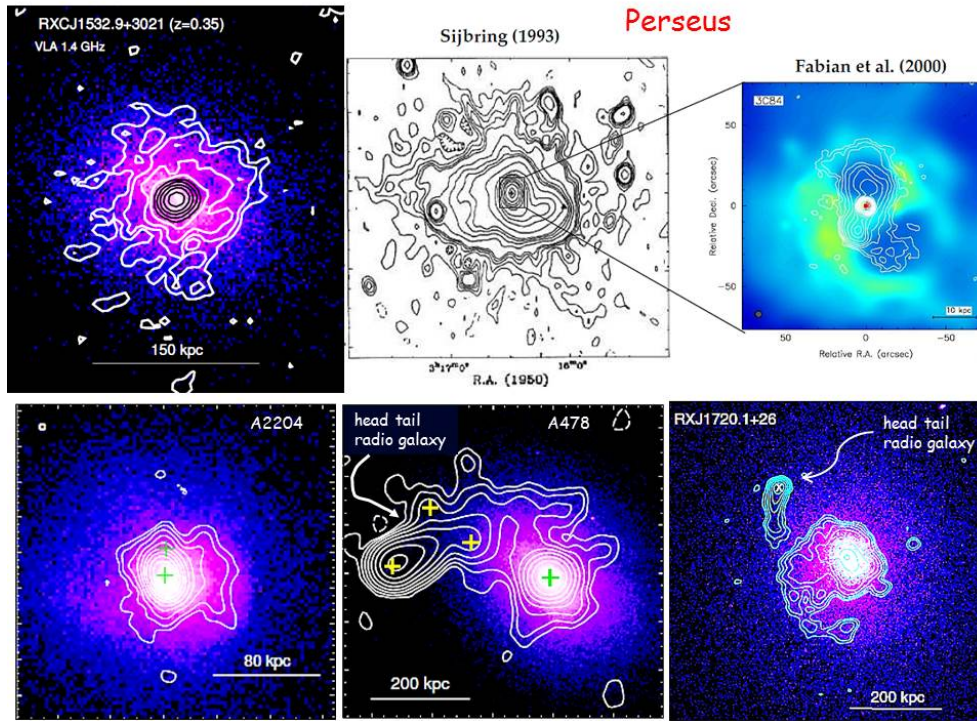


Fig. 15. Images of radio mini-halos (contours) and the X-ray emission from the hosting clusters (colors). Credits:<sup>212</sup> for RXCJ1532, A2204, A478, Giacintucci in prep. for RXCJ1720, and<sup>213</sup> for Perseus.

regions of galaxy clusters (Sect. 2.1). In principle these AGNs could represent the primary source of the CRs in mini halos, however they are not sufficient by themselves, at least without some dynamical assistance, to explain the diffuse radio emission. In particular, a *slow diffusion problem* once again exists for mini halos; that is, the energy loss time scale of the radio emitting CRE is still much shorter than the time needed by these particles to diffuse efficiently across the emitting volume.

Similarly to giant halos, two physical mechanisms have been identified as possibly responsible for the radio emission in mini halos: i) re-acceleration of CRE (leptonic models or re-acceleration models) and ii) generation of secondary CRE (hadronic or secondary models).

According to leptonic models mini halos originate due to the re-acceleration of pre-existing, relativistic CRE in the ICM by turbulence in the core region, e.g.<sup>279</sup> So, this model is similar in character to the turbulence model for giant halos, except that the responsible turbulence is concentrated in the cluster core region. In this case obvious sources of the seed CRE are, for example, the buoyant bubbles that are inflated by the central AGN and disrupted by gas motions in the core.<sup>121, 122, 277</sup> A key question in this model is the origin of the turbulence responsible for re-accelerating the electrons. Unlike giant halos, merger shocks and Mpc-scale motions/flows would not be candidates. Gitti et al.(2002)<sup>279</sup> originally proposed

that the cooling flow of gas inward within the core could generate the needed turbulence. More recent X-ray observations however have shown that these “classical cooling flows” do not materialize, e.g.<sup>280</sup> On the other hand, observations suggest that even relatively relaxed clusters have large-scale gas motions in their cores at significant fractions of the local sound speed. The clearest observational signatures of these gas motions are spiral-shaped cold fronts seen in the majority of cool-core clusters.<sup>281</sup> These cold fronts are believed to be produced by the cold gas of the core sloshing in the clusters deep potential well, in response to passing dark matter subhalo motions, for example. Those sloshing motions, can advect ICM across the cluster core and can also produce turbulence there.<sup>132, 282–284</sup> Remarkably, a correlation between radio mini halos and cold fronts has been discovered in a few clusters and has been used to suggest a connection between radio mini halos and turbulence generated by the sloshing motions.<sup>285</sup> Recent simulations<sup>286</sup> support this hypothesis and have shown that the motions and turbulence generated by core sloshing in galaxy clusters can re-accelerate and spatially redistribute seed CRE. Those CRE and magnetic fields amplified at the same time produce radio emission that resembles mini halos, being diffuse, steep spectrum, and connected with the spatial features of the X-ray emitting gas. As noted early in this review, AGN activity also can dump considerable kinetic energy into the ICM and drive cluster-core scaled ICM motions (Sect. 2.2.2). While these motions can mix CRE into ICM relatively near the AGN outflows, larger scale flows, such as sloshing are probably necessary for those CRE to become broadly distributed across the full cluster cores. Current observational information on turbulent motions in cool cluster cores coming from X-ray emission lines is limited by relatively poor available spectral resolution. In the few cases of compact cool cores the turbulent velocities have been constrained and the turbulent pressures (due to fluctuations on scales much smaller than the size of these compact cores) are found to be less than  $\sim 10\%$  of the thermal pressures.<sup>287, 288</sup> Future observations with ASTRO-H will provide much better constraints as they will be able to reveal the presence of small-scale turbulence (with velocities down to about 100 km/s) from the study of X-ray lines.<sup>154, 155</sup>

The second mechanism proposed for the origin of mini halos is, just as for giant halos, based on the generation of secondary particles via inelastic collisions between CRp and thermal protons.<sup>24, 239, 274</sup> In this case the primary CRp could be provided by the central AGN and then advected, streamed or diffused across the cluster core. In this case an interesting issue is the possible connection between these CRp, which ultimately generate the observed mini halos in this picture, and the heating of the ICM in the region of the cool core. Colafrancesco & Marchegiani (2008)<sup>289</sup> proposed a scenario where the cooling of the gas in the cool cores is balanced by the heating due to the CRp via Coulomb and hadronic interactions. In order to balance the cooling of the gas, these models assume that CRs in cool cores carry a substantial fraction of the energy of the ICM, a condition that however is ruled out by current  $\gamma$ -ray observations that put severe limits to the energy budget of CRs (Sect. 3.3) in core regions.<sup>33</sup> More recent approaches that model the CRp-driven heating mechanism rely on the possibility that CRp streaming and the related generation of MHD waves can heat the ICM in the cool cores with an efficiency that may be much larger than that due to Coulomb and hadronic interactions.<sup>290, 291</sup> Under this hypothesis several calcu-



lations have derived consistent pictures of cool-core heating and generation of radio mini halos.<sup>292</sup>

Discrimination between a leptonic and hadronic origin of radio mini halos is very challenging due to severe limitations of current observational constraints. Although a correspondence between radio mini halos and cool core clusters is well established, current radio studies do not provide an exhaustive view of the occurrence of radio mini halos in galaxy clusters more generally. For example, it is still not clear whether these radio sources are common or rare in cool cores.<sup>212</sup> In addition,  $\gamma$ -ray upper limits from the Fermi satellite and ground based Cherenkov telescopes are not yet deep enough to put strong constraints on the origin of these radio sources. For example, these limits do not put significant tension on a purely hadronic origin of mini halos.<sup>27,31</sup> Generally, in comparison with the case of giant halos, the combination of radio and  $\gamma$ -rays constraints are less restrictive for mini halos, because the ratio of  $\gamma$ -ray luminosity to radio luminosity is smaller. This is due to the fact that the likely value of the average magnetic field in the much smaller and more central volume occupied by mini halos is larger than that in the much bigger volume of giant halos (see eq. 26). In addition, we note that for the best test case, the mini halo in the nearby Perseus cluster, the presence of strong  $\gamma$ -ray emission from the central radio source 3C 84 (NGC 1275) does not allow one to put stringent limits on the diffuse emission from the cluster core in the critical 0.2-10 GeV band.<sup>30</sup>

One possibility to discriminate between different models is to look for differences in the integrated spectrum and spectral index maps. For example, compelling evidence for very steep spectra and/or for the existence of spectral breaks at high frequencies would favour a re-acceleration scenario rather than a hadronic origin in the mini halos. Similarly to the case of giant halos, current mini halo radio observations cover too short a frequency range to constrain spectral curvatures. Furthermore, the fractional contribution to the observed flux that is provided by discrete radio sources embedded in the halo volume is larger for mini halos, making good spectral measurements more challenging than in the case of giant halos.<sup>38,212</sup> Better spectral constraints might come from future observations at low (e.g. with LOFAR) and higher (JVLA) radio frequencies. These radio telescopes, and their combination, should allow deeper imaging, with unprecedented dynamic range, and measurement of the diffuse synchrotron spectrum over a fairly wide frequency range.

#### 4.3.1. *A connection between giant and mini radio halos ?*

An obvious, interesting question is whether there is any connection between mini halos and giant radio halos or do they have independent physical origins? Despite the apparently distinct population distributions, there are, in principle, several arguments in support of a possible connection. Indeed, one could argue that the driven flows and turbulent motions that destroy the ICM cores of clusters during merger could also transport and re-accelerate CRs on larger, Mpc, scales. This, in fact, is a “generic” candidate-scenario that we propose to switch off bright mini halos and to begin powering giant radio halos in dynamically active systems. In this scenario complex situations where a central mini-halo is embedded in a lower brightness radio emission on larger scales should exist in dynamically “intermediate”

systems; Abell 2142 could be one example.<sup>219,293</sup>

In a recent work Zandanel et al.(2013)<sup>274</sup> proposed that mini-halos are primarily of hadronic origin, while giant radio halos experience a transition from central hadronic emission to leptonic emission component in the external regions due to CRe re-acceleration. Potentially, also diffusion and advective transport of CRs in the ICM can induce an evolution from mini to giant halos (and vice-versa), assuming that this process is sufficiently fast (i.e.,  $\leq$  Gyr) on spatial scales of clusters cores<sup>w</sup>. A similar evolution could be driven by the evolution (amplification and dissipation) of the magnetic field in the cluster core and periphery in response to mergers.<sup>239,250</sup>

Observations with the next generation of observational facilities and similar advances in numerical simulations will hopefully clarify these issues in the near future.

#### 4.4. *Giant Radio Relics*

Some merging clusters host peripheral, giant radio relics. As in the case of giant radio halos, a few tens of giant relics have been discovered so far. Radio relics differ from radio halos in the morphologies, peripheral locations and polarization (typically being up to 30% level in integrated linear polarization)<sup>38</sup> (Figure 16). These properties provide a clear starting point in establishing their origin. Specifically, there is broad consensus that the giant radio relics trace shocks outside cluster cores, probably relatively strong merger shocks, where the emitting CRe can be accelerated or re-accelerated.<sup>23,39,97–99,196,214,294–300</sup> This model is based on the physics described in Sect. 2.2.1.

In addition to probing the origin of CRs in galaxy clusters, relics are also important probes of the magnetic field properties in the ICM periphery, as they are found at distances up to a large fraction of the cluster virial radius, e.g.<sup>39</sup>

##### 4.4.1. *Shock–relics connection*

The association between giant radio relics and shocks is based partly on the usually elongated morphologies of the relics, consistent with a shock seen relatively edge-on. In addition, the fact that in some cases the relics occur in pairs on opposite sides of the cluster core<sup>214,216,294,301</sup> is telling, since emerging merger shocks should form in such pairs. In those paired relic cases a line between the relics is typically consistent with an apparent merger axis, as established by other observations, such as in the X-rays. In addition, the fact that relics are strongly polarized with an orientation that generally implies the magnetic field is aligned with the long axis of the relic, suggests that they originate in regions where the magnetic field is compressed in the shock plane.<sup>39,214,302</sup> Most important, in a number of cases merger shocks that have been detected using X-ray observations coincide closely with radio relics (or with sharp edges of radio halos) reinforcing the idea of a direct connection between shocks and the acceleration of the radio emitting CRe in those regions.<sup>78,303–310</sup>

<sup>w</sup>Streaming has also been proposed to explain the bimodality of giant radio halo populations<sup>46,192</sup>

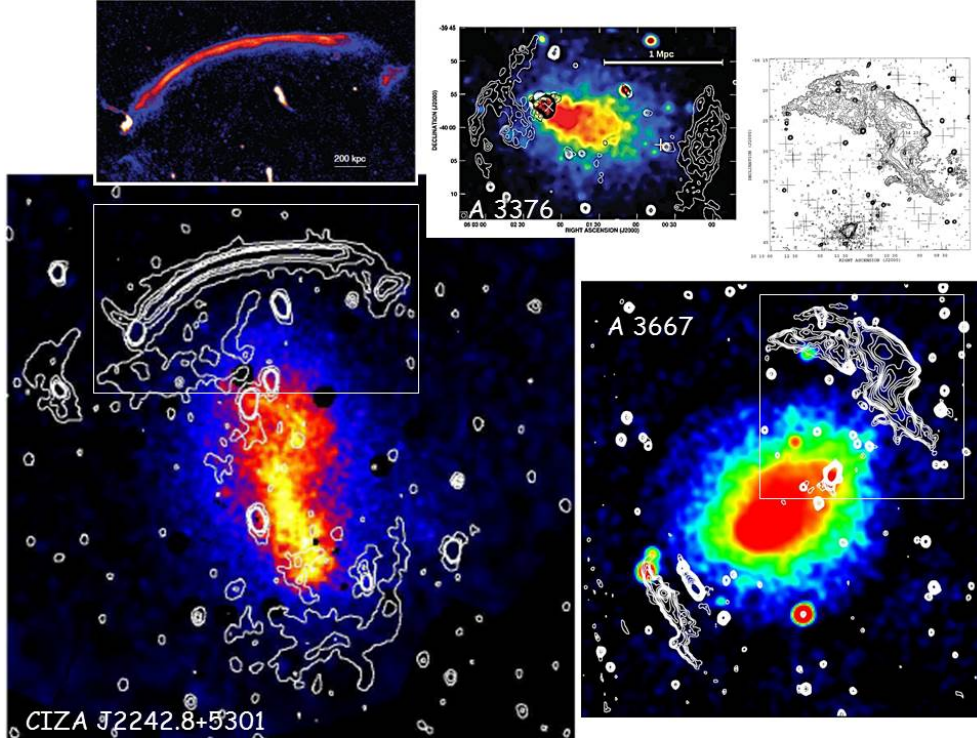


Fig. 16. Images of giant radio relics (contours) overlaid on the X-ray emission from the hosting systems (colors). The three radio relics are reported with the same physical scale. Upper-left and upper-right panels highlight the high-resolution radio images of the northern relics in CIZA2242 and A3667, respectively (credits:<sup>214,215</sup> for CIZA2242,<sup>216</sup> for A3667,<sup>217</sup> for A3376).

Presumably the observed CRE are accelerated or re-accelerated at these shocks. Those CRE are then advected into the downstream region at the velocity of the downstream flow,  $V_d$  as they cool from ICS and synchrotron losses. This process sets the thickness of radio relics as seen at different frequencies; the emitting CRE can travel a maximum distance from the shock  $= V_d \tau$ , where  $\tau$  is the radiative life-time of CRE emitting at the observed frequency  $\nu_o$ ,  $\tau \propto \nu_o^{-1/2}$ . Typically the life-time of CRE radiating in the radio band is of the order of 100 Myr implying a transverse size of radio relics  $\sim 100$  kpc for a reference downstream velocity  $V_d = 1000 \text{ km s}^{-1}$  and ICS dominated losses (with  $z \sim 0 - 0.3$ ). This is consistent with observations, once projection effects are properly taken into account. In this case radio synchrotron spectral steepening with distance from the shock front is expected in radio relics with spatially resolved cross sections as a consequence of the fact that the oldest population of CRE is also the most distant from the shock. This expectation is in agreement with several observations that provide evidence for steepening in radio relics along their transverse direction, from their front to the back.<sup>214,302,303</sup> Furthermore, recent analyses have shown evidences for synchrotron spectral curvatures along the transverse dimension of a few particularly favorable relics and also that the curvature increases

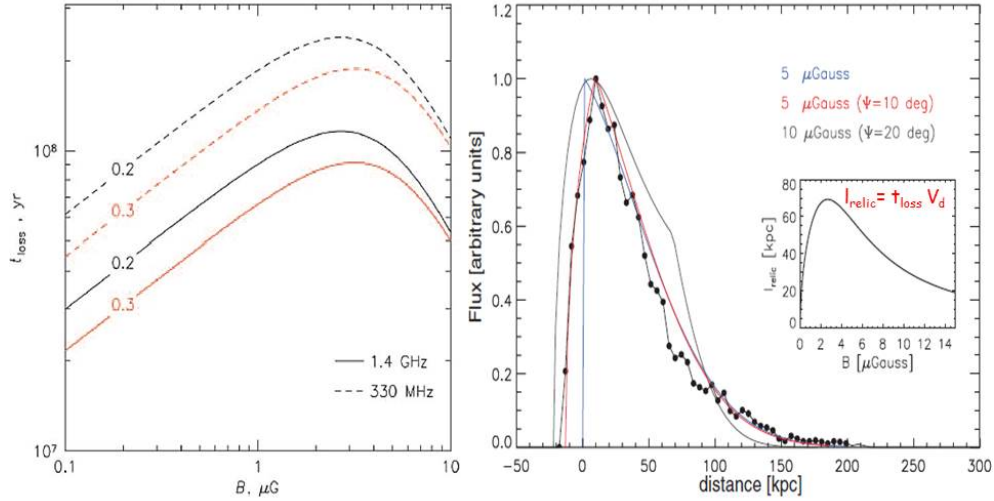


Fig. 17. Left panel: the life-time due to synchrotron and inverse Compton losses of CRE emitting at 330 and 1400 MHz (dashed and solid lines, respectively) as a function of the magnetic field strength in the downstream region. Calculations are shown for redshift  $z = 0.2$  and  $0.3$  (black (upper) and red (lower) lines, respectively) (adapted from<sup>299</sup>). Right panel: the brightness profile of the northern radio relic in CIZA2242 (data-points) compared to scenarios that assume different magnetic fields in the downstream regions and inclination angles. The inset shows the life time of the emitting particles as a function of the magnetic field and the relationship between the thickness of the relic,  $l_{relic}$  (distance), the life-time,  $\tau_{loss}$ , and the downstream velocity,  $V_d$  (adapted from<sup>214</sup>).

with distance in the downstream area.<sup>311,312</sup> The life-time of radio-emitting CRE in the downstream region depends also on the magnetic field,  $\tau \propto E_e^{-1} B^{1/2} / (B^2 + B_{IC}^2)$ , and the energy of electrons emitting at frequency  $\nu_o$  is  $E_e \propto (\nu_o/B)^{1/2}$ . For this reason the measure of the transverse size of relics at a given frequency  $\nu_o$ , that is  $= V_d \tau$ , provides also constraints on the magnetic field strength in these sources, provided the downstream velocity is known;<sup>299</sup> this is shown in Figure 17. The downstream velocity,  $V_d = c_s(M^2 + 3)/(4M)$  ( $c_s$  is the sound speed in the upstream region and  $M$  is the shock Mach-number), can be derived from the density/temperature jumps at the shock measured by X-ray observations, or alternatively from the synchrotron injection spectrum measured at the leading edge of the relic (assuming this is the location of the physical shock), using  $\alpha_{inj} = (\delta_{inj} - 1)/2$  (eq.3).

#### 4.4.2. Open problems & particle re-acceleration at shocks

The above observational facts support a connection between giant radio relics and merger shocks, suggesting that CRe are energized locally at these shocks and then age in the downstream region. However these observations do not tell us more about the physics of the acceleration mechanisms. Shocks discovered in the X-rays, including those that coincide with radio relics, are apparently weak, with Mach numbers determined from the X-rays estimates for density and/or temperature jumps across the shock region,  $M \approx 1.5 - 3$ .<sup>77,281</sup> High resolution cosmological simulations are consistent with the observational data, suggesting that shocks with  $M > 3$  are rare well inside cluster virial radii.<sup>13,71-73,79,313</sup> This, however, poses a problem for the origin of giant radio relics, because, as discussed in Sect. 2.2.1, weak shocks are expected to be relatively ineffective as particle accelerators, especially if they are accelerating CR from nonrelativistic energies. This is partly because the equilibrium DSA spectrum of locally injected CRs in such shocks is quite steep (eq. 3), so most particles injected at the shock carry away relatively little energy. In addition, thermal leakage injection is likely to be less effective in weak shocks than strong shocks.<sup>91</sup> Using reasonable parameters for shocks with  $M \leq 3$ , less than  $\sim 0.01\%$  of the thermal ion flux through such shocks should be injected into the CRp population and less than a few percent of the shock energy flux should be transferred to freshly injected CRp.<sup>92,196</sup> It is important to keep in mind that all the above efficiencies refer to CRp, while CRe are the particles observed in radio relics. Again, as pointed out above, primary CRe are much more difficult to inject from the thermal pool into the CR population than CRp (Sect.2.2.1). In the galactic CRs  $N_{CRe}/N_{CRp} \sim 1/100$ , presumably reflecting that constraint. An electron fraction even that large, and likely representing DSA at strong shocks, is already a theoretical challenge. Thus, merger shocks seem very unlikely to inject thermal electrons and then to accelerate them to relativistic energies with efficiencies high enough to extract more than a tiny fraction of a percent of the energy flux through the shock.<sup>106</sup> Thus, the question is whether radio relics can be powered by the acceleration of the thermal particles of the ICM at weak shocks. This may point to an alternate source for the CRe that are available to be re-accelerated in the shocks by the DSA process.

The synchrotron luminosity that is emitted in the radio band by assuming that a fraction  $\eta_{CRe}$  of the kinetic energy flux through the shock-surface,  $S$ , is transferred to supra-thermal (and relativistic) CRe is (see also<sup>99</sup>):

$$v_o P_{Syn}(v_o) \sim 1/2 \rho_u V_{sh}^3 \eta_{CRe} S \left(1 + \left(\frac{B_{IC}}{B}\right)^2\right)^{-1} \mathcal{F}^{-1}(\alpha(M)) \quad (29)$$

where the dimensionless function  $\mathcal{F}$  is a few for  $\alpha_{inj} = 0.5$  and rapidly decreases for steeper spectra (weaker shocks, eq. 3). That drop results from the fact that a progressively smaller fraction of the energy of the accelerated CRe is associated with GeV radio-emitting electrons at these shocks. Figure 18 shows the radio luminosity (left panel) and luminosity per unit surface area (right panel) of 25 giant radio relics as a function of their projected distance from cluster centers (see Figure caption for details). Figure 18 highlights that a large scatter exists in the radio luminosity of relics at a given distance. This may be due

to projection effects (namely the relics with lower radio power are seen at large angles) or it may imply large variations of either the acceleration efficiency,  $\eta_{CRe}$ , or the magnetic field strength in radio relics. The most luminous radio relics in Fig. 18 put tension on the standard scenario where the radio-emitting CRe are accelerated at shocks from the thermal pool. Indeed if we adopt typical parameters of the ICM at the location of peripheral radio relics,  $V_{sh} \sim 3000 \text{ km s}^{-1}$  and  $\mathcal{F} \sim \text{few}$ , Eq. 29 implies that  $\eta_{CRe} \geq 10^{-4}$  is necessary to generate relics with synchrotron luminosity above  $\sim 10^{41} \text{ erg/s}$ . For some of the most

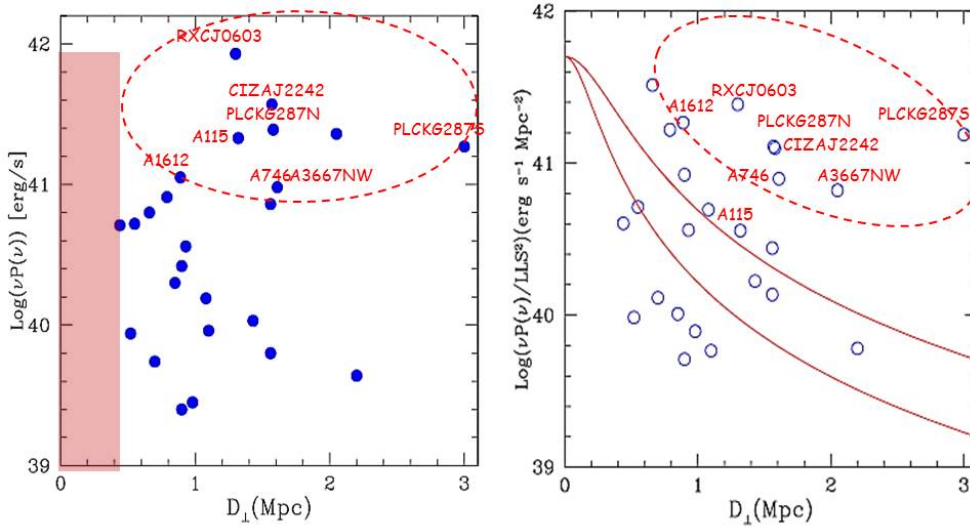


Fig. 18. Left panel : the synchrotron radio luminosity ( $vP(\nu)$ ) evaluated at 1400 MHz) as a function of projected distance from cluster center for 25 giant radio relics with unambiguous classification. Data are taken from the compilations in,<sup>38,42</sup> although we only use the 25 sources that can be “unambiguously” classified as giant radio relics. Right panel : the synchrotron radio luminosity ( $vP(\nu)$ ) evaluated at 1400 MHz) per unit relic-surface area as a function of projected distance for the same relics in the left panel. Solid lines mark reference radial behaviours of the kinetic energy flux per unit area through shocks with equal velocity (in arbitrary units); they are obtained using typical beta-models for the gas-density distribution in the hosting clusters. The pink vertical band in the left panel marks the typical minimum distance where giant radio relics are found.<sup>314</sup>

powerful relics in Fig. 18, such as RXCJ0603, A3667 and CIZAJ2242, a Mach number 2.4-3 shock is seen by X-ray observations.<sup>307,309</sup> In these cases if we assume a reference acceleration efficiency of CRp at weak,  $M \sim 2 - 3$ , shocks of about 1%, e.g.,<sup>81</sup> an unusually large CRe/CRp ratio  $\sim 0.1$  is required to match the observed synchrotron luminosity. Another problem faced by the standard scenario where relics originate from shock accel-

eration of thermal particles is that in several cases the observed radio spectrum is flatter than that expected from DSA by assuming the Mach number of shocks derived from X-ray observations (eq. 3).<sup>307,309</sup> For example, the well studied relic in CIZA J2242.8+55301 has a radio spectra at the putative shock location  $\alpha_{inj} = (\delta_{inj} - 1)/2 = 0.6$  (so,  $\delta_{inj} = 2.2$ ), implying from eq. 3 a rather large shock Mach number  $M = 4.6$ ,<sup>214</sup> if the radiating electrons represent a locally injected population. On the other hand, X-ray observations with Suzaku derived a Mach number  $\sim 3$  from the temperature jump at the relic,<sup>307</sup> which would imply  $\alpha_{inj} \simeq 0.75$ . In this respect it is worth mentioning that numerical simulations show variations of the Mach number over shocks<sup>315</sup> that potentially might produce some differences in the shock Mach numbers derived from X-rays (temperature or density jumps) and from radio. In this case the radio Mach number would be biased high because synchrotron emission is likely to be locally stronger in regions with higher Mach number.

In principle, all the challenges discussed above can be naturally circumvented by adopting a scenario where radio relics are generated by the re-acceleration of pre-existing (seed) CRe at merger shocks.<sup>97,299,300</sup> If a pre-existing population of CRs with a hard (flat) spectrum passes through such weak shocks, DSA can enhance the energy content of those CRs by a factor of a few. This makes DSA re-acceleration at merger shocks a relatively more efficient process.<sup>196</sup> Additionally, the re-accelerated particle spectrum is similar to the spectrum of the pre-existing population if the latter is flat, so not the classic DSA spectrum for shock injected CRs given in eq. 3.<sup>92,196</sup> The physical acceleration is still DSA, however; the change reflects only the assumed source of particles being accelerated. The potentially higher efficiency of re-acceleration in these shocks is possible because the acceleration time needed to double the energy of each CR can still be relatively short (see eq. 4). In this case a model that can account for the observed properties of CIZA J2242.8+55301 could involve a Mach 2 shock re-accelerating an upstream CRe population with an energy spectral index,  $\delta = 2.2$  and a plausible upstream CRe pressure  $\sim 10^{-4}$  compared to the upstream thermal pressure.<sup>97</sup> Then the challenge becomes defining acceleration processes just upstream of the shock (since radiative lifetimes are still very short), such as, e.g., turbulence, that can account for the CRe population entering the shock (Sects. 2.2.2, 4.2-4.3).

$\gamma$ -ray upper limits (Sect. 3.3) may provide a complementary way to constrain the origin of radio relics, because the ratio of  $\gamma$  and radio-relic luminosities essentially resembles the ratio of the acceleration-efficiency of CRp and CRe at clusters shocks. In principle this also applies to the case of re-acceleration, as the same shocks would re-accelerate both CRe and CRp. Their relative abundances are then the principal uncertainty. According to Vazza & Bruggen (2013),<sup>316</sup> by assuming the standard paradigm for the origin of giant radio relics, based on shock acceleration or re-acceleration, and a “canonical” ratio CRp/CRe, too many CRp should be produced in galaxy clusters violating current  $\gamma$ -ray limits. One possibility to reconcile a shock-acceleration origin for radio relics with the current lack of  $\gamma$ -rays from clusters, would be to assume that cluster shocks accelerate CRe and CRp with an “unusually” large CRe to CRp energy ratio  $\geq 0.1$ . Apparently, this is in contrast with constraints based on SNR (which, however, refer to very different environments and strong shocks) and with several theoretical arguments (Sect. 2.2.1). However recent PIC simulations (that are focused however on strong shocks) suggest that the configuration of the magnetic field

may play an important role, with quasi-perpendicular shocks being efficient CRe accelerators.<sup>106</sup> This explanation for relics generally, would seem, then, to require magnetically perpendicular shocks over Mpc scales, or at least perpendicular shock geometry being exceedingly common. As we will discuss in Section 5.2 an “unusually” large ratio CRe/CRp at clusters shocks would also have consequences for the  $\gamma$ -ray emission from galaxy clusters produced via ICS.

However, we also mention that another possibility to reconcile a shock-re-acceleration origin of relics with  $\gamma$ -ray limits is that the spectra of the pre-existing CRe differs from a power law and breaks at a maximum Lorentz factor  $\gamma \sim 1000$ ; this does not apply to shock acceleration. In this case re-acceleration from weak shocks could provide high-energy CRe without accelerating CRp too much, e.g.<sup>316</sup> Rather the pre-existing electron population is “bumped-up” in energy enough at the shock to take it from an invisible to a visible state. We note that this scenario for the pre-existing CRe is somewhat similar to that assumed in several calculations of turbulent re-acceleration for giant radio halos (Sect. 4.2 and also Fig. 7) and could be motivated by the fact that the life-time of CRe in the ICM is maximum at energies in the range 0.1-0.3 GeV (Fig. 8).

## 5. High energy emissions from galaxy clusters

Non-thermal high energy emission from galaxy clusters is an unavoidable consequence of the presence of energetic CRe in the ICM as shown by radio observations (Sect. 4). High energy emission is also expected from the theoretical scenario of CR acceleration and confinement discussed in Sects. 2 & 3. Standard mechanisms for the production of high energy photons from the ICM are supra-thermal bremsstrahlung from supra-thermal and primary CRe, ICS of seed photons from primary and secondary CRe, and the decay of  $\pi^0$  generated by CRp-p collisions. In addition, if ultra-high-energy CRs are present in the ICM, the CRe produced through the interaction of these CRs with ambient photons will produce both synchrotron and ICS emission at high energies. In this Section we will discuss the relevant processes, current observational constraints and future prospects for hard-X-ray emission and  $\gamma$ -ray emission from galaxy clusters.

### 5.1. *Hard x-ray emission from nonthermal electrons*

While thermal emission dominates ICMs in the keV energy range, it declines rapidly at higher energies, allowing the possibility of detection of non-thermal excess emission at energies  $> 10$ -20 keV. ICS of CMB photons (from both primaries and secondary CRe) and supra-thermal bremsstrahlung are expected to be the most important mechanisms responsible for hard X-rays in the ICM.<sup>11,317-320</sup> Their relative contributions depend on the spectral energy distributions of supra-thermal electrons and more energetic CRe in the ICM. The formation of prominent hard, supra-thermal tails of electrons in the ICM is difficult, because Coulomb collisions with the thermal ICM induce a relatively efficient thermalization of the supra-thermal particles.<sup>160,161,163</sup> At the same time, however, a population of ultra-relativistic CRe exists in the ICM, as demonstrated by the diffuse radio sources (halos and relics) discussed in Sects. 4.2-4.4. Consequently, ICS of CMB photons is an unavoidable



process that produces some level of high energy emission in galaxy clusters.<sup>321</sup> The typical energy of ultra-relativistic electrons emitting photons observed in the hard X-ray band (with energy  $E_{ph}$ ) via ICS of the seed CMB photons is:

$$E_e(\text{GeV}) \approx 3 \left( \frac{E_{ph}}{30\text{keV}} \right)^{\frac{1}{2}}, \quad (30)$$

while that of CRe emitting synchrotron radiation, emitted at redshift  $z$  and observed at frequency  $\nu_0$  is

$$E_e(\text{GeV}) \approx 7 \left( \frac{\mu\text{G}}{B} \frac{\nu_0}{\text{GHz}} \right)^{\frac{1}{2}} (1+z)^{\frac{1}{2}} \quad (31)$$

which means that the two processes sample pretty much the same population of CRe. More specifically, by assuming a power law energy distribution of the emitting CRe, in the form  $N(E_e) = K_e E_e^{-\delta}$ , both the synchrotron and ICS spectrum are power-laws with slope  $\alpha = (\delta - 1)/2$  and the ICS flux received by the observer at frequency  $\nu_X$  can be calculated from the synchrotron flux received at the frequency  $\nu_R$  :

$$F_{ICS}(\nu_X) = 1.38 \times 10^{-34} \left( \frac{F_{Syn}(\nu_R)}{\text{Jy}} \right) \frac{(1+z)^{\alpha+3}}{\langle B_{\mu\text{G}}^{1+\alpha} \rangle} \left( \frac{\nu_X/\text{keV}}{\nu_R/\text{GHz}} \right)^{-\alpha} \mathcal{C}(\alpha) \quad (32)$$

where  $F_{ICS}$  is in c.g.s. units,  $\langle \dots \rangle$  denotes the emission-weighted quantity in the emitting volume and the dimensionless function  $\mathcal{C}$  is given in Table 1 for different values of  $\alpha$ .

Table 1. Numerical values of the function  $\mathcal{C}$  in eq. 32

$\alpha$	0.7	0.8	0.9	1.0	1.1	1.2	1.3
$\mathcal{C}$	$4.78 \times 10^2$	$9.09 \times 10^2$	$1.70 \times 10^3$	$3.16 \times 10^3$	$5.83 \times 10^3$	$1.07 \times 10^4$	$1.95 \times 10^4$
$\alpha$	1.4	1.5	1.6	1.7	1.8	1.9	2.0
$\mathcal{C}$	$3.55 \times 10^4$	$6.45 \times 10^4$	$1.17 \times 10^5$	$2.11 \times 10^5$	$3.80 \times 10^5$	$6.83 \times 10^5$	$1.23 \times 10^6$

Eq. 32 shows the well known fact that measuring ICS from galaxy clusters in the hard X-ray band constrains (essentially provides a measure for, if the emission is detected) the average value of the magnetic field in the emitting region.

The search for diffuse ICS emission from galaxy clusters at hard X-ray energies has been underway for many years. One of the most persistent discussions of possible ICS detections involve the Coma cluster that hosts the prototype of giant radio halos (Fig. 1, and Sect. 4.2). Non-thermal hard X-ray excess emission has been claimed from Coma by Rephaeli & Gruber (1999, 2002)<sup>322,323</sup> with the Rossi X-ray Timing Explorer (RXTE) and by Fusco-Femiano et al. (1999, 2004)<sup>324,325</sup> with BeppoSAX. However, the detection has remained controversial.<sup>326–330</sup> We note that a  $\simeq 4\sigma$  hard X-ray excess emission, at a level consistent with that in,<sup>325</sup> was also found by<sup>330</sup> with the Suzaku HXD-PIN assuming a best fit value of the cluster temperature = 8.2 keV as derived from XMM-Newton data, that was consistent

with the temperature adopted in the analysis of.<sup>325</sup> However,<sup>330</sup> concluded that there was no statistical evidence for ICS emission within the field of view of Suzaku HXD-PIN because these authors used an higher temperature,  $= 8.45 \pm 0.06$  keV, that was obtained from a more complex fit combining XMM-Newton and Suzaku HXD-PIN data. Recently Wik et al.<sup>331</sup> performed a joint analysis of 58-month Swift Burst Alert Telescope (BAT) and of the XMM-Newton EPIC-pn spectrum derived from mosaic observations of the Coma cluster and found no evidence for ICS emission at the level expected from previous detections even if the such emission is assumed to be very extended. More recently Fusco-Femiano et al.(2011)<sup>332</sup> attempted to reconcile the limits and detections obtained from different instruments by carrying out a complex joint model-analysis based on the temperature and density profiles, derived from XMM-Newton and ROSAT data, and on the BeppoSAX data. So far, additional candidate clusters for ICS emission are the Ophiucus cluster<sup>333</sup> (but see<sup>334</sup>) and the Bullet cluster.<sup>335,336</sup> Other few cases where a detection of hard X-ray excess emission has been claimed are at low significance level.<sup>337-339</sup> Based on that we would reach the conservative conclusion that there is no compelling evidence for a detection of ICS emission from any ICM with current instruments and that limits imply (averaged) fields  $B \geq 0.1 - 0.3 \mu\text{G}$ . Thus future observations are necessary to solve current controversies.

In the next years the detectors onboard of NuSTAR<sup>x</sup> and ASTRO-H will improve the sensitivity in the hard X-ray band by more than one order of magnitude with respect to the current facilities.

From eq. 32, clusters hosting bright radio halos, with fluxes at Jy level at 1 GHz (such as Coma, Perseus, A2319), should have ICS fluxes integrated in the band 20-80 keV of several  $\times 10^{-13} \text{erg/s/cm}^2$ , if we assume an average magnetic field  $\simeq 1 \mu\text{G}$  in the halo region. Coma is a relevant example. Current analysis of the Coma cluster using RM<sup>205</sup> favor a value  $\simeq 2 \mu\text{G}$  for the magnetic field averaged on  $\text{Mpc}^3$ -volume. This implies an expected ICS flux  $\sim 2 \times 10^{-13} \text{erg/s/cm}^2$  in the 20-80 keV band measured on an aperture radius  $= 35$  arcmin, if we adopt the radio flux of the halo measured on the same aperture radius<sup>266</sup> and a synchrotron spectral index  $\alpha = 1.25$ . Such a flux distributed on a 35 arcmin aperture-radius is probably difficult to detect with ASTRO-H. However, even a relatively small departure from that magnetic field value, say a factor 2 lower, may be sufficient to lead to a detection. In fact, the important point here is that even the non detection of nearby clusters hosting bright radio halos in the hard X-rays at the sensitivity level of the ASTRO-H telescope would be a result, providing very meaningful constraints on the magnetic field strength in these systems.

Similar considerations apply for clusters with giant radio relics. Some clusters host bright relics, with fluxes at Jy level at 1 GHz (A2256, A3367), and should produce ICS fluxes in the hard X-rays of several  $\times 10^{-13} \text{erg/s/cm}^2$ , provided that the average magnetic field in the relic region is  $\simeq 1 \mu\text{G}$ . On one hand radio relics cover an aperture angle that is smaller than giant radio halos and have peripheral locations, making their detection in the hard X-rays less problematic. On the other hand, however, relics are associated with shock compression

<sup>x</sup><http://www.nustar.caltech.edu/>, was launched in 2012 and first results on the Bullet cluster are in preparation<sup>340</sup>

regions (Sect. 4.4) where the average magnetic fields is presumably larger than that (averaged) in the region of giant halos, thus reducing the expected ICS flux. A textbook example is the relic A3667-NW, the brightest giant radio relic. Suzaku observations put a limit to the cluster ICS hard X-ray emission of about  $5 \times 10^{-12} \text{ erg/s/cm}^2$ .<sup>306,341</sup> Deeper limits have been obtained in the X-rays with Suzaku XIS and XMM-Newton, taking advantage of the peripheral location of the relic where thermal cluster's emission is fainter.<sup>306,341,342</sup> These constraints imply  $B \geq 2 - 3 \mu\text{G}$  if the power law spectrum measured in radio (corresponding to the energies of ICS emitting CRe in the hard X-rays, eq. 30-31) is extrapolated at energies about 10 times smaller (producing ICS at keVs). Constraints become significantly shallower in the case that the spectrum of CRe in the relic-downstream flattens at lower energies, e.g.<sup>341</sup> We note that such a flattening might result from the fact that the life-time of CRe producing ICS photons at keV energies becomes comparable to the shock life-time, implying that their spectrum gradually approaches the injection spectrum (with slope  $\sim \delta_{inj}$ , see Sect. 2.2.1). The future ASTRO-H or NuSTAR observations will overcome these uncertainties. From eq. 32 and assuming the spectrum and flux of the radio relic,  $\alpha = 1.1$  and 3.7 mJy at 1.4 GHz,<sup>343</sup> we obtain an expected ICS flux in the 10-40 keV band  $\simeq 2.5 \times 10^{-13} / (B_{\mu\text{G}}/3)^{2.1} \text{ erg/s/cm}^2$ . We note that  $B \sim 3 - 5 \mu\text{G}$  is derived from Faraday RM in the relic region.<sup>343</sup>

As a general conclusion, however, it is worth stressing that, unless the magnetic field strength in galaxy clusters is much smaller than that constrained from Faraday rotation measurements, future telescopes with 10 times more effective area than ASTRO-H are needed to explore non-thermal electron emission from galaxy clusters in the hard X-rays.

## 5.2. Gamma ray emission

The initial motivation for the interest in the  $\gamma$ -ray emission from clusters arose from the possibility of significant CRp confinement in the ICM (Sect. 2).<sup>17,19,344</sup> As already discussed, a natural byproduct of CR confinement is the emission of  $\gamma$  radiation from both the decay of secondary  $\pi^0$  and the ICS of CMB photons by high energy secondary CRe (Sect. 2.3). The latter channel becomes sub-dominant when integrated over a cluster at energies  $> 100 \text{ MeV}$ .<sup>96,206</sup> (Figure 19, left, for an example of the expected  $\gamma$ -ray spectrum).

After the first pionereing theoretical attempts<sup>11,12,16,17,22,96,344,345</sup> in the last decade numerical simulations allowed useful estimates of the expected  $\gamma$ -ray emission from galaxy clusters, under different assumptions. These simulations, that include some models for CR physics and the acceleration of CRs at cosmological shocks provided a picture of the radio to  $\gamma$ -ray properties of galaxy clusters. The first simulations of this kind predicted that clusters would be potentially detectable in  $\gamma$ -rays with the Fermi-LAT telescope<sup>83,206,207</sup> (Figure 19). The most important assumption in these simulations is in the efficiency of particle acceleration at weak shocks that, as explained in Sect. 2.2, is, however, poorly known. Subsequent simulation studies have attempted to reconcile expectations with the limits from 18 months observations with Fermi-LAT and from Cherenkov telescopes observations of the Perseus cluster.<sup>198,202,209</sup> However the most recent limits, that are derived using almost 5 years of Fermi-LAT data and stacking procedures, are definitely inconsistent with the

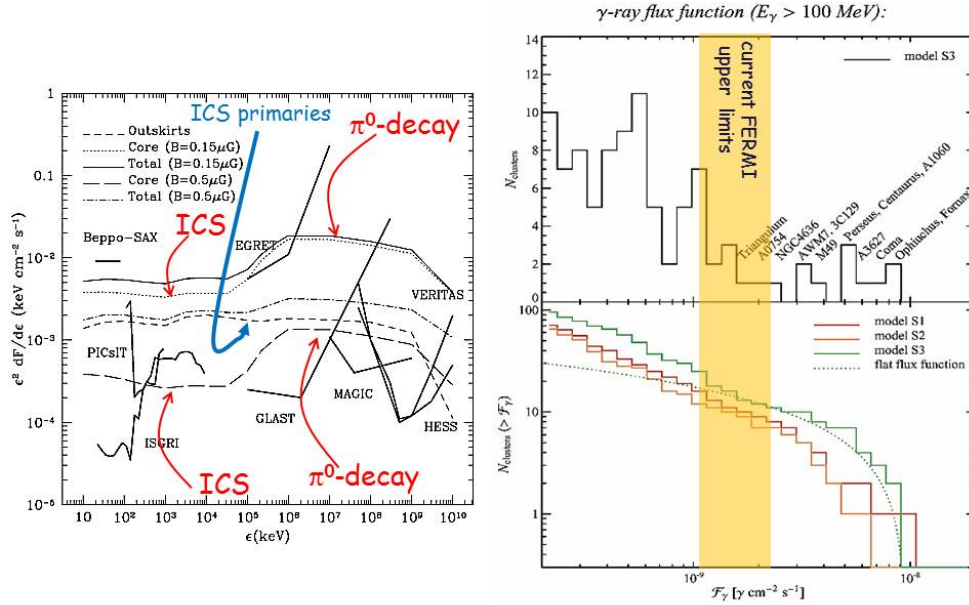


Fig. 19. Left panel: the  $\gamma$ -ray spectrum of the Coma cluster obtained by assuming that the radio halo is due to secondary CRp generated by CRp-p collisions in the ICM (adapted from<sup>206</sup>). Calculations account for the  $\pi^0$ -decay and ICS of CMB photons by secondary pairs and are obtained assuming an average magnetic field = 0.15 and = 0.5  $\mu$ G. The dashed line is the contribution from ICS of primary CRp accelerated at strong shocks in the cluster outskirts. Expectations are compared to the sensitivities of several high energy instruments. Right panel: the expected number counts of galaxy clusters in the  $\gamma$ -rays from simulations by<sup>207</sup> (adapted from<sup>207</sup>). The reference range of sensitivity of Fermi-LAT observations is reported as a yellow area.

predictions of these simulations.<sup>32,33</sup> That outcome may imply that the models of particle acceleration adopted in these simulations were too optimistic, in which case current limits can be used to constrain the acceleration efficiency. For example, by assuming the CRp spectral slope and spatial distribution that are predicted by simulations in,<sup>202</sup> Ackermann et al. (2013)<sup>32</sup> and Zandanel & Ando (2013)<sup>201</sup> derived limits on the maximum efficiency of shock acceleration in the ICM which refers to the case of strong shocks,  $\eta_{CRp} \leq 0.15$ . Alternatively one may speculate that the spatial distribution of CRp is much broader than that expected from these simulations and also than that of the thermal ICM. That would also indicate that the diffusion/transport of CRp with energy  $< \text{TeV}$  is fairly efficient, putting meaningful constraints on the physics discussed in Sect. 3.2.

In reality, the microphysics of the ICM and of CRs in galaxy clusters is very complicated and, unfortunately, well beyond the capabilities of current simulations (Sects. 2.2, 3.2). A way to circumvent these difficulties for now is to derive expectations by anchoring model parameters to the properties of the diffuse synchrotron emission in the form of

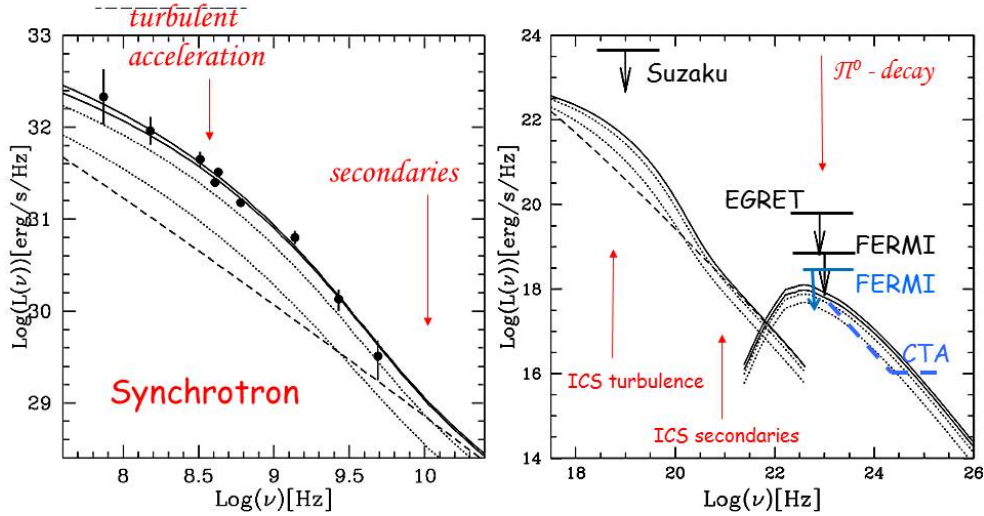


Fig. 20. Left panel: the synchrotron spectrum of the Coma radio halo (data-points) is compared with expectations based on turbulent reacceleration of secondary particles (tick-solid lines) (adapted from<sup>172</sup>). Dotted-lines show the time-evolution of the emission that is produced during different stages of the mergers. The dashed line shows the expected emission for a non-turbulent relaxed system that is powered via pure-hadronic cascades (see<sup>172</sup> for details). Right panel: the high-energy (ICS and  $\pi^0$  decay) emission of the Coma cluster compared with current limits (blue is the Fermi-LAT limit based on about 4 years of data<sup>32</sup>). The style of the lines is the same of the left panel (adapted from<sup>172</sup>). In all models/calculations the magnetic field is fixed to the value and radial profile that are favoured by current RM analysis.<sup>205</sup> The bump in both the radio and hard X-ray spectra is produced by the combined effect of turbulent reacceleration and radiative losses on the CRE spectrum.

radio halos in nearby clusters<sup>34,260,262,344</sup> (Sect. 4.2, 4.3). Potentially this also allows one to put combined constraints on both the origin of diffuse cluster-scale emission (such as radio halos) and on the expected high energy emissions from the hosting clusters. In Sect. 4.2 we have already discussed that, at least in a few observed cases, the combination of radio-halo properties and of the Fermi-LAT upper limits disfavor a purely hadronic origin of these radio sources. That limits the role played by secondaries for the origin of the observed radio emission and, consequently, also the expected  $\gamma$ -ray luminosity generated by CRp-p collisions. In particular for the Coma cluster, where the most stringent constraints have been derived using the properties of the radio halo at lower frequencies, Fermi-LAT upper limits imply a magnetic energy density in the cluster that is much larger than that constrained by Faraday rotation measures.<sup>262</sup>

Based on that, one way to obtain meaningful expectations of the level of  $\gamma$ -rays from galaxy

clusters expected because of the existence of radio halos is provided by joint modelings of the production of secondary particles and of the re-acceleration of these secondaries (and of the primary CRp) due to MHD turbulence in the ICM.<sup>177</sup> Our ability to apply turbulent re-acceleration to refine the picture based on CRp confinement and injection of secondaries in the ICM is limited primarily by our limited understanding of ICM turbulence, its origins, evolution distribution and spectral properties, especially on scales where resonant interaction with CR take place (Sect. 2.2.2). Pioneering calculations in this direction have been recently developed in<sup>172</sup> assuming that compressible MHD turbulence, generated in galaxy clusters at large scales during cluster-cluster mergers, cascades to smaller scales and also assuming that a pre-existing population of long-living CRp is mixed with the ICM. These calculations allow one to model the temporal evolution of the non-thermal emission from galaxy clusters, from radio (radio halos) to  $\gamma$ -rays, and to connect the evolution with cluster merger histories (Figure 20). These calculations show that radio halos and cluster-scale ICS emission are generated in a turbulent ICM (presumably in merging systems), while a fainter long-living radio (and ICS) emission sustained by the process of continuous injection of high energy secondary CRE is expected to be common in clusters more generally. The strength of this latter, persistent component is proportional to the energy density of the primary CRp in the ICM and, in the context of these modelings, it can be constrained by the upper limits to the cluster-scale radio emission in galaxy clusters without radio halos (Fig. 12, Sect. 4.2). Contrary to the *transient* nature of giant radio halos and hard X-ray emission in galaxy clusters,  $\gamma$ -ray emission is expected to be common at a moderate level in all clusters and not directly correlated with the presence of the currently observed giant radio halos. Since the CRp population of a cluster reflects its integrated history (assuming CRp do not escape) there should be a moderate range in  $\gamma$ -ray luminosities, e.g.<sup>23</sup> We note that expectations of  $\gamma$ -ray emission (from  $\pi^0$  decay and ICS from secondaries) according to these calculations are optimistic, because they are still based on a secondary origin of the seed electrons to re-accelerate. They can be used to constrain the minimum level of  $\gamma$ -rays from galaxy clusters *under the hypothesis that secondaries play an important role* for the origin of halos, being the only seed electrons to re-accelerate in the ICM. Figure 20 shows that the expected level of  $\gamma$ -ray emission from a Coma-like cluster is at a level few times below present Fermi-LAT limits. Note that expectations in Fig. 20 are obtained by assuming the magnetic field in the Coma cluster that is favored by current analysis of Faraday RM, namely a central magnetic field  $B = 4.6\mu\text{G}$  and a radial decline of the magnetic energy with the thermal energy density.<sup>205</sup> A lower value of the field would imply a larger  $\gamma$ -ray luminosity (eq. 26).

In general the population of CRE in the ICM is a mix of re-accelerated primaries and of locally injected secondaries. The  $\gamma$ -ray luminosity should roughly scale with the ratio of secondaries to primary CRE, because primary CRE (re)accelerated in Mpc-scale turbulent regions cannot produce  $\gamma$ -rays (as explained in Sect. 2.2.2, their maximum energy does not exceed significantly about a few times 10 GeV). Consequently if the secondary particles play a minor role and radio halos are powered by primary CRE the expected  $\gamma$ -ray luminosity is much smaller than that in Figure 20. For this reason future  $\gamma$ -ray observations with a sensitivity level few times better than current ones, using 10 years of Fermi-LAT data

or with the Cerenkov Telescope Array (CTA), are extremely important as they will definitely clarify the role of CRp and their secondaries for the origin of non-thermal emission in galaxy clusters.

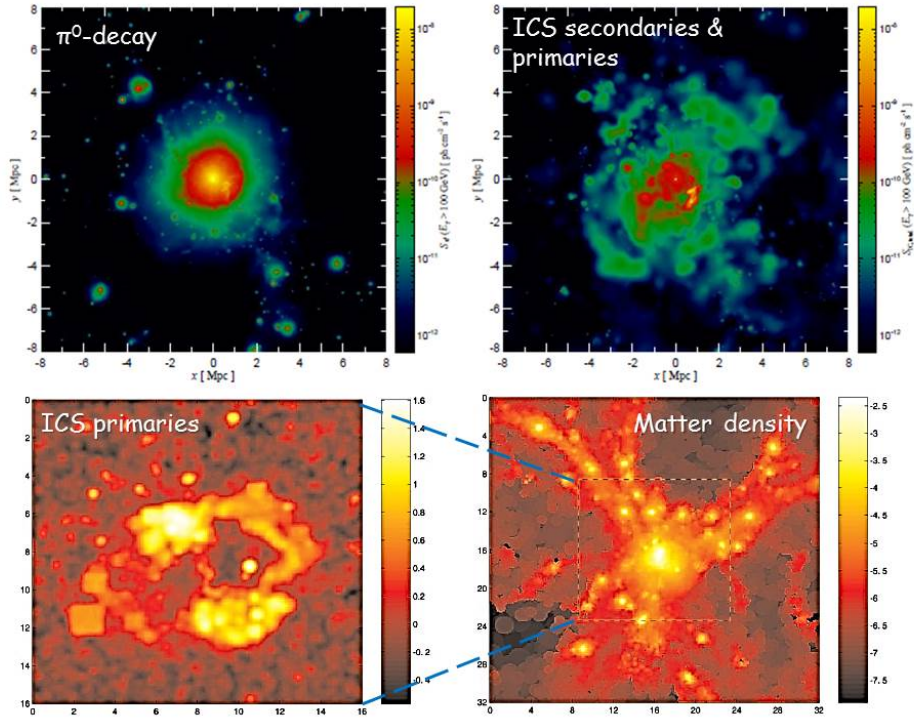


Fig. 21. Upper panels (adapted from<sup>202</sup>):  $\gamma$ -ray emission from a simulated cluster due to  $\pi^0$ -decay (left panel) and due to the combined ICS of CMB photons from shock-accelerated (primary) CRE and secondary CRE (right panel). Bottom panels (adapted from<sup>346</sup>):  $\gamma$ -ray emission from a simulated cluster due to shock-accelerated (primary) CRE (left panel), and projected matter density distribution in a simulated box containing that cluster (right panel); the square-region in the right-panel highlights the region shown in the left panel.

Primary CRE can be accelerated at cosmological shocks up to energies of tens of TeV (Sect 2.2.1), and the resulting ICS emission extends to multi-TeV energies.<sup>11, 12, 25, 83, 96, 202, 346</sup> There is agreement that the expected  $\gamma$ -ray spectrum of galaxy clusters should be dominated by the decay of the neutral pions in the central cluster regions and by ICS of primary CRE accelerated by strong shocks in cluster outskirts<sup>25, 83, 202, 347</sup> (Figs. 19, 21). The relative importance of the two mechanisms depends on the ratio of the efficiency of acceleration of CRp and CRE at shocks (Sect. 2.2.1) and on the dynamics/transport of CRp in the ICM (Sect. 3.2).<sup>206, 207, 347</sup> Under the assumption of CRp confinement and of “canonical” CRp/CRE ratios at shocks, the  $\pi^0$  decay is the dominant channel for the production of  $\gamma$ -rays from clusters.

Instead of the rather centrally concentrated  $\gamma$ -ray emission from  $\pi^0$ -decay, the ICS from

primary CRe accelerated at strong shocks should appear very different, giving rise to a spatially extended (rather flat) emission, potentially edge brightened, on scales comparable to the cluster virial region (Figure 21). The ICS luminosity from CRe accelerated at the strong shocks that surround clusters outskirts (assuming  $B_{IC} \gg B$ ) is :

$$v_o P_{ICS}(v_o) \sim 1/2 \rho_u V_{sh}^3 \eta_{CRe} S_{cl} \mathcal{F}^{-1}(\alpha(M)) \quad (33)$$

where  $\mathcal{F}(\alpha(M))$  is of the order of few for strong (external) shocks that are of interest for this discussion. Numerical simulations allow estimates of the shock-kinetic energy flux across the cluster surface,  $1/2 \rho_u V_{sh}^3 S_{cl} \sim 10^{41-42}$  erg/s (e.g., Fig. 3), implying that a luminosity  $\geq 10^{40}$  erg/s, that might become detectable in nearby clusters with future  $\gamma$ -ray observations, can be generated only provided that the acceleration of CRe at these shocks is “unusually” efficient, about  $\eta_{CRe} \geq 0.01$ . Although this is theoretically challenging and also not supported by current observations of SNR (Sect. 2.2.1), we note that the possibility of an efficient CRe (re-)acceleration at clusters shocks is also under discussion for the origin of radio relics (see Sect. 4.4). Consequently data from 10 years of Fermi-LAT observations will provide very important constraints.

Other mechanisms for the production of  $\gamma$ -rays in the ICM include non thermal bremsstrahlung<sup>25,96,206</sup> and ICS from pairs generated by Bethe-Heitler processes (photo-pair and photo-pion production) due to the interaction between Ultra High Energy protons ( $E \geq 10^{18}$  eV) and photons of the CMB.<sup>348,349</sup> As discussed in Sect. 2.2.1, the acceleration of these ultra high energy CRp in galaxy clusters is a theoretical challenge (Figure 5 for an “optimistic” view). However if EeV CRp are present, the high energy electron-positron pairs that are produced should radiate synchrotron and ICS emission peaking in the hard X-ray and TeV energy bands, respectively,<sup>350,351</sup> where future observations with ASTRO-H and CTA may obtain interesting constraints.

## 6. Concluding Remarks

The importance of non-thermal components in galaxy clusters is twofold. One point is that they are complementary probes of the mechanisms that dissipate energy at micro-physical scales; that is, especially the gravitational energy associated with the hierarchical sequence of mergers and accretion of matter that lead to the formation of clusters and cosmic filaments. The second is that non-thermal components, magnetic fields and CRs, actually strongly affect the physics of the ICM and evolve somewhat distinctly from thermal plasma components. Thus, they could also have a role in the evolution of clusters themselves.

In this review we have discussed the physics of CRs in galaxy clusters, including their acceleration and transport in the ICM, and the most relevant observational milestones that have provided relevant constraints on this physics. Finally, looking forward, we have placed emphasis on what appear to be the most important prospects for the near future from radio and high-energy observations.

As we have discussed in Sect. 3, the bulk of CR protons deposited within the cluster volume would be magnetically confined there for cosmological times. Therefore, due to



their long life-times they should accumulate at increasing levels over time as the cluster is assembled. The amount of energy that is associated with these CRp depends on the efficiency of particle acceleration mechanisms in the ICM. This has been discussed in Sect. 2. CRs, and CR protons in particular, should be accelerated at shocks associated with cluster formation and in turbulent regions. Galaxies within the cluster may also supply CRs by way of supernovae and high energy outflows from supermassive black holes in their nuclei (that is, AGNs). A notable and unavoidable consequence of CR proton acceleration and confinement in the ICM is  $\gamma$ -ray emission resulting from decay of neutral pions produced by inelastic collisions involving CR protons and thermal protons (Sect. 2.3). For this reason  $\gamma$ -ray observations are powerful tools to constrain the physics of acceleration and transport of CRs in galaxy clusters. This has been discussed in Sects. 3.3 and 5.2. The non-detection of galaxy clusters after almost 5 years of observations with the Fermi-LAT telescope is one of the most relevant recent observational milestones in this field (Sect. 3.3). It contradicts several optimistic expectations that had been developed from attempts to model CR production in these environments. The failure, so far, to detect GeV - TeV  $\gamma$ -rays in any cluster generally limits the energy budget of CR protons in the central (Mpc-scale) regions of galaxy clusters to the percent level of the thermal energy. However, this observed limit does not yet imply that CRs are dynamically unimportant everywhere in the ICM, because CRs may still be able to contribute significantly to the cluster energy budget in the outermost regions of these systems<sup>y</sup>. Most important, current  $\gamma$ -ray limits do not constrain the most significant aspect of having CRs and magnetic fields in the ICM; that is, radical changes of the (micro-)physics of the ICM that are potentially induced by these non-thermal components. Even weak magnetic fields will control important transport processes within the ICM, including viscosity and thermal and electrical conductivities. CRs can also play important roles in damping turbulence as well as driving instabilities that influence the small-scale structure of the cluster magnetic field.

Radio observations of synchrotron radiation from the ICM provide the most important guide-lines for understanding the physics of CRs acceleration in galaxy clusters. This has been discussed extensively in Sect. 4. Observations detect diffuse, steep spectrum, cluster-scale synchrotron emission clearly associated with the ICM in the form of giant radio halos and relics. One of the most significant observational milestones for galaxy clusters in the last decade was the establishment of a connection between these giant radio sources and cluster mergers. That connection provides a starting point to understand radio emission origins and, most important, to identify a theoretical link between CR acceleration/transport in the ICM and the effects induced by cluster mergers on the physics of the ICM itself. In this respect it is quite commonly accepted that giant radio halos trace turbulent regions that form during mergers and where particles are trapped and accelerated/generated by some mechanism (Sect. 4.2) and where magnetic fields are amplified. On the other hand, giant radio relics are associated with cosmological shock waves where particles can be accelerated from the upstream thermal particle pool reaccelerated from nonthermal par-

---

<sup>y</sup>For a fixed ratio of CRp to thermal energy the luminosity of secondary  $\gamma$ -rays scales with the square of the thermal gas density (eq. 16, 17).

ticle populations somehow resident in the inflowing plasma (Sect. 4.4). In Sect. 4.3 we have also discussed the case of radio-mini halos. These diffuse radio sources are found in relaxed, cool-core clusters and have a size comparable to that of the cool-core region, so substantially smaller than the giant halos. The fact that mini-halos are always found in dynamically relaxed systems suggests that situations other than cluster mergers can also drain energy “in situ” into CRs and, probably, magnetic fields. Yet, as we have discussed in Sect. 4.3, whether or not the underlying physical mechanisms that accelerate the CRE in mini halos differ substantially from the analogous mechanisms in giant radio halos is still unclear.

### **6.1. Radio Emission**

The challenges to explain the origin of radio halos and relics triggered a lively debate in the literature. Although fundamental steps have been successfully obtained in the last years, several important aspects of the physics of these sources are still unclear. The most relevant observational and theoretical breakthroughs have been summarised in Sect. 4 along with the future observational prospects in the field.

As motivated in Sect. 4.2, a promising model for giant radio halos is based on the hypothesis that CRs are re-accelerated by turbulence generated in the ICM during cluster mergers. Turbulence will not accelerate CR electrons directly out of the thermal electron population; some other injection sources are needed. Such seed electrons probably come in various proportions from large scale shocks within the ICM, from energetic phenomena associated with individual galaxies and as secondary  $e^\pm$  also produced in  $CRp - p$  collisions. The last of these contributors has received much attention. In fact direct secondary CRE generation without any re-acceleration was also proposed by itself to explain giant radio halos. Indeed one of the most relevant theoretical discussions for the origin of giant radio halos is the role of these secondary particles. One way to constrain the importance of these secondaries starts from the Fermi-LAT limits to  $\gamma$ -ray emission. This is especially meaningful when combined with radio frequency information in nearby clusters hosting radio halos. In particular deep radio observations allow detection of the radio emission in these clusters up to their largest spatial scales and provide constraints on the spectrum of radio halos. These studies appear to challenge the classical, pure secondary injection model for radio halos.

A unique and clear expectation of radio halo models based on turbulent acceleration is the existence of a large population of radio halos with very steep spectra. This prediction reflects the intrinsic difficulties of the mechanisms of stochastic acceleration by turbulence in accelerating CRE to very high energies, and suggests that clusters with weaker turbulence will produce steeper radio spectra. In the next few years the LOFAR radio telescope will survey the northern sky at (as yet) unexplored low radio frequencies, thus allowing to unveil a large number of these sources if they exist.

Giant, peripheral radio relics have recently attracted much attention. This has been discussed in Sect. 4.4. There is general agreement on the fact that radio relics originate at shock waves that cross galaxy clusters during mergers. A shock connection is motivated by

strong arguments, including their morphology, polarization and spectral properties, but also by the observed spatial coincidence between radio relics and shocks found in some cases by X-ray observations. On the other hand, theory and X-ray observations agree on the fact that merger shocks are relatively weak, with Mach numbers less than a few. Significantly, they are much weaker than shocks in supernova remnants, where efficient CRs acceleration is proved and strong magnetic field amplification is strongly suggested. There are very good reasons to expect particle acceleration to be much less efficient in weak shocks. So, these processes, that are so important in SNR shocks, should be much less effective in cluster merger shocks and, so long as the accelerated population is locally injected at low energies, lead to a rather steep spectrum compared to those seen in some relics. In this respect radio relics are “unique laboratories” to study the acceleration of particles at large-scale, weak shocks in high-beta plasma environments. While first order, diffusive shock acceleration (DSA) at these shocks is the apparent candidate to explain the CR electron population seen in relics, there are fundamental concerns about the detailed, micro-physical mechanisms. In fact the most relevant concern is whether shocks in galaxy clusters are efficient enough to accelerate the emitting CRe from the thermal pool to observed multi-GeV energies. As discussed in Sect. 4.4 this appears not to be the case. Although the classical model of DSA for locally injected CR electrons could account for properties of some relics, such a model is challenged by energy arguments combined with simulations of CR acceleration at weak shocks. This is especially a concern in the case of the most powerful relics and those with relatively flat spectra giant radio relics (we note that very steep spectra of giant relics also challenge the classical DSA model due to associated energy arguments). A natural candidate-mechanism is the re-acceleration of pre-existing CRe at these shocks, provided there is a scenario that produces them in sufficient numbers and maintains a sufficiently flat spectrum upstream of the shock. DSA is more efficient at extracting shock energy in this situation and does not constrain the spectrum of the downstream CR population to the “classical DSA” value if the CR population entering the shock has a flatter spectrum than this. Radio relics pin-point the (re)acceleration of CRe at shocks in the ICM. However, what about CRp ? As discussed in Sect. 2, shock acceleration is generally expected to be more efficient for CRp acceleration rather than for CRe. In this respect a consequence of current models of radio relics is the likely acceleration of a substantial population of CRp in galaxy clusters. That, however, is strongly constrained by current luminosity limits in  $\gamma$ -rays. Consequently we can expect in the coming years the combination of radio and  $\gamma$ -ray observations to provide interesting constraints on the physics of (re-)acceleration of CRs at clusters shocks and on the ratio CRp/CRe at these shocks.

## **6.2. High Energy Emission**

High energy emission from galaxy clusters has been discussed in Sect. 5. Galaxy clusters should be high energy sources. This is not only due to theoretical arguments based on acceleration and confinement of CRs in these systems, but it is unavoidably expected at some level from the existence of the high energy CRe that produce the synchrotron radiation observed in the radio band.

In particular hard X-ray emission is expected from ICS of the CMB photons by essentially the same CRe that produce synchrotron radiation in the radio band. In this case the expected ICS luminosity depends on the magnetic field strength in the ICM. As a conservative summary in Sect. 5.1 we stated that no ICS emission is convincingly detected in the hard X-ray band, implying a lower limit to the cluster magnetic field of about 0.1-0.3  $\mu\text{G}$  in the cases of several nearby clusters hosting radio halos. These limits are substantially smaller than the current estimates of the magnetic field strength based on Faraday RM. Consequently the expected ICS emission could very well be much smaller and well below current observational capabilities.

Gamma-ray emission from galaxy clusters is discussed in Sect. 5.2 (and Sect. 3.3). These emissions are mainly expected from the combination of  $\pi^0$ -decay from CRp-p collisions and ICS from primary CRe. The former mechanism should dominate in cluster central regions, while the latter one could be the most important mechanism in cluster outskirts. The  $\gamma$ -ray luminosity of galaxy clusters and the expected ratio between  $\pi^0$ -decay and ICS components are uncertain, as a consequence of our poor understanding of several aspects of the CRs acceleration and transport processes in the ICM. These mechanisms are, however, strongly connected with the physics of the observed radio sources. For this reason multi-frequency modelings and the combination of observations at both radio frequencies and high-energies have allowed derivation of important constraints on the origin of halos and relics, and also meaningful expectations for the resulting high energy emission from galaxy clusters. This has been extensively discussed in Sect. 5.2.

Another important point that has been discussed in this review is the maximum energy of CRs that can be achieved in galaxy clusters. This has been discussed to some extent in Sect. 2 where we focus on CRe and CRp; we do not study the case of nuclei. Of course, this is still very uncertain. Based on current understanding of CRs acceleration and transport/confinement in galaxy clusters it is possible to conclude that CRe can be accelerated to multi-TeV energies, while CRp might also reach EeV energies. In particular the possibility to accelerate EeV protons in the ICM is very appealing. As we mention in Sect. 5.2, one possible way to unveil these particles, if they exist in galaxy clusters, is to detect the synchrotron hard X-rays and ICS  $\gamma$ -rays (TeV) that are emitted by the secondary pairs that are produced through the interaction of these EeV CRp with the CMB photons.

### **6.3. The Future**

The next decade represents a “golden age” for studies of non-thermal components in galaxy clusters. This is one of the reasons that motivated us to write a review at this time.

This expectation is especially true in radioastronomy, thanks to a new generation of radio telescopes, such as LOFAR and the SKA pathfinders/precursors (ASKAP, MeerKAT, MWA, LWA). They will enter into unexplored territories, reaching unprecedented sensitivities to cluster scale emission over a broad frequency range. These telescopes will also allow polarization and Faraday Rotation studies of background and cluster radio sources with unprecedented statistics, frequency and dynamic range, probing cluster scale magnetic fields. As we briefly discussed in Sect. 4.1 (and Sect. 4.2-4.4), magnetic field properties and

the polarization of diffuse cluster-scale sources are indeed central ingredients also for our understanding of CRs acceleration and transport in the ICM.

One of the most notable examples of new, expected information is the spectrum of halos and relics. As discussed in Sect. 4, the spectrum of these sources provide crucial information for the origin of the emitting CRe. However, current observations allow derivation of high quality spectra only for a few cases. Most important, spectra are typically measured in a limited frequency range  $\nu_{max}/\nu_{min} \leq 10$  that probes the energy spectra of the emitting CRe over a very narrow energy range. The combination of LOFAR with JVLA observations (potentially also in combination with data from single dish radio telescopes) will allow spatially resolved and accurate measurements of halo and relic spectra over a frequency range 10 times bigger. That extension will open the possibility of deriving meaningful constraints of the CRe energy distributions and their spatial evolution/variation.

As discussed in Sect. 4, the surveys planned with the next generation of radio telescopes have the potential to probe the formation and evolution of cluster scale radio sources along with the evolution of the hosting clusters themselves. The apparent connection between halos and mergers suggests that these sources are valuable probes of the clusters merging history throughout the cosmic epochs. In this respect combined X-ray – radio and SZ – radio statistical studies of the occurrence of radio halos in clusters will provide unique information on the origin of non-thermal components and on their connection with the clusters thermal properties. In this respect LOFAR surveys will be of great interest, as they will probe an unexplored frequency range where current models predict the existence of cluster-scale radio emission with very steep spectrum.

In our review we also stressed that presumably *current observations* detect only the *tip of the iceberg* of the non-thermal radio emission from the Cosmic Web. In this respect, what is still unseen is the most attractive science case of the new generation of radio telescopes. In principle, according to the current theoretical picture, one may speculate that halos and relics pin-point only the regions where CRe acceleration is most efficient. Fainter synchrotron emission might be much more common and it may extend to scales even larger, thus tracing the complex pattern of shocks and turbulence that embed clusters and filaments. Unfortunately, our current ignorance of plasma-physics in these environments does not yet allow physically solid attempts to establish whether the SKA and its pathfinders will be able to detect these signals.

The future is bright also at high photon energies. First of all the hard X-ray telescopes NuSTAR and ASTRO-H will shortly derive constraints on the presence of non-thermal excess emission in galaxy clusters at a level that is about 10 times fainter than current studies. As discussed in Sect. 5.1 the detection of ICS emission from the brightest halos and relics is only possible if the magnetic field is substantially smaller, at least a factor 2-3, than that estimated from current RM analysis. However, even the non detection of nearby clusters hosting bright radio halos and relics at the sensitivity level of these telescopes would be a valuable result, providing very meaningful constraints on the magnetic field strength in these systems.

However, one of the most desired results from ASTRO-H is the first measure, from the study of metal lines, of turbulent motions in the ICM. This has been mentioned in Sects.

2 and 4. Turbulence is a fundamental ingredient for current theoretical scenario, not only because it is important for the acceleration and transport of CRs, but also because it is expected to strongly affect the micro-physics of the ICM. In this respect we also mention that a gigantic step forward represented by measured turbulent motions in galaxy clusters is a central science case of X-ray telescopes with much better spectral resolution and effective area, such as *Athena+*, that may be launched in about 15 years.

Current constraints from  $\gamma$ -ray observations allowed a gigantic step in our understanding of the CRs content in galaxy clusters. This has been discussed in Sects. 3.3, 4 and 5 also in the context of the impact of these constraints on models of giant halos and relics, and mini-radio halos. Better constraints are expected from future and ongoing observations with the Fermi-LAT and from observations with the next generation of Cherenkov telescopes, such as the CTA. As discussed in Sect. 5 these observations will allow derivation of fundamental constraints on the physics of CRE/CRp acceleration and transport in the ICM, and on the role played by secondary particles in the origin of giant and mini-radio halos.

### Acknowledgments

This work was supported in part by the National Science Foundation under Grant No. PHYS-1066293 and the hospitality of the Aspen Center for Physics. GB acknowledges the Simons Foundation for support. TWJ is supported by NASA grant NNX09AH78G, by US NSF grants AST0908668 and AST1211595 and the Minnesota Supercomputing Institute. We thank Kaustuv Basu, Marcus Bruggen, Reiner Beck, Damiano Caprioli, Rossella Cassano, Julius Donnert, Yutaka Fujita, Roberto Fusco-Femiano, Myriam Gitti, Joseph Lazio, Hui Li, Franco Vazza and Fabio Zandanel for comments and discussions. We also thank help from Franco Vazza for Fig. 2, from Paul Edmond for Fig. 5, from Simona Giacintucci for Figs. 11 & 15, and from Rossella Cassano and Fabio Zandanel for Fig. 14.

### References

1. Sarazin, C. L., *X-ray emission from clusters of galaxies*, Cambridge: Cambridge University Press (1988).
2. Kravtsov, A. V., & Borgani, S. 2012, *Annual Rev. of Astronomy & Astrophysics*, 50, 353
3. Briel, U. G., Henry, J. P., Lumb, D. H., et al. 2001, *A&A*, 365, L60
4. Planck Collaboration, Ade, P. A. R., Aghanim, N., et al. 2011, *A&A*, 536, A8
5. Brown, S., & Rudnick, L. 2011, *MNRAS*, 412, 2
6. Carlstrom, J. E., Holder, G. P., & Reese, E. D. 2002, *Annual Rev. of Astronomy & Astrophysics*, 40, 643
7. Norman, M. L., & Bryan, G. L. 1999, *The Radio Galaxy Messier 87*, LNP, 530, 106
8. Ryu, D., Kang, H., Cho, J., & Das, S. 2008, *Science*, 320, 909
9. Kaastra, J. S., Bykov, A. M., Schindler, S., et al. 2008, *Space Science Reviews*, 134, 1
10. Norman, C. A., Melrose, D. B., & Achterberg, A. 1995, *ApJ*, 454, 60
11. Sarazin, C. L. 1999, *ApJ*, 520, 529
12. Loeb, A., & Waxman, E. 2000, *Nature*, 405, 156
13. Ryu, D., Kang, H., Hallman, E., & Jones, T. W. 2003, *ApJ*, 593, 599
14. Cassano, R., & Brunetti, G. 2005, *MNRAS*, 357, 1313
15. Brunetti, G., Giacintucci, S., Cassano, R., et al. 2008, *Nature*, 455, 944

16. Völk, H. J., Aharonian, F. A., & Breitschwerdt, D. 1996, *Space Science Reviews*, 75, 279
17. Berezhinsky, V. S., Blasi, P., & Ptuskin, V. S. 1997, *ApJ*, 487, 529
18. Ensslin, T. A., Biermann, P. L., Kronberg, P. P., & Wu, X.-P. 1997, *ApJ*, 477, 560
19. Blasi, P., & Colafrancesco, S. 1999, *Astroparticle Physics*, 12, 169
20. Lazarian, A., & Brunetti, G. 2011, *MmSAIt*, 82, 636
21. Colafrancesco, S., & Blasi, P. 1998, *Astroparticle Physics*, 9, 227
22. Völk, H. J., & Atoyan, A. M. 1999, *Astroparticle Physics*, 11, 73
23. Miniati, F., Jones, T. W., Kang, H., & Ryu, D. 2001, *ApJ*, 562, 233
24. Pfrommer, C., & Enßlin, T. A. 2004, *MNRAS*, 352, 76
25. Blasi, P., Gabici, S., & Brunetti, G. 2007, *International Journal of Modern Physics A*, 22, 681
26. Reimer, O., Pohl, M., Sreekumar, P., & Mattox, J. R. 2003, *ApJ*, 588, 155
27. Perkins, J. S., Badran, H. M., Blaylock, G., et al. 2006, *ApJ*, 644, 148
28. Kiuchi, R., Mori, M., Bicknell, G. V., et al. 2009, *ApJ*, 704, 240
29. Aharonian, F., Akhperjanian, A. G., Anton, G., et al. 2009, *A&A*, 495, 27
30. Ackermann, M., Ajello, M., Allafort, A., et al. 2010, *ApJ*, 717, L71
31. Aleksić, J., Alvarez, E. A., Antonelli, L. A., et al. 2012, *A&A*, 541, A99
32. The Fermi-LAT Collaboration : Ackermann, M., et al. 2013, arXiv:1308.5654
33. Huber, B., Tchernin, C., Eckert, D., et al. 2013, *A&A*, 560, A64
34. Reimer, A., Reimer, O., Schlickeiser, R., & Iyudin, A. 2004, *A&A*, 424, 773
35. Brunetti, G., Venturi, T., Dallacasa, D., et al. 2007, *ApJ*, 670, L5
36. Brown, S., Emerick, A., Rudnick, L., & Brunetti, G. 2011, *ApJ*, 740, L28
37. Ferrari, C., Govoni, F., Schindler, S., Bykov, A. M., & Rephaeli, Y. 2008, *Space Science Reviews*, 134, 93
38. Feretti, L., Giovannini, G., Govoni, F., & Murgia, M. 2012, *Astronomy & Astrophysics Rev.*, 20, 54
39. Brügggen, M., Bykov, A., Ryu, D., Röttgering, H. 2012, *Space Science Reviews*, 166, 187
40. Brunetti, G. 2011, *MmSAIt*, 82, 515
41. Sarazin, C. L. 2004, *Journal of Korean Astronomical Society*, 37, 433
42. Nuza, S. E., Hoeft, M., van Weeren, R. J., Gottlöber, S., & Yepes, G. 2012, *MNRAS*, 420, 2006
43. Kang, H., Ryu, D., & Jones, T. W. 1996, *ApJ*, 456, 422
44. Fujita, Y., Takizawa, M., & Sarazin, C. L. 2003, *ApJ*, 584, 190
45. Brunetti, G., & Lazarian, A. 2007, *MNRAS*, 378, 245
46. Ensslin, T., Pfrommer, C., Miniati, F., & Subramanian, K. 2011, *A&A*, 527, A99
47. Jones, T. W. 2011, *Journal of Astrophysics and Astronomy*, 32, 427
48. Morlino, G., & Caprioli, D. 2012, *A&A*, 538, A81
49. Miley, G. 1980, *Annual Rev. of Astronomy & Astrophysics*, 18, 165
50. Burns, J. O. 1990, *Astronomical Journal*, 99, 14
51. Best, P. N., von der Linden, A., Kauffmann, G., Heckman, T. M., & Kaiser, C. R. 2007, *MNRAS*, 379, 894
52. Mittal, R., Hudson, D. S., Reiprich, T. H., & Clarke, T. 2009, *A&A*, 501, 835
53. McNamara, B. R., & Nulsen, P. E. J. 2007, *Annual Rev. of Astronomy & Astrophysics*, 45, 117
54. Gitti, M., Brighenti, F., & McNamara, B. R. 2012, *Advances in Astronomy*, 2012, 950641
55. Rafferty, D. A., McNamara, B. R., Nulsen, P. E. J., & Wise, M. W. 2006, *ApJ*, 652, 216
56. Dunn, R. J. H., & Fabian, A. C. 2006, *MNRAS*, 373, 959
57. O'Neill, S. M., & Jones, T. W. 2010, *ApJ*, 710, 180
58. Gitti, M., Nulsen, P. E. J., David, L. P., McNamara, B. R., & Wise, M. W. 2011, *ApJ*, 732, 13
59. Hardcastle, M. J., & Croston, J. H. 2010, *MNRAS*, 404, 2018
60. Croston, J. H., & Hardcastle, M. J. 2013, arXiv:1312.5183
61. De Young, D. S. 2006, *ApJ*, 648, 200
62. Dursi, L. J., & Pfrommer, C. 2008, *ApJ*, 677, 993

68 *G. Brunetti & T. W. Jones*

63. Dong, R., & Stone, J. M. 2009, *ApJ*, 704, 1309
64. O'Neill, S. M., De Young, D. S., & Jones, T. W. 2009, *ApJ*, 694, 1317
65. Stocke, J. T., Hart, Q. N., & Hallman, E. J. 2009, *American Institute of Physics Conference Series*, 1201, 206
66. Burns, J. O. 1998, *Science*, 280, 400
67. Hardcastle. M. J., & Sakelliou, I. 2004, *MNRAS*, 349, 560
68. Cassano, R., Etori, S., Giacintucci, S., et al. 2010, *ApJ*, 721, L82
69. Takizawa, M., & Naito, T. 2000, *ApJ*, 535, 586
70. Gabici, S., & Blasi, P. 2003, *ApJ*, 583, 695
71. Pfrommer, C., Springel, V., Enßlin, T. A., & Jubelgas, M. 2006, *MNRAS*, 367, 113
72. Skillman, S. W., O'Shea, B. W., Hallman, E. J., Burns, J. O., & Norman, M. L. 2008, *ApJ*, 689, 1063
73. Vazza, F., Brunetti, G., & Gheller, C. 2009, *MNRAS*, 395, 1333
74. Vazza, F., Brügggen, M., Gheller, C., & Brunetti, G. 2012, *MNRAS*, 421, 3375
75. Roettiger, K., Stone, J. M., & Burns, J. O. 1999, *ApJ*, 518, 594
76. Dolag, K., Bartelmann, M., & Lesch, H. 2002, *A&A*, 387, 383
77. Markevitch, M., & Vikhlinin, A. 2001, *ApJ*, 563, 95
78. Markevitch, M. 2010, *arXiv:1010.3660*
79. Vazza, F., Brunetti, G., Gheller, C., & Brunino, R. 2010, *New Astronomy*, 15, 695
80. Berrington, R. C., & Dermer, C. D. 2003, *ApJ*, 594, 709
81. Kang, H., Ryu, D., Cen, R., & Ostriker, J. P. 2007, *ApJ*, 669, 729
82. Vazza, F., Dolag, K., Ryu, D., et al. 2011, *MNRAS*, 418, 960
83. Miniati, F., Ryu, D., Kang, H., & Jones, T. W. 2001, *ApJ*, 559, 59
84. Pfrommer, C., Enßlin, T. A., Springel, V., Jubelgas, M., & Dolag, K. 2007, *MNRAS*, 378, 385
85. Bell, A. R. 1978, *MNRAS*, 182, 147
86. Drury, L. O. 1983, *Reports on Progress in Physics*, 46, 973
87. Blandford, R., & Eichler, D. 1987, *Physics Reports*, 154, 1
88. Jones, F. C., & Ellison, D. C. 1991, *Space Science Reviews*, 58, 259
89. Malkov, M. A., & O'C Drury, L. 2001, *Reports on Progress in Physics*, 64, 429
90. Blasi, P. 2002, *Astroparticle Physics*, 16, 429
91. Kang, H., Jones, T. W., & Gieseler, U. D. J. 2002, *ApJ*, 579, 337
92. Kang, H., & Jones, T. W. 2005, *ApJ*, 620, 44
93. Kang, H., Ryu, D., & Jones, T. W. 2009, *ApJ*, 695, 1273
94. Kang, H., Jones, T. W., & Edmon, P. P. 2013, *ApJ*, 777, 25
95. Kang, H., & Jones, T. W. 2002, *Journal of Korean Astronomical Society*, 35, 159
96. Blasi, P. 2001, *Astroparticle Physics*, 15, 223
97. Kang, H., Ryu, D., & Jones, T. W. 2012, *ApJ*, 756, 97
98. Ensslin, T. A., Biermann, P. L., Klein, U., & Kohle, S. 1998, *A&A*, 332, 395
99. Hoeft, M., & Brügggen, M. 2007, *MNRAS*, 375, 77
100. Berezhinskii, V. S., & Grigor'eva, S. I. 1988, *A&A*, 199, 1
101. Blasi, P. 2004, *Journal of Korean Astronomical Society*, 37, 483
102. Vink, J., & Yamazaki, R. 2014, *ApJ*, 780, 125
103. Amato, E., & Arons, J. 2006, *ApJ*, 653, 325
104. Burgess, D. 2006, *ApJ*, 653, 316
105. Amano, T., & Hoshino, M. 2009, *ApJ*, 690, 244
106. Riquelme, M. A., & Spitkovsky, A. 2011, *ApJ*, 733, 63
107. Gargaté, L., & Spitkovsky, A. 2012, *ApJ*, 744, 67
108. Caprioli, D., & Spitkovsky, A. 2013, *arXiv:1310.2943*
109. Park, J., Workman, J. C., Blackman, E. G., Ren, C. & Siller, R., *Physics of Plasmas*, 19, 2904, 2012



110. Bell, A. R. 1978, *MNRAS*, 182, 443
111. Lucek, S. G., & Bell, A. R. 2000, *MNRAS*, 314, 65
112. Bell, A. R. 2004, *MNRAS*, 353, 550
113. Amato, E., & Blasi, P. 2009, *MNRAS*, 392, 1591
114. Biermann, L. 1950, *Zeitschrift Naturforschung Teil A*, 5, 65
115. Weibel, E. S. 1959, *Physical Review Letters*, 2, 83
116. Gedalin, M., Medvedev, M., Spitkovsky, A., Krasnosolskikh, V., Balikhin, M., Vaivads, A. & Perri, S, *Physics of Plasmas*, 17, 2108, 2010
117. Davies, G., & Widrow, L. M. 2000, *ApJ*, 540, 755
118. Caprioli, D. 2012, *Journal of Cosmology and Astroparticle Physics*, 7, 38
119. Jaffe, W. J. 1977, *ApJ*, 212, 1
120. Deiss, B. M., & Just, A. 1996, *A&A*, 305, 407
121. Heinz, S., Brüggén, M., Young, A., & Levesque, E. 2006, *MNRAS*, 373, L65
122. Brüggén, M., & Scannapieco, E. 2009, *MNRAS*, 398, 548
123. Parrish, I. J., & Stone, J. M. 2007, *ApJ*, 664, 135
124. Ricker, P. M., & Sarazin, C. L. 2001, *ApJ*, 561, 621
125. Subramanian, K., Shukurov, A., & Haugen, N. E. L. 2006, *MNRAS*, 366, 1437
126. Vazza, F., Brunetti, G., Kritsuk, A., et al. 2009, *A&A*, 504, 33
127. Dolag, K., Vazza, F., Brunetti, G., & Tormen, G. 2005, *MNRAS*, 364, 753
128. Iapichino, L., & Niemeyer, J. C. 2008, *MNRAS*, 388, 1089
129. Keshet, U., Markevitch, M., Birnboim, Y., & Loeb, A. 2010, *ApJ*, 719, L74
130. Iapichino, L., Schmidt, W., Niemeyer, J. C., & Merklein, J. 2011, *MNRAS*, 414, 2297
131. Paul, S., Iapichino, L., Miniati, F., Bagchi, J., & Mannheim, K. 2011, *ApJ*, 726, 17
132. ZuHone, J. A., Markevitch, M., & Lee, D. 2011, *ApJ*, 743, 16
133. Hallman, E. J., & Jeltema, T. E. 2011, *MNRAS*, 418, 2467
134. Vazza, F., Brunetti, G., Gheller, C., Brunino, R., & Brüggén, M. 2011, *A&A*, 529, A17
135. Vazza, F., Roediger, E., & Brüggén, M. 2012, *A&A*, 544, A103
136. Nagai, D., Lau, E. T., Avestruz, C., Nelson, K., & Rudd, D. H. 2013, *ApJ*, 777, 137
137. Miniati, F. 2013, arXiv:1310.2951
138. Beresnyak, A., Xu, H., Li, H., & Schlickeiser, R. 2013, *ApJ*, 771, 131
139. Lazarian, A. 2006, *ApJ*, 645, L25
140. Schekochihin, A. A., Cowley, S. C., Kulsrud, R. M., Hammett, G. W., & Sharma, P. 2005, *ApJ*, 629, 139
141. Schekochihin, A. A., Cowley, S. C., Rincon, F., & Rosin, M. S. 2010, *MNRAS*, 405, 291
142. Levinson, A., & Eichler, D. 1992, *ApJ*, 387, 212
143. Pistinner, S., Levinson, A., & Eichler, D. 1996, *ApJ*, 467, 162
144. Brunetti, G., & Lazarian, A. 2011, *MNRAS*, 412, 817
145. Yan, H., & Lazarian, A. 2011, *ApJ*, 731, 35
146. Wentzel, D. G. 1974, *Annual Rev. of Astronomy & Astrophysics*, 12, 71
147. Pistinner, S. L. 1997, in *Galactic Cluster Cooling Flows*, ASP Conf. Series, 115, 165
148. Weatherall, J. C., & Eilek, J. 1999, in *Diffuse Thermal and Relativistic Plasma in Galaxy Clusters*, 255
149. Schuecker, P., Finoguenov, A., Miniati, F., Böhringer, H., & Briel, U. G. 2004, *A&A*, 426, 387
150. Sanders, J. S., Fabian, A. C., Churazov, E., et al. 2013, *Science*, 341, 1365
151. Schuecker, P., Finoguenov, A., Miniati, F., Böhringer, H., & Briel, U. G. 2004, *A&A*, 426, 387
152. Sunyaev, R. A., Norman, M. L., & Bryan, G. L. 2003, *Astronomy Letters*, 29, 783
153. Vazza, F., Gheller, C., & Brunetti, G. 2010, *A&A*, 513, A32
154. Takahashi, T., Mitsuda, K., Kelley, R., et al. 2010, *Proceedings of the SPIE*, 7732, 77320Z-77320Z-18
155. Zhuravleva, I., Churazov, E., Kravtsov, A., & Sunyaev, R. 2012, *MNRAS*, 422, 2712

70 *G. Brunetti & T. W. Jones*

156. Zhuravleva, I., Churazov, E., Sunyaev, R., et al. 2013, MNRAS, 435, 3111
157. Melrose, D. B., *Plasma astrophysics. Nonthermal processes in diffuse magnetized plasmas*, New York: Gordon and Breach, (1980)
158. Schlickeiser, R., *Cosmic ray astrophysics*, Springer (2002)
159. Lazarian, A., & Vishniac, E. T. 1999, ApJ, 517, 700
160. Petrosian, V., & East, W. E. 2008, ApJ, 682, 175
161. Chernyshov, D. O., Dogiel, V. A., & Ko, C. M. 2012, ApJ, 759, 113
162. Brunetti, G., Setti, G., Feretti, L., & Giovannini, G. 2001, MNRAS, 320, 365
163. Petrosian, V. 2001, ApJ, 557, 560
164. Jokipii, J. R. 1966, ApJ, 146, 480
165. Schlickeiser, R., & Achatz, U. 1993, Journal of Plasma Physics, 49, 63
166. Miller, J. A., & Roberts, D. A. 1995, ApJ, 452, 912
167. Foote, E. A., & Kulsrud, R. M. 1979, ApJ, 233, 302
168. Yan, H., & Lazarian, A. 2004, ApJ, 614, 757
169. Dung, R., & Petrosian, V. 1994, ApJ, 421, 550
170. Kirk, J. G., Schneider, P., & Schlickeiser, R. 1988, ApJ, 328, 269
171. Skilling, J. 1975, MNRAS, 172, 557
172. Brunetti, G., & Lazarian, A. 2011, MNRAS, 410, 127
173. Ohno, H., Takizawa, M., & Shibata, S. 2002, ApJ, 577, 658
174. Brunetti, G., Blasi, P., Cassano, R., & Gabici, S. 2004, MNRAS, 350, 1174
175. Chandran, B. D. G. 2000, Physical Review Letters, 85, 4656
176. Yan, H., & Lazarian, A. 2002, Physical Review Letters, 89, 1102
177. Brunetti, G., & Blasi, P. 2005, MNRAS, 363, 1173
178. Moskalenko, I. V., & Strong, A. W. 1998, ApJ, 493, 694
179. Stecker, F. W. 1970, Astrophysics and Space Science, 6, 377
180. Badhwar, G. D., Golden, R. L., & Stephens, S. A. 1977, Physical Review D, 15, 820
181. Stephens, S. A., & Badhwar, G. D. 1981, Astrophysics and Space Science, 76, 213
182. Dermer, C. D. 1986, ApJ, 307, 47
183. Dermer, C. D. 1986, A&A, 157, 223
184. Kamae, T., Abe, T., & Koi, T. 2005, ApJ, 620, 244
185. Kelner, S. R., Aharonian, F. A., & Bugayov, V. V. 2006, Physical Review D, 74, 034018
186. Dolag, K., & Ensslin, T. A. 2000, A&A, 362, 151
187. Kamae, T., Karlsson, N., Mizuno, T., Abe, T., & Koi, T. 2006, ApJ, 647, 692
188. Bhattacharjee, P. 2000, Physics Reports, 327, 109
189. Goldreich, P., & Sridhar, S. 1995, ApJ, 438, 763
190. Cho, J., Lazarian, A., & Vishniac, E. T. 2003, in *Turbulence and Magnetic Fields in Astrophysics*, ed. E. Falgarone, and T. Passot., Lecture Notes in Physics, 614, 56
191. Beresnyak, A., Yan, H., & Lazarian, A. 2011, ApJ, 728, 60
192. Wiener, J., Oh, S. P., & Guo, F. 2013, MNRAS, 434, 2209
193. Cho, J., & Lazarian, A. 2004, Journal of Korean Astronomical Society, 37, 557
194. Richardson, L. F. 1926, Royal Society of London Proceedings Series A, 110, 709
195. Rebusco, P., Churazov, E., Böhringer, H., & Forman, W. 2005, MNRAS, 372, 1840
196. Kang, H., & Ryu, D. 2011, ApJ, 734, 18
197. Aharonian, F., Akhperjanian, A. G., Anton, G., et al. 2009, A&A, 502, 437
198. Aleksić, J., Antonelli, L. A., Antoranz, P., et al. 2010, ApJ, 710, 634
199. Arlen, T., Aune, T., Beilicke, M., et al. 2012, ApJ, 757, 123
200. Prokhorov, D. A., & Churazov, E. M. 2013, arXiv:1309.0197
201. Zandanel, F., & Ando, S. 2013, arXiv:1312.1493
202. Pinzke, A., & Pfrommer, C. 2010, MNRAS, 409, 449
203. Clarke, T. E., Kronberg, P. P., Böhringer, H. 2001, ApJ, 547, L111

204. Carilli, C. L., & Taylor, G. B. 2002, *Annual Rev. of Astronomy & Astrophysics*, 40, 319
205. Bonafede, A., Feretti, L., Murgia, M., et al. 2010, *A&A*, 513, A30
206. Miniati, F. 2003, *MNRAS*, 342, 1009
207. Pfrommer, C. 2008, *MNRAS*, 385, 1242
208. Colafrancesco, S., & Marchegiani, P. 2008, *A&A*, 484, 51
209. Pinzke, A., Pfrommer, C., & Bergström, L. 2011, *Physical Review D*, 84, 123509
210. Govoni, F., Markevitch, M., Vikhlinin, A., et al. 2004, *ApJ*, 605, 695
211. Venturi, T., Giacintucci, S., Dallacasa, D., et al. 2013, *A&A*, 551, A24
212. Giacintucci, S., Markevitch, M., Venturi, T., et al. 2014, *ApJ*, 781, 9
213. Gitti, M., Brunetti, G., Feretti, L., & Setti, G. 2004, *A&A*, 417, 1
214. van Weeren, R. J., Röttgering, H. J. A., Brüggen, M., & Hoeft, M. 2010, *Science*, 330, 347
215. Ogrear, G. A., Brüggen, M., Röttgering, H., et al. 2013, *MNRAS*, 429, 2617
216. Röttgering, H. J. A., Wieringa, M. H., Hunstead, R. W., & Ekers, R. D. 1997, *MNRAS*, 290, 577
217. Kale, R., Dwarakanath, K. S., Bagchi, J., & Paul, S. 2012, *MNRAS*, 426, 1204
218. Venturi, T. 2011, *MmSAIt*, 82, 499
219. Farnsworth, D., Rudnick, L., Brown, S., & Brunetti, G. 2013, *ApJ*, 779, 189
220. Rudnick, L., Alexander, P., Andernach, H., et al. 2009, *astro2010: The Astronomy and Astrophysics Decadal Survey*, 2010, 253
221. Dolag, K., Grasso, D., Springel, V., & Tkachev, I. 2005, *Journal of Cosmology and Astroparticle Physics*, 1, 9
222. Brüggen, M., Ruszkowski, M., Simionescu, A., Hoeft, M., & Dalla Vecchia, C. 2005, *ApJ*, 631, L21
223. Dubois, Y., & Teyssier, R. 2008, *A&A*, 482, L13
224. Donnert, J., Dolag, K., Lesch, H., Müller, E. 2009, *MNRAS*, 392, 1008
225. Xu, H., Li, H., Collins, D. C., Li, S., & Norman, M. L. 2010, *ApJ*, 725, 2152
226. Xu, H., Li, H., Collins, D. C., Li, S., & Norman, M. L. 2011, *ApJ*, 739, 77
227. Ensslin, T. A. & Vogt, C., 2003, *A&A*, 401, 835
228. Cho, J. & Ryu, D. 2009, *ApJ*, 705, L90
229. Vogt, C. & Ensslin, T. A. 2005, *A&A*, 434, 67
230. Murgia, M., Govoni, Feretti, L., Giovannini, Dallacasa, G., Fanti, R., Taylor, G. B. & Dolag, K., 2004, *A&A*, 424, 429
231. Govoni, F. 2006, *Astronomische Nachrichten*, 327, 539
232. Guidetti, D., Murgia, M., Govoni, F., et al. 2008, *A&A*, 483, 699
233. Kuchar, P., & Enßlin, T. A. 2011, *A&A*, 529, A13
234. Vacca, V., Murgia, M., Govoni, F., et al. 2012, *A&A*, 540, A38
235. Bonafede, A., Vazza, F., Brüggen, M., et al. 2013, *MNRAS*, 433, 3208
236. Donnert, J., Dolag, K., Brunetti, G., & Cassano, R. 2013, *MNRAS*, 429, 3564
237. Petrosian, V., & Bykov, A. M. 2008, *Space Science Reviews*, 134, 207
238. Dennison, B. 1980, *ApJ*, 239, L93
239. Keshet, U., & Loeb, A. 2010, *ApJ*, 722, 737
240. Hanisch, R. J. 1982, *A&A*, 111, 97
241. Giovannini, G., Tordi, M., & Feretti, L. 1999, *New Astronomy*, 4, 141
242. Kempner, J. C., & Sarazin, C. L. 2001, *ApJ*, 548, 639
243. Venturi, T., Giacintucci, S., Brunetti, G., et al. 2007, *A&A*, 463, 937
244. Venturi, T., Giacintucci, S., Dallacasa, D., et al. 2008, *A&A*, 484, 327
245. Cassano, R., Brunetti, G., Venturi, T., et al. 2008, *A&A*, 480, 687
246. Cassano, R., Ettori, S., Brunetti, G., et al. 2013, *ApJ*, 777, 141
247. Kale, R., Venturi, T., Giacintucci, S., et al. 2013, *A&A*, 557, A99
248. Brunetti, G., Cassano, R., Dolag, K., & Setti, G. 2009, *A&A*, 507, 661

249. Buote, D. A. 2001, *ApJ*, 553, L15
250. Kushnir, D., Katz, B., & Waxman, E. 2009, *Journal of Cosmology and Astroparticle Physics*, 9, 24
251. Basu, K. 2012, *MNRAS*, 421, L112
252. Planck Collaboration, Ade, P. A. R., Aghanim, N., et al. 2013, arXiv:1303.5089
253. Sommer, M. W., & Basu, K. 2014, *MNRAS*, 437, 2163
254. Govoni, F., Enßlin, T. A., Feretti, L., & Giovannini, G. 2001, *A&A*, 369, 441
255. Planck Collaboration, Ade, P. A. R., Aghanim, N., et al. 2013, *A&A*, 554, A140
256. Brunetti, G. 2003, in *Matter and Energy in Clusters of Galaxies*, ASP Conf. Series, 301, 349
257. Brunetti, G. 2004, *Journal of Korean Astronomical Society*, 37, 493
258. Marchegiani, P., Perola, G. C., & Colafrancesco, S. 2007, *A&A*, 465, 41
259. Donnert, J., Dolag, K., Cassano, R., & Brunetti, G. 2010, *MNRAS*, 407, 1565
260. Brunetti, G. 2009, *A&A*, 508, 599
261. Jeltama, T. E., & Profumo, S. 2011, *ApJ*, 728, 53
262. Brunetti, G., Blasi, P., Reimer, O., et al. 2012, *MNRAS*, 426, 956
263. Willson, M. A. G. 1970, *MNRAS*, 151, 1
264. Venturi, T., Giovannini, G., & Feretti, L. 1990, *Astronomical Journal*, 99, 1381
265. Thierbach, M., Klein, U., & Wielebinski, R. 2003, *A&A*, 397, 53
266. Brunetti, G., Rudnick, L., Cassano, R., et al. 2013, *A&A*, 558, A52
267. Schlickeiser, R., Sievers, A., & Thiemann, H. 1987, *A&A*, 182, 21
268. Kale, R., & Dwarakanath, K. S. 2010, *ApJ*, 718, 939
269. van Weeren, R. J., Röttgering, H. J. A., Rafferty, D. A., et al. 2012, *A&A*, 543, A43
270. Macario, G., Venturi, T., Brunetti, G., et al. 2010, *A&A*, 517, A43
271. Macario, G., Venturi, T., Intema, H. T., et al. 2013, *A&A*, 551, A141
272. Cassano, R., Brunetti, G., & Setti, G. 2006, *MNRAS*, 369, 1577
273. Cassano, R., Brunetti, G., Norris, R. P., et al. 2012, *A&A*, 548, A100
274. Zandanel, F., Pfrommer, C., & Prada, F. 2013, arXiv:1311.4795
275. Cassano, R., Brunetti, G., Röttgering, H. J. A., & Brüggem, M. 2010, *A&A*, 509, A68
276. Enßlin, T. A., Röttgering, H. 2002, *A&A*, 396, 83
277. Cassano, R., Gitti, M., & Brunetti, G. 2008, *A&A*, 486, L31
278. Murgia, M., Govoni, F., Markevitch, M., et al. 2009, *A&A*, 499, 679
279. Gitti, M., Brunetti, G., & Setti, G. 2002, *A&A*, 386, 456
280. Peterson, J. R., & Fabian, A. C. 2006, *Physics Reports*, 427, 1
281. Markevitch, M., & Vikhlinin, A. 2007, *Physics Reports*, 443, 1
282. Fujita, Y., Matsumoto, T., & Wada, K. 2004, *ApJ*, 612, L9
283. Ascasibar, Y., & Markevitch, M. 2006, *ApJ*, 650, 102
284. ZuHone, J. A., Markevitch, M., & Johnson, R. E. 2010, *ApJ*, 717, 908
285. Mazzotta, P., & Giacintucci, S. 2008, *ApJ*, 675, L9
286. ZuHone, J. A., Markevitch, M., Brunetti, G., & Giacintucci, S. 2013, *ApJ*, 762, 78
287. Sanders, J. S., Fabian, A. C., Smith, R. K. & Peterson, J. R. 2010, *MNRAS*, 402, L11
288. Bulbul, G. E., Smith, R. K., Foster, A., Cottam, J., Loewenstein, M., Mushotzky, R. & Shafer, R. 2012, *ApJ*, 747, 32, 2012
289. Colafrancesco, S., & Marchegiani, P. 2008, *A&A*, 484, 51
290. Guo, F., & Oh, S. P. 2008, *MNRAS*, 384, 251
291. Fujita, Y., & Ohira, Y. 2012, *ApJ*, 746, 53
292. Fujita, Y., & Ohira, Y. 2013, *MNRAS*, 428, 599
293. Rossetti, M., Eckert, D., De Grandi, S., et al. 2013, *A&A*, 556, A44
294. Bagchi, J., Durret, F., Neto, G. B. L., & Paul, S. 2006, *Science*, 314, 791
295. Roettiger, K., Burns, J. O., & Stone, J. M. 1999, *ApJ*, 518, 603
296. Enßlin, T. A., & Gopal-Krishna 2001, *A&A*, 366, 26

297. Hoeft, M., Brüggén, M., Yepes, G., Gottlöber, S., & Schwöpe, A. 2008, *MNRAS*, 391, 1511
298. Skillman, S. W., Hallman, E. J., O'Shea, B. W., et al. 2011, *ApJ*, 735, 96
299. Markevitch, M., Govoni, F., Brunetti, G., & Jerius, D. 2005, *ApJ*, 627, 733
300. Pinzke, A., Oh, S. P., & Pfrommer, C. 2013, *MNRAS*, 435, 1061
301. Bonafede, A., Brüggén, M., van Weeren, R., et al. 2012, *MNRAS*, 426, 40
302. Clarke, T. E., & Ensslin, T. A. 2006, *Astronomical Journal*, 131, 2900
303. Giacintucci, S., Venturi, T., Macario, G., et al. 2008, *A&A*, 486, 347
304. Finoguenov, A., Sarazin, C. L., Nakazawa, K., Wik, D. R., & Clarke, T. E. 2010, *ApJ*, 715, 1143
305. Macario, G., Markevitch, M., Giacintucci, S., et al. 2011, *ApJ*, 728, 82
306. Akamatsu, H., Takizawa, M., Nakazawa, K., et al. 2012, *PASJ*, 64, 67
307. Akamatsu, H., & Kawahara, H. 2013, *PASJ*, 65, 16
308. Bourdin, H., Mazzotta, P., Markevitch, M., Giacintucci, S., & Brunetti, G. 2013, *ApJ*, 764, 82
309. O'Greehan, G. A., Brüggén, M., van Weeren, R. J., et al. 2013, *MNRAS*, 433, 812
310. Owers, M. S., Nulsen, P. E. J., Couch, W. J., et al. 2014, *ApJ*, 780, 163
311. van Weeren, R. J., Röttgering, H. J. A., Intema, H. T., et al. 2012, *A&A*, 546, A124
312. Stroe, A., van Weeren, R. J., Intema, H. T., et al. 2013, *A&A*, 555, A110
313. Ryu, D., & Kang, H. 2009, *Astrophysics and Space Science*, 322, 65
314. Vazza, F., Brüggén, M., van Weeren, R., et al. 2012, *MNRAS*, 421, 1868
315. Skillman, S. W., Xu, H., Hallman, E. J., et al. 2013, *ApJ*, 765, 21
316. Vazza, F., & Brüggén, M. 2014, *MNRAS*, 437, 2291
317. Enßlin, T. A., Lieu, R., & Biermann, P. L. 1999, *A&A*, 344, 409
318. Blasi, P. 2000, *ApJ*, 532, L9
319. Dogiel, V. A. 2000, *A&A*, 357, 66
320. Petrosian, V., Bykov, A., & Rephaeli, Y. 2008, *Space Science Reviews*, 134, 191
321. Rephaeli, Y. 1979, *ApJ*, 227, 364
322. Rephaeli, Y., Gruber, D., & Blanco, P. 1999, *ApJ*, 511, L21
323. Rephaeli, Y., & Gruber, D. 2002, *ApJ*, 579, 587
324. Fusco-Femiano, R., dal Fiume, D., Feretti, L., et al. 1999, *ApJ*, 513, L21
325. Fusco-Femiano, R., Orlandini, M., Brunetti, G., et al. 2004, *ApJ*, 602, L73
326. Rossetti, M., & Molendi, S. 2004, *A&A*, 414, L41
327. Fusco-Femiano, R., Landi, R., & Orlandini, M. 2007, *ApJ*, 654, L9
328. Eckert, D., Neronov, A., Courvoisier, T. J.-L., & Produit, N. 2007, *A&A*, 470, 835
329. Lutovinov, A. A., Vikhlinin, A., Churazov, E. M., Revnivtsev, M. G., & Sunyaev, R. A. 2008, *ApJ*, 687, 968
330. Wik, D. R., Sarazin, C. L., Finoguenov, A., et al. 2009, *ApJ*, 696, 1700
331. Wik, D. R., Sarazin, C. L., Finoguenov, A., et al. 2011, *ApJ*, 727, 119
332. Fusco-Femiano, R., Orlandini, M., Bonamente, M., & Lapi, A. 2011, *ApJ*, 732, 85
333. Eckert, D., Produit, N., Paltani, S., Neronov, A., & Courvoisier, T. J.-L. 2008, *A&A*, 479, 27
334. Ajello, M., Rebusco, P., Cappelluti, N., et al. 2009, *ApJ*, 690, 367
335. Petrosian, V., Madejski, G., & Luli, K. 2006, *ApJ*, 652, 948
336. Ajello, M., Rebusco, P., Cappelluti, N., et al. 2010, *ApJ*, 725, 1688
337. Fusco-Femiano, R., Dal Fiume, D., De Grandi, S., et al. 2000, *ApJ*, 534, L7
338. Rephaeli, Y., & Gruber, D. 2003, *ApJ*, 595, 137
339. Nevalainen, J., Oosterbroek, T., Bonamente, M., & Colafrancesco, S. 2004, *ApJ*, 608, 166
340. Wik, D. R., Hornstrup, A., Molendi, S., et al. 2013, *AAS/High Energy Astrophysics Division*, 13, #401.0
341. Nakazawa, K., Sarazin, C. L., Kawaharada, M., et al. 2009, *PASJ*, 61, 339
342. Finoguenov, A., Sarazin, C. L., Nakazawa, K., Wik, D. R., & Clarke, T. E. 2010, *ApJ*, 715, 1143

74 *G. Brunetti & T. W. Jones*

343. Johnston-Hollitt, M. 2004, in *The Riddle of Cooling Flows in Galaxies and Clusters of galaxies*, ed. T. H. Reiprich, J. C. Kempner & N. Soker, 51
344. Pfrommer, C., & Enßlin, T. A. 2004, *A&A*, 413, 17
345. Gabici, S., & Blasi, P. 2004, *Astroparticle Physics*, 20, 579
346. Keshet, U., Waxman, E., Loeb, A., Springel, V., & Hernquist, L. 2003, *ApJ*, 585, 128
347. Kushnir, D., & Waxman, E. 2009, *Journal of Cosmology and Astroparticle Physics*, 8, 2
348. Aharonian, F. A., Belyanin, A. A., Derishev, E. V., Kocharovskiy, V. V., & Kocharovskiy, V. V. 2002, *Physical Review D*, 66, 023005
349. Rordorf, C., Grasso, D., & Dolag, K. 2004, *Astroparticle Physics*, 22, 167
350. Inoue, S., Aharonian, F. A., & Sugiyama, N. 2005, *ApJ*, 628, L9
351. Vannoni, G., Aharonian, F. A., Gabici, S., Kelner, S. R., & Prosekin, A. 2011, *A&A*, 536, A56